AMB-REP-004

AMBER

the near-infrared interferometric instrument

ESO/VLTI Conceptual Design Review

Report prepared by the AMBER team

January 20, 1999

F. Malbet (editor), R. Petrov, U. Beckmann, E. Le Coarer, F. Lisi, D. Mouillet,
K. Perraut, A. Richichi, S. Robbe, M. Sacchettini

Contents

List of Figures

List of Tables

Chapter 1

Introduction

AMBER is the nickname of the near infrared / red focal instrument developed for the interferometric mode of the VLT (the VLTI). In a first phase starting in end of 2001, AMBER will be operated with two 8 m Unit Telescopes (UTs) in the near infrared, from 1 to 2.5 microns, with a priority for the K band. When the 1.8 m Auxiliary Telescopes (ATs) and an additional delay line become available, Amber will permit to measure phase closures with 1 UT and 2 ATs or with 3 ATs. When the ATs are equiped with the same kind of Adaptive Optics than the UTs, Amber will be extended to operation in the R band around the Hα line by the adjonction of visible spectrograph and detector. Some provisions are also made for later extensions to the L and M bands.

1.1 Scope of the report

This report concerns the near infrared instrument and has been prepared for the "Conceptual Design Review"(CDR) of the AMBER which takes place at ESO in January 99. This document is also intented to serve as a reference document for the preliminary design phase starting immediately after the CDR. With some updates and additions it will also be the base of the Memorandum of Understanding describing the collaboration between ESO and the Amber consortium.

1.2 VLTI context

AMBER will be installed in the focal laboratory of the VLTI. There, ESO will deliver beams from two or more telescopes, stabilized in position and direction and corrected for the piston variations introduced by the atmosphere thanks to a fringe tracking device. If the beams come from 8-m Unit Telescopes (UTs), ESO will at least partially correct the atmospheric wavefront perturbations with low-order adaptive optics. These adaptive optics modules are expected to have fair performances in the K band, with Strehl ratios reaching between 0.1 and 0.5 and to be usable down to the H and J band. ESO plans

to install a dual beam facility, called the PRIMA facility, which will allow to use an off-axis star for wavefront and fringe sensing. The distance between the science source and the reference star can reach 1 arcminute. The sky coverage dramatically depends on the limiting magnitude of the fringe sensor unit (FSU). If the FSU uses an infrared detector with approximatively 20 $e^-$of read-out noise (RON), its limiting magnitude is $K \sim 13$ and the sky coverage is about 1%. With coming detectors with RON of the order of 1 e^-, the limiting magnitude would be better than 15 and the sky coverage could reach 50%. Besides AMBER, two more instruments will equip the VLTI focus in the first phase: VINCI and MIDI. VINCI is a commissioning and first-light instrument able to measure very accurately contrasts on bright sources with no spectral resolution. MIDI is a science instrument to be operated in the mid infrared between 8 and 12 microns.

1.3 Science objectives

As explained in chapter 2, the potential astrophysical program of an near infrared instrument at the focus of an interferometer with baselines ranging from 40 m in the first phase to 200 m in the latest version is quite large (cf. review by the ESO Interferometry Science Advisory Committee 1996). We have selected three key programs for the first observations and we have used their instrumental needs as guidelines for the selection of the instrument concept. These programs are:

- study of disks, jets, multiplicity around young stellar objects (YSOs);
- detection, masses and spectra of extrasolar giant planets (EGPs) around solar type stars (such as 51 Peg);
- dust tori (and later broad line regions) of active galactic nuclei (AGNs).

The YSO program requires the measurements of visibilities with an accuracy better than 1% on stars with magnitudes ranging from 6 to 12 in K. The spectral coverage should include JHK. A spectral resolution of the order of 1000 will enhance the results by providing cinematic information. Imaging such objects is an ultimate goal which will be achievable thanks to the combination of 3 beams.

The EGP program is aimed only to relatively bright stars ($K \sim 5$) with extremely small effects on the measured quantities ($\sim 10^{-4}$) because of the large magnitude difference between the star and the planet. The first method consists in measuring the small visibility variation introduced by the planet when it orbits the star (Coudé du Foresto, Mariotti & Perrin 1996). The visibility variations will be smaller than 0.01% with a period ranging from a few days to a few weeks. For this approach, it is necessary to have visibility measurements with bias smaller than 10^{-4}. A second approach is to measure the difference in visibility or in phase between two spectral channels produced by the rapid variation of the magnitude difference with wavelength. The variations are smaller than 10^{-4} in fringe contrast or in fringe position, however the calibration is eased by the fact that the different channels are simultaneously analyzed. An additional advantage is that measuring

a variation as in function of λ actually yields to the spectrum of the planet and can therefore give much stronger constraints on its physical properties. In any case, an extreme care will be devoted to the calibration of the measurements and the suppression of atmospheric and instrumental biases.

The main difficulty of the AGN program is the faintness of the objects ($K \geq 11$). The requirements on the visibility accuracy can be limited to about 1%, at least in a first phase. Imaging capability is also foreseen to determine their morphological aspect at the scale of 1 parsec.

1.4 Instrument concept

The main characteristics of AMBER result from the combined needs of the latter three programs with the additional requirement of using phase closure to get imaging information as soon as more than two telescopes are available. The need to obtain extremely well calibrated visibilities on relatively bright objects points toward the spatial filtering techniques illustrated by the FLUOR experiment (Coudé du Foresto et al. 1996). When a single mode is selected in each interferometric beam, then all atmospheric and instrumental defects before the filter are reduced to photometric and piston fluctuations. The photometric variations are monitored in real time and the piston fluctuations do not affect the visibility of the fringes if the individual exposure times are short compared to the atmospheric time scale. This technique has now been demonstrated in details (Coudé du Foresto 1996). Its main limitation is the need of very short exposure times that reduce the limiting magnitude. This situation is not really changed when a fringe tracker is available, except in the rare case when a really bright reference star is available and allows to stabilize the fringes at very high accuracy, of the order of $\lambda/40$ or better. If the reference star is too faint, the quality of fringe tracking will be worse than $\sim \lambda/4$ and there will be a seeing dependent fringe degradation. The GI2T interferometer (Mourard et al. 1994) and other instruments have demonstrated that a good way to calibrate the measures is to use their variations with wavelength. AMBER concept combines the strong points from FLUOR and GI2T by using spatial filtering and dispersed fringes (see Malbet 1997a, b).

Spectral resolution is achieved by a dispersion spectrograph since AMBER is not dominated by background noise. It must however be cooled even at the relatively low 1000 resolution for the observation of sources fainter than magnitude 12. The maximum spectral resolution results from a trade-off between the needs of a larger range of programs and the technical and cost possibilities. The study of stellar structures and circumstellar matter will benefit strongly from a resolution of the order of 10000 (30 km/s). A more modest spectrograph with a 1000 resolution would have been sufficient in the first two years of operation of AMBER, but the gain in cost and in development time will have been too small to justify the additional overall burden represented by the development of two successive infrared spectrographs and their installation with the corresponding modifications of the beam combiner (change in the beam sizes). We have therefore chosen to build directly the instrument for spectral resolutions of about 5 (no dispersion), 70, 1000 and 10000 even if

the highest resolution will not be used in a first phase and the corresponding observing, data reduction and calibration procedures will be implemented later.

The multi-axial beam combiner has been chosen to ease the feed of the fringes in the spectrograph and to allow the transition from a two- to a three-telescope interferometer.

1.5 Phases of implementation

AMBER will be implemented in several phases. The first phase that we call phase A corresponds to two telescopes and to the JHK bands. Our objective is to use AMBER as soon as interferometric beams from two UTs are available with low order adaptive optics (phase A1). In the ESO current timetable this corresponds to end of 2001. When the first 2 ATs becomes operational in 2002, AMBER will have the possibility to observe more frequently at the cost of the ultimate sensitivity (phase A2).

In the second phase that we call phase B, which starts when the 3 Delay Lines become available, we will implement a third beam in AMBER to permit phase closure with 3 telescopes (Phase B1). We also plan to equip the ATs with low-order adaptive optics which allow us to extend the instrument wavelength coverage down to the Hα line and to develop a visible spectrograph and detector (Phase B2). One of the most interesting program permitted by this extension will be the resolution of the Broad Line Regions of AGNs and quasars. Another possible extension is the installation of a spectrograph and a detector for the L and M bands (Phase B3), which are not yet covered by any instrument. The space reservations for this L and M extension are included in the AMBER specifications of AMBER but at the moment no timetable has been established. Besides the phases for hardware implementation, there will be different steps in the development of the software and of the observing and calibration procedures.

Our objective is to combine a relatively ambitious long term program with a simplified but fully operational instrument for the first observations.

1.6 Expected performance

At this stage of the project, the expected performance are still subject to several uncertainties linked to exact specifications of optics throughput, detector and electronics characteristics, as well as fringe tracker and adaptive optics performances. At present[1] (see Table 1.1), we estimate that AMBER coupled to the VLT UTs will allow us to reach $K \sim 20 - 21$ in broad band and $K \sim 15 - 16$ at a resolution of 1000 when a reference is available for wavefront and fringe sensing. When the interferometer uses the object itself as a reference, the limiting magnitude is $K \sim 13 - 14$ depending on seeing conditions.

[1] see also section 3.8

Table 1.1: Expected K limiting magnitudes for two UTs (left) and two ATs (right) in average seeing conditions (in excellent seeing conditions in parenthesis).

	2 UTs				2 ATs			
Visibility accuracy	moderate		high		moderate		high	
Self-reference	**13** (14.2)		**10.5** (11.7)		**12** (12.1)		**9.5** (9.7)	
Spectral resolution	*5*	*70*	*1000*	*10000*	*5*	*70*	*1000*	*10000*
Off-axis reference	**20.4**	**17.7**	**14.8**	**12.3**	**19.4**	**16.7**	**13.8**	**11.3**
	(21.6)	(18.9)	(16.0)	(13.5)	(19.5)	(16.8)	(13.9)	(11.4)

1.7 ESO framework

In the definition of the software organization, a particular attention is being devoted to the simplification and the standardization of the observing, calibration and data reduction procedures. Our goal is to arrive at Paranal with at least a basic mode of operation (short exposures and low dispersed fringes) for which everything has been simulated, developed and tested in advance. The observing sequences is predefined from well analyzed templates, the parameters is established from simulations of the targets prepared by the science group and estimation of signal-to-noise ratio based on realistic simulations of the instrument prepared by the observing support group and updated in the integration and test phase. The data processing sequence and all the corresponding calibrations is automatically unfold as a result of the observing sequence. The single task remaining to the scientist is the interpretation of calibrated visibilities or phase differences.

Of course this is an ideal situation, but we want to reach it as fast as possible. We also believe that such an approach will permit the operation of the instrument by ESO or other non-members of the AMBER consortium as soon as an observing mode is fully commissioned. However, it would be unrealistic to expect that all important modes are commissioned simultaneously and we think that there will be a coexistence between instrument modes which can be operated by ESO for an *interferometrically conscious* general user and more advanced modes accessible only to AMBER members during their first uses.

In the same philosophy, the software and hardware architectures of the instrument control have been selected to be compliant with ESO standards and therefore with ESO operation and maintenance at least in their highest functionalities. As explained in chapter 7, we need to obtain some dispensation from the strict ESO standards for some low level motor and actuator boards and all the electronics of the detector head, in order to maintain the cost and the manpower load in AMBER compatible with the timetable and our resources.

1.8 Report outline

Chapter 2 details the science objectives. Chapter 3 presents the conceptual design and chapter 4 an extensive system analysis of AMBER. Chapter 5 lists the interfaces between AMBER and the VLTI. Chapter 6 details the optical lay-out of the beam combiner, the spectrograph and the detector. Chapter 7 describes a preliminary software functional analysis of the instrument control and architecture solutions. Chapter 8 explicates the assembly, integration and tests. Chapter 9 presents the project structure, schedule, budget and operation plan.

Chapter 2

Science objectives

A definition of the science objectives of AMBER is important in at least two respects.

Firstly, we note that AMBER will be the only instrument to cover the short-wavelength range at VLTI. This includes the near-infrared JHK bands (1 to 2.5μm), with later extensions to the red part of the visible spectrum and to the L and M bands (3.5 to 5μm). This wavelength range represents a window open on almost every aspect of modern astronomical research, and offers a combination of the highest angular resolution and deepest sensitivity available from the ground in the next decade. It should be stressed that AMBER will take advantage of some of the longest baselines among all large interferometric facilities, with some of the largest photon-collecting areas. This accounts for a very competitive coverage of many key scientific areas.

Secondly, many aspects in the practical design of AMBER are strongly dependent on its scientific use. Specifically, some technical choices in the subsystems need an assessment of the observational priorities to steer the design between different —and often contrasting— options. Also the software development, which will eventually provide the general user tools to prepare observations and evaluate them, must be coordinated with the diverse needs of the scientific use of AMBER.

In order to tackle these issues, a science group has been created. In this chapter, we give an overview of the objectives and the initial work of the science group. Then we provide a necessarily sketched description of the science targets that are being singled out for further study. We conclude with a list of technical choices driven by the scientific objectives.

2.1 Aim and working plan of the science group

The main aim of the AMBER science group is to define the key targets and priorities during the scientific operation of AMBER (see also document AMB-SGR-001). This comes from the necessity to make the best use of the scientific time in phase A: firstly because the UT time will be precious and relatively short, and secondly because it is essential to prove the ability to achieve adequate science with the UTs in order to apply competitively for open time. Given the potential of VLTI and AMBER in terms of sensitivity and angular

resolution, the spectrum of scientific applications is very wide. Our aim is to select a list of *key targets*, which have the potential to provide a sufficiently competitive scientific return with relatively short observing time. The key factor in this selection is to aim at what is feasible, without hunting for results which are repetitions or obvious extensions of what has been or is being done elsewhere.

This initial sample of key targets will be further subjected to modelling and simulations, in order to quantify explicitly the needs for number of baselines, integration times, minimum SNR, etc. On this basis, specific objects will be selected, and priorities will be assigned. This should include different scenari of the actual performance of the VLTI+AMBER, and will eventually be used as a guide to schedule observations during scientific time in Phase A.

What we have just defined as modelling and simulations needs some clarification, since interferometric measurements are intrinsically different from standard imaging and intuitive assumptions can be misleading. With imaging, one measures the brightness distribution over a field, $I(x, y)$. Such *brightness map* is usually contiguous, i.e. all points in the field are measured. With interferometry, one measures the points in a *Fourier map* $\tilde{I}(u, v)$. Although the two maps are related by a simple Fourier transformation, interferometry with a sparse array such as that of VLTI can measure only a few (u, v) points. The situation can be aggravated by the fact that, in the absence of closure phase (which is the case for AMBER in Phase A, but should be overcome when 3 telescopes become available in Phase B or when the PRIMA facility will allow to achieve phase referencing), one can measure only the modulus $|\tilde{I}|$ of the Fourier map. As a result, interferometric maps are generally not easily converted into true brightness maps[1]. In the case of the VLTI, which has a relatively large of possible baselines but only a few telescopes, the problem is really in the amount of time required to obtain the widest possible coverage of the (u, v) plane.

Therefore, one should begin to think in advance about the scientific output of an interferometric observation, in terms of sparse Fourier maps rather than true brightness maps. We intend to provide models of typical key targets in terms of Fourier components, and try to establish which features of the Fourier map can constrain or identify unambiguously a given physical parameter. To provide one example, in the case of a circumstellar dust shell the key physical parameters might be the density law of the dust, the size of the dust particles, the temperature law. We are currently generating model Fourier maps as a function of these parameters, which will be investigated in order to determine which (u, v) points (i.e., baselines of the VLTI) should be favored in the observations.

After this initial modelling phase, we will begin simulations to determine the amount of observing time required with the given baselines and depending on external parameters (seeing, level of AO correction, detector noise, etc.), in order to reach a minimum level of SNR for the given object, necessary to extract the required information on the physical parameter(s).

Understandably, this is at the moment an ideal plan of the science group work, which must be verified and corrected if necessary at each step. Note however the strong overlap

[1]Note exceptions for simple geometries, such as the case of a binary star.

Table 2.1: Scientific requirements.

Key Target	Visib. Accur.	Limit Magn.	Wavelength Coverage	Spectr. Resol.	Large Field[a]	Phase Closure[a]
Hot Exoplanets	10^{-4}	K>5	K	5-100	N	N
Star Forming Regions	10^{-2}	K>7	JHK+lines	5-1000	Y	Y
Circumstellar matter	10^{-2}	K>4	JHK+lines	5-1000	Y	Y
AGN dust tori	10^{-2}	K>11	K	5-100	Y	Y
Binaries	10^{-3}	K>4	K	5-100	N	N
Stellar Structure	10^{-4}	K>1	lines	10000	N	Y

[a] Not mandatory, but interesting in the long term.

between some of the software developments required by this plan of modelling and simulations, with the tasks of the observing software described in chapter 7. This relieves the science group from a large part of the practical work in the area of programming. Similarly, we are in contact with ESO personnel to follow the development of the ESO end-to-end model, which is also a viable tool for some of the simulations required.

2.2 Initial list of key targets

An initial list of key targets has been selected, based on assumptions and considerations about limiting magnitudes, visibility accuracy, spectral resolutions which have been detailed already in previous documents (see for instance AMB-REP-001, AMB-REP-002, AMB-REP-003 and Petrov et al. 1998). In particular, we refer to these references for a detailed discussion of the various observing modes foreseen for AMBER. As a rule of thumb, the expected limiting magnitudes are $K \sim 13$ and 12 with the UTs and the ATs respectively in pessimistic case and respectively 14.7 and 12.1 in optimistic case (see section 3.8 in chapter 3). A considerable improvement will be achieved when the PRIMA dual feed facility currently being designed by ESO and scheduled to be implemented in a very early phase of the VLTI operations will be available. In this case, at least on a fraction of the sky where a suitable reference star is available within a $\approx$1 arcmin field, the limiting sensitivity will be pushed by several magnitudes (up to 20 with the UTs).

In Table 2.1, we list some of the targets of investigation foreseen for AMBER, grouped as wide categories. Here below, we give some more details on the main scientific issues relative to each topic. For reasons of space, the description will be necessarily of a general nature. For convenience, we divide the topics between stellar, extragalactic and solar system-related astronomy. Three objectives among those ones have been selected as **key** targets:

- disks, jets, multiplicity around youg stellar objects (YSOs);

- detection, masses and spectra of extrasolar giant planets (EGPs) around solar type stars (such as 51 Peg);
- dust tori (and later broad line regions) of active galatic nuclei (AGNs).

2.2.1 Stellar astronomy

The broad area of stellar astronomy is congenial to the range of angular resolution and sensitivity projected for VLTI+AMBER, and also offers a higher probability of finding natural guide stars for the AO necessary with UTs operation. On the other hand, this is also the area where the competition from other ground-based interferometric facilities will be stronger, and therefore it is essential to scrutinize attentively the research possibilities in order to find the best possible cutting edge for new results during Phase A .

Star formation, young stars, jets

The area of star formation, involving many physical processes acting over a broad range of values in density, temperatures and chemical composition are traditionally the focus of investigations by several observing techniques from the radio to the visual bands. This area of research is also particularly interesting because of the consequences on the formation of single and multiple stars, of circumstellar disks, possibly of planets. The processes through which stars form also have a permanent signature on the way they will evolve through the greater part of their existence as normal stars.

One should mention first that AMBER in Phase A, coupled to the long baselines offered by VLTI, would allow us to extend the study of binary frequency in the early stage of star formation. Recent studies have shown that this appears to be significantly higher than for stars on the main sequence, implying that binarity is the rule rather than an exception in the formation processes. However, this conclusion is based on studies conducted in 2 or 3 star-forming regions only, because of the limits in angular resolution intrinsic with speckle interferometry on monolithic mirror telescopes. AMBER would be able not only to sample smaller separation ranges, but also to extend these studies to much larger distances and therefore increase significantly the statistics.

The physical understanding of complex structures such as circumstellar and proto-planetary disks, as well as the determination of flux distributions of pre-main sequence binaries, would benefit from observations in Phase A covering the near-IR domain. This is a particular area which will attract significant attention from all interferometric facilities with individual meter-sized collecting areas operating in the near-IR and therefore which will be very competitive (see the results already obtained with small interferometers like IOTA and PTI: Malbet et al. 1998 and Millan-Gabet et al. 1998). Another characteristic of the early stages of stellar formation is the presence of large amounts of dust and the consequent strong extinction of many of the interesting sources. This implies that this is an area in which the coordinated use of the two first-light VLTI intruments AMBER and MIDI should be highly stressed.

One point of distinction for AMBER investigation could be that of jets around young stars. Many young stars exhibit jets of ionized material, which have striking properties of alignment and symmetry. The exact nature of their energy source and the physics of their propagation are still being speculated, and require additional information which is precluded in normal observations. For example, the typical transversal scales of such jets are of order 3×10^{15}cm, which at the distance of the Orion region (450 pc) corresponds to 0.4". At the same time, they present a fine structure (nodules, bow-shocks) which must be investigated at the highest possible resolution and reaching as close as possible to the central star. Because of the ionization conditions, several emission lines are present. Although the jets are bright and visible also in the near-IR (typically H_2 at 2.12μm), they are best studied in the red part of the visible spectrum: Hα , SII$\lambda\lambda$6716,6731Å, OIλ6300Å, NIIλ6583Å are some examples. In the latter case, AMBER could exploit the red-spectrum, large-field operation and closure phase capability foreseen for Phase B, to map the central region of the jets with high-dynamic range and investigate the alignment mechanisms and energy sources.

Be stars, LBV

Hot stars such as Be, B[e] stars and luminous blue variables often exhibit strong stellar winds. The kinematic study of such winds is important to determine the physical conditions on the central star, and often represents an important means of studying the past history of stellar evolution. In addition, they often interact with the surrounding interstellar medium producing complex geometries. These objects are best studied in the visible part of the spectrum where they are brighter but also in the near infrared domain, and where a higher spectral resolution can be achieved. As such, they also constitute ideal targets for Phase A and B. In this case, AMBER would be an ideally suited instrument in virtue of the ability to obtain closure phases, allowing us to study the complex structures with a high dynamic range. Also spectral resolution would be highly desirable, with the need to reach $\sim 10^4$.

Giants, Supergiants, AGB stars, post-AGB stars

Cool giant and supergiant stars, having the largest angular diameters of all stars for a given luminosity, have represented a traditional goal of speckle interferometry and long-baseline interferometry. More than the mere measurement of the angular diameters[2], AMBER in phase A would be more suited to the investigation of the dust shells that are often present around such objects in the late stages of stellar evolution. Such shells have complex geometries, often dictated by the recent history of mass ejection from the star as well as by its interaction with the surrounding interstellar medium. In this respect, the ability to obtain imaging thanks to closure phase capability in AMBER phase B1 or the phase referencing facility will provide the means to investigate properties such as phases of mass ejection, dust characteristics, evolution of the ejecta in a second.

[2]These are already well sampled in the range 0.001" to 0.06" for $> 10^2$ objects

The example of IRC+10216 can be considered a prototypical case, with a complex structure of a dust shell on scales of ≈0.1" surrounded by several blobs of earlier dust emissions on scales ≤1". Accurate spectroscopic investigations as well as color and polarimetric maps of the individua blobs would allow us to understand the history of mass ejections, and the properties of the dust particles. There are several tens of objects that could be profitably studied in this sense by the VLTI+AMBER.

As an example of a future target for AMBER, we present in Fig. 2.1 the case of the source IRAS06088+1909. This previously anonymous source has recently been studied by combining several techniques in the visual and near-IR, including lunar occultations, speckle interferometry, polarimetry and imaging (see Richichi et al. 1998). The picture that emerges is that of a very reddened carbon star, surrounded by what appears to be an elongated, compact dust shell. Many characteristics of this object indicate a close resemblance to IRC+10216, but a detailed study is hampered by the larger distance which in this case is estimated to be ≈2kpc. Objects such as these need spectral coverage and resolution, imaging capability and angular resolution at the milliarcsecond level to be investigated. AMBER holds the potential to carry out investigations of many objects such as this to distances of a few kpc, thus allowing a substantial improvement in our understanding of the late stages of AGB evolution.

For what concerns planetary nebulae, quite a few of the central stars are at present known to be binaries. AMBER coupled to the maximum VLTI baseline offers the opportunity to reveal the duplicity in the galactic planetary nebulae with separations < 1AU at a distance of 1kpc. This is particularly useful to study the relationship between binarity and morphological characteristics of the nebulae.

Close binaries; symbiotic systems

It is known that the majority of stars live their lives as members of binary or multiple systems. A significant statistics of such systems has been obtained already by traditional observations, has been subsequently extended by methods such as speckle, lunar occultations or interferometry, and is likely to be further expanded by observations with more modern facilities. In addition to the study of separation and motions of binary systems, which at any rate is well suited also for other similar facilities, an important contribution by AMBER+VLTI in this field would rather be in the study of the mass loss and exchange phenomena that are often associated with very close binary systems.

Galactic center

Recent observations are beginning to shed light into the physics and kinematics of the very central part of our Galaxy. The picture that emerges is that of a large number of stars, moving at high speed (up to $> 10^3$km/s) in a restricted volume of space, $(0.2\ \mathrm{pc})^3$. The dynamical center seems to coincide with Sgr A*, but the uncertainty is still relatively large (0.1") to leave space to other suggestions. What is important is that the general kinematics seems consistent with density constraints that imply the presence of a central black hole.

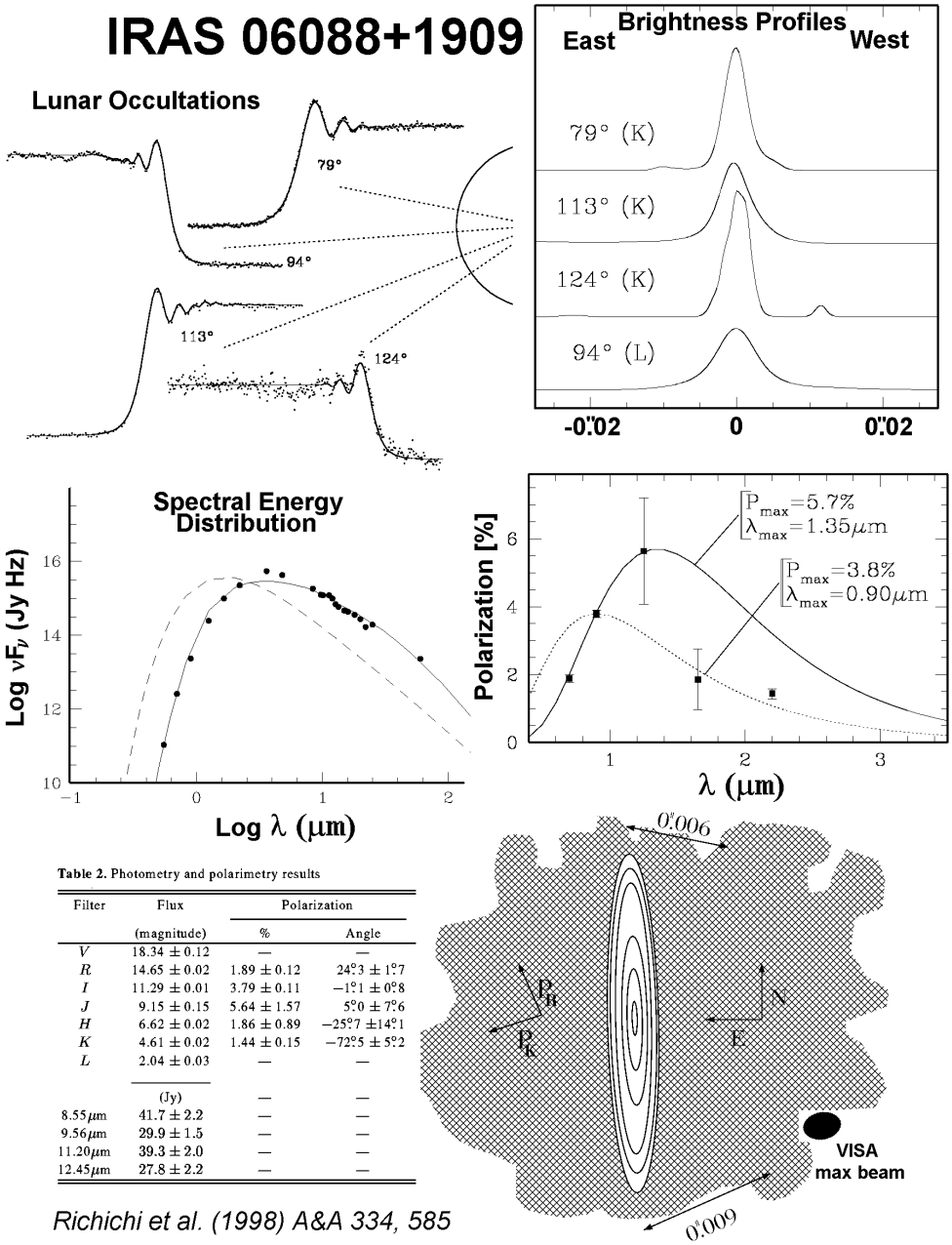

Table 2. Photometry and polarimetry results

Filter	Flux	Polarization	
	(magnitude)	%	Angle
V	18.34 ± 0.12	—	—
R	14.65 ± 0.02	1.89 ± 0.12	24°.3 ± 1°.7
I	11.29 ± 0.01	3.79 ± 0.11	−1°.1 ± 0°.8
J	9.15 ± 0.15	5.64 ± 1.57	5°.0 ± 7°.6
H	6.62 ± 0.02	1.86 ± 0.89	−25°.7 ±14°.1
K	4.61 ± 0.02	1.44 ± 0.15	−72°.5 ± 5°.2
L	2.04 ± 0.03	—	—
	(Jy)	—	—
8.55μm	41.7 ± 2.2	—	—
9.56μm	29.9 ± 1.5	—	—
11.20μm	39.3 ± 2.0	—	—
12.45μm	27.8 ± 2.2	—	—

Richichi et al. (1998) A&A 334, 585

Figure 2.1: IRAS 06088+1909 is a IRC+10216–like carbon star, recently investigated and whose characteristics are illustrated in the figure. This serves an example of a class of objects for which observations by AMBER are needed to provide a qualitative step in our understanding of stellar properties.

This is sufficient to describe the importance of this area of research, which however is quite demanding in its needs of both high spatial resolution and spectroscopic resolution. Because of the very crowded field, this is a difficult target for classical interferometers which do not have closure phase and are restricted to very small field of views. AMBER at the VLTI (especially in Phase B1) would have the capability to disentangle the complex field to extract information at much higher angular resolution than achieved today. The large density of stars also ensures an ideal target for adaptive optics operation, and it should be further stressed that the location of the Galactic Center is almost at the zenith from Paranal, while it is a low-altitude object for many Northern hemisphere interferometers (with the exception of Keck).

2.2.2 Extragalactic astronomy

Extragalactic astronomy is a more challenging area for interferometers such as VLTI (as well as for its competitor Keck and similar ones), because of the faintness of the targets but even more because of the relative scarcity of suitable natural guide stars for the wavefront correction. Nevertheless, a preliminary analysis shows that within the magnitude limits of the VLTI+AMBER there is a sufficient large number of objects to deserve a dedicated observational program. This will be expecially true in view of the availability of the PRIMA dual feed facility.

Active galactic nuclei

AGNs constitute a heterogeneous class of galaxies (Seyfert galaxies, QSOs, radio galaxies, blazars) characterized by a strong nuclear energy source that is thought to be powered by an accreting supermassive black hole. Strong emission lines come both from a compact sub-pc scale region (the broad line region) and from an extended 100 pc scale region (narrow line region). Also, collimated jets are often present. The unified model of AGNs ascribes some of the differences between different classes of active nuclei to the orientation of a circumnuclear 1-10 pc scale dusty torus.

The high angular resolution provided by VLTI combined with the high sensitivity of AMBER and later its phase closure capability could tackle several of the important open issues in this field. Furthermore the physics of the narrow line region is still poorly constrained. More specifically, it is not clear what is the relative role played by the nuclear photoionizing source and jet-induced shocks in the excitation and dynamics of the narrow line region. It would be possible to directly test the "unified model" by detecting 1-10 pc scale circumnuclear dusty torus in the near-IR bands (H and K), either in emission (hot dust) or in absorption (reddening maps). A positive detection of the torus has already been obtained by means of near-IR adaptive optics; AMBER would further probe such structures at much higher resolution and would extend the investigation to more distant objects (see Malbet, Petitjean and Henri 1997). An extension by a factor of $\approx$10 in radius would imply an enormous increase in the available statistics, allowing us in particular to sample a wider range of AGN luminosities and characteristics.

Except for the brightest sources, like NGC1068 ($K = 8$ but with an estimated core magnitude of $K \sim 11$), the latter studies implies almost invariably the need of the dual feed facility, and the presence of a nearby foreground star (or perhaps a local supernova) to provide adaptive optics wavefront correction and/or fringe tracking. In such cases, AMBER would be able to probe more distant and fainter QSOs and Radio Galaxies. The high angular resolution should also provide information on the host galaxy of these objects, that is relevant to the issues of the formation of AGNs and their connection to the galaxy evolution.

Low redshift galaxies

Also in the local universe, there are several research topics where the predicted performance of AMBER in terms of sensitivity and angular resolution can lead to very competitive scientific results. For instance, it would be of fundamental importance to be able to determine color-luminosity (H-R) diagrams in relatively distant galaxies. Again, this is subject to the availability of suitable reference sources for wavefront and piston correction. This should be feasible at least in a small fraction of cases even at intermediate and high galactic latitudes. Some of the applications would be the production of color-luminosity diagrams for distances $\gg$ 10Mpc (the limit of HST), and the possibility to trace Cepheids to relatively distant galaxies (subject to good photometric calibration of the interferometric measurements). In the first case, we would be able to measure the age of the stellar population. This in turn is a key to determining the age of initial stellar formation, and should provide clues to the processes of disk and bulge formation and evolution, expecially if we can probe regions and galaxy characteristics sufficiently different from those sampled up to now. In the second case, we would be able to obtain a wider and more accurate calibration of the Cepheids distance scale. Finally, more extensive estimations of Cepheid distances would be available to compare with peak brightnesses of type Ia supernovae. Eventually, a substantial refinement of the galactic distance scale and of the cosmological constant would be possible.

2.2.3 Solar system-related astronomy

Until recently astronomy has been focused mostly on stars and galaxies, but with the latest evidence of possible planets and protoplanetary disks around nearby stars, the field of solar system-related studies is gaining momentum and is in fact among the key targets for the new generation of ground-based and space-born telescopes. Also in this area, AMBER could provide a tool for competitive research.

Hot Exoplanets

The search for exoplanets is currently at the forefront of scientific interest both from the purely scientific point of view, and thanks to a more general interest from the media and the public. In the case of VLTI, the full capability will be achieved when AMBER will

benefit from the dual-feed feature of PRIMA, which will allow astrometric monitoring of a star's motion by comparison with one (or more) reference stars in a field of ≈ 30".

However, already without PRIMA there is a mode in which relatively hot exoplanets could be detected: to measure the fringe phase shifts of the central star, caused by the displacement of the photocenter due to the planet. This method has been investigated quantitatively by the science group, and the magnitude of the expected effect should be within the limits of detection by AMBER for a 51 Peg-type system. It must be noted that because the expected phase shift is very small, it is impossible to achieve the required precision in an absolute sense. Therefore, one has to rely on a relative measurement of the phase shift, which can be accomplished by measuring *simultaneously* the fringes over a wide baseline of wavelengths. This is one of the drivers for the low-resolution mode of the spectrograph.

Post-planetary disks

The observation of post-planetary disks is well suited to the resolution offered by VLTI, and to the limited imaging capability achievable with three baselines. The prototype of this class of objects can be considered to be β Pic. With AMBER, similar objects could be studied at much larger distances. The most demanding requirement is the contrast which in model fitting methods can be directly translated to visibility accuracies.

Solar system objects

Without entering their very diverse physical characteristics, we list here only a few solar system objects where the baselines of VLTI combined with the sensitivity and phase closure capability offered by AMBER would provide a very competitive scientific return:

- asteroids (dimensions, duplicity, surface structure).
- surfaces of the major satellites of the outer planets.
- imaging and monitoring of active features such as Io's volcanoes.
- Pluto/Charon system.

2.3 Scientific drivers in the AMBER design

In the course of the initial design of AMBER, several technical points were raised in which different options were available and needed an input from the science group. We summarize them here for reference:

Wavelength Coverage. We have enumerated the needs in terms of minimum vs. desirable wavelength coverage, and of spectral resolution. It has been agreed that AMBER will cover initially the JHK bands, with extensions to RI in the visual (first

priority, phase B2), and LM in the infrared (second priority, phase B3). Each band will benefit from 4 spectral resolution settings, with a maximum of $\lambda/\Delta\lambda \approx 10^4$.

Detector Format. Choice of the HAWAII versus PICNIC, in view of the read-out noise (≤ 10 e^-) and the need for a large number of pixels in some specific applications (e.g., low dispersion coverage of 2 bands simultaneously for phase-referenced observations of exoplanets).

Field of View. A field of view (FOV) larger than a simple UT-Airy disk in Phase A. The point is not to make a full coverage of the available field (which would be practically infeasible over the nominal 2 arcseconds FOV with the VLTI resolution), but to make sure that selected objects are not vignetted and to sample specific features. Also the problem of a correct centering of the objects has been raised. A FOV of many Airy disks (a value of 0.3 arcseconds has been recommended) is a strong requirement in the AMBER design. It has been decided to leave this option open as long as it does not create practical conflicts with other design options, or until it does not delay the work of other subsystems.

Polarization A lower priority on polarimetric observations capability has been recommended, simply due to the fact that they are time-consuming. It was estimated that a sufficient volume of key science can be tackled in Phase A (when observational time at the UTs is precious) without polarimetry.

Fringe Tracker The need for the best (i.e. most sensitive) fringe tracking possible is obvious from the science point of view. Initially, the point has been to upgrade the ESO/OCA PFSU to charge-integrating InSb or even a NICMOS detector. This would have provided a gain of 2-3 magnitudes to the expected PFSU magnitude limit. With the development of new 1 e^- RON near-infrared detectors, we strongly suggest ESO to think of using such devices, with the possibility of opening significantly broader targets for the AMBER science.

Chapter 3

Conceptual design

We present here the keys to the AMBER concept. Detailed numbers and arguments will be given in chapter 4 where the choices are presented.

3.1 VLTI infrastructure

AMBER is the final stage of an overall infrastructure. It is part of a VLTI well defined plan. The general concept of the VLTI is to provide an interferometric focus to the instruments, like modern telescopes provide almost diffraction-limited beams to their instruments. Therefore the VLTI infrastructure works like a general facility which supplies the following functions:

- sampling of the (u, v) plane with 4 fixed UTs and 3 movable ATs with baselines ranging from 8m to 200m.
- collection of light with 4 large telescopes (UTs, 8m) and 3 small telescopes (ATs, 1.8m).
- wavefront correction at the telescopes (only for the UTs in the first phase)
- star separators which allows to extract two fields of $2''$ within a field of $1'$, called respectively the primary and secondary fields.
- transportation of the primary and secondary beams from the telescopes to the focal lab.
- compensation by the delay lines (DLs) of the optical path difference due to the sidereal motion.
- correction of the fluctuations of optical path length due to the atmospheric piston with a fringe sensor and active delay lines.
- stabilization of the beams in direction and lateral position.
- longitudinal position of the pupil at any point thanks to a variable curvature mirror (VCM).

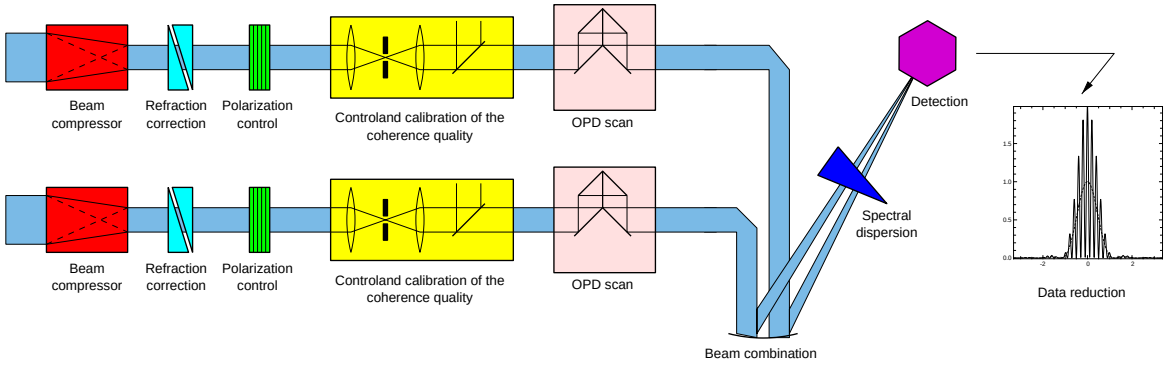

Figure 3.1: Functional diagram of AMBER

- compensation by the differential delay lines (DDLs) of the optical path difference due to the sidereal motion between the primary star and the secondary star.
- metrology system to measure the optical path difference between the primary and secondary beams to allow phase referencing and narrow-angle astrometry.

All these functions should be available at the very beginning, except for the metrology system which will be delivered later. Only two UTs will be available during the first two years starting in 2001, then 3 ATs starting in 2003.

3.2 Global functional analysis

AMBER measures the complex degree of coherence of the wave received by the set of the pupils which composed the interferometer. It must therefore accept the beams provided by the VLTI infrastructure, correct them from some atmospheric and instrumental effects, combine them to form interference fringes, and measure the contrast and the phase of these fringes in one or several spectral channels. The main functions of AMBER are (see Fig. 3.1):

F01 Match of the optical characteristics from the VLTI beams

F02 Compensation of the atmospheric systematic effects

F03 Control of the polarization state

F04 Control and calibration of the coherence quality

F05 Scan of the optical path difference (OPD)

F06 Interferometric beam combination

F07 Spectral dispersion

F08 Signal detection and acquisition

F09 Transformation of the signals into calibrated coherence measures

3.3 Implementation phases

3.3.1 Phase A

AMBER will focus on the combination of two UTs in the near infrared and 2 ATs when they become available. AMBER is then composed of the following elements:

- two-way beam combiner
- beam quality control (polarization, spatial filter, photometry monitoring , etc)
- cooled spectrograph (spectral resolution up to 10000)
- infrared detector (1 μm $\leq \lambda \leq$ 2.6 μm)
- control software + data reduction software

3.3.2 Phase B – Extensions

The following phases of AMBER will happen when 2 or 3 ATs become available in 2003. The following extensions are foreseen by order of priority:

1. 3-way beam combiner allowing to achieve phase closure
2. visible spectrograph and detector (0.6 μm $\leq \lambda \leq$ 1 μm) and adaptive optics for the ATs for observations in the visible domain
3. extension to L and M bands (2.5-3 μm) using a dedicated spectrograph and detector.

3.4 AMBER interferometric requirements

3.4.1 Instrumental visibility

The interferometric requirements consists mainly in contrast loss and contrast accuracy. The first one is easily calibrated with a star used as a calibrator (we know its intrinsic visibility and deduce therefore the instrumental visibility). The second one is a requirement on the contrast stability: what is the stability of the instrumental visibility measured on a calibrator so that we are able to average the visibility measurements to increase the accuracy?

The scientific requirement for the visibility accuracy is to detect a final visibility change of the order of 10^{-4} on a 51 Peg-like star (see section 1.3). The observing cycle described in section 3.7 and in more details in section 4.11.3 lasts about 5 minutes (see AMB-IGR-007). Observing a 51 Peg-like star during 8 hours leads to 100 independent measures which can fit the expected variation of visibility in function of the brightness ratio, the orbit position angle and the orbit inclination. Consequently, 3 nights lead to an accuracy of 10^{-4} if the measures obtained in one cycle are accurate at the level of 10^{-3}. The AMBER requirement

on the **visibility stability and accuracy in 5 minutes is** 10^{-3}. For comparison, FLUOR achieves presently an accuracy of 3×10^{-3} on a (Coudé du Foresto, Mariotti & Perrin 1996).

The phase requirement derives simply from the visibility amplitude requirement: 10^{-n} in amplitude leads to 10^{-n} in fringes for the phase. However in differential mode, the requirements benefit from independent measurements at different wavelengths and therefore the measure on a 51 Peg-like star can be achieved in much less than 3 nights.

The requirement in terms of contrast loss is the one found in the error budget for the VLTI. **The requirement is 5% of maximum contrast loss for AMBER**.

3.4.2 Optical throughput

The main requirement on throughput is driven by the AGN program. We wish to observe AGN with magnitude $K > 11$. This leads to a transmission budget of 45% for AMBER in K .

The details of the computation are: with a VLTI transmission of 30%, a coupling factor of 70% and a Strehl ratio of 0.1 for an average seeing and an adaptive optics with 31 actuators, a detector read-out noise of 10 e^- and an instrument throughput of 45% excluding the coupling already taken into account, we obtain a limiting magnitude of $K \sim 13$. Any gain in the throughput will increase this limiting magnitude and the requirement is therefore an **optical throughput greater than 45%**.

3.5 Fundamental specifications

- **Atmospheric refraction** The effect is important for the J and H band and nearly negligible for the K band. However, the effects between bands can be large. The adaptive optics system will give a direction at a given wavelength (the one uses for image sensing in the lab). The angle between this latter direction and the actual direction at the observing wavelength will vary with time and implies coupling degradations. We therefore conclude that **an Atmospheric Refraction Compensator is needed before AMBER and actually before any instruments which operates at a different wavelength than the image sensor (ESO module?).**

- **Atmospheric differential dispersion** Its effect is rather negligible except at long baselines, at the H_α wavelength and at the lower resolution. **We do not correct for atmospheric differential dispersion** and recommend to use higher spectral resolution when the effect is no longer negligible since the dispersion decreases with $\Delta\lambda$. We still have to evaluate the impact on faint sources for which we do not want to disperse the signal.

- **Polarization** We can **select one polarization direction** with a polarizer if the contrast appears to be too small because of unexpected instrumental polarization.

- **Spatial filtering** All incoming beams are spatially filtered thanks to **single-mode optical fibers** .
- **Photometry calibration** For each beam, **35% of the flux** is used for photometric calibrations.
- **OPD** AMBER is able to **adjust the zero-OPD** and to **center the fringes**. The OPD modulation is done thanks to the VLTI delay lines .
- **Beam combination** The beam combination is **multi-axial** using a non-redundant 1-D array. The incoming beams are compressed with an anamorphic factor of 4.8 for 2 beams and 14.4 for 3 beams.
- **Spectral dispersion** The interferometric signal is dispersed with $\mathcal{R}$ **~5, 70, 1000 or 10000**. The photometric signals are **spectrally dispersed with low resolution**.
- **Detection** The AMBER detector is the **HAWAII detector** from Rockwell with a read-out noise less than 10 e^-.
- **Data reduction.** Use a generalization of the **ABCD algorithm** to the multiaxial lay-out.

3.6 Operating modes

3.6.1 Observing modes

The observing modes correspond to different values of the parameters to achieve a given visibility accuracy and/or sensitivity. They are derived from the scientific requirements (cf. Table 2.1 in chapter 2) and are summarized in Table 3.1.

With an elementary exposure time τ = 10ms and no fringe tracking, the fringe stabilization is better than 0.03 μm(see Table 4.2), leading to a visibility accuracy of $\leq 10^{-2}$. Because consecutive visibility measures are statistically independent, the visibility accuracy increases with the number of measures. In 2 minutes, one can expect to have $N \sim 10\,000$ measurements, so the accuracy is increased by a factor 100.

Therefore to reach the visibility requirements, we need elementary exposures of 100ms for the imaging mode, 10ms for the high precision visibility mode. An elementary exposure time of 100s seems reasonable when fringe tracking is available.

3.6.2 Acquisition modes

The acquisition modes which have been identified are the different ways to acquire the fringes. These modes are summarized in Table 3.2. They do not take into account the specifications in term of visibility accuracy or sensitivity.

Table 3.1: Characteristics of observing modes.

Observing Modes	Visibility accuracy	Sensitivity (mag)	Spectral resolution	Exposure time	Acquisition modes
Imaging mode (IM)	1%	$K \geq 11$	$\mathcal{R} \leq 1000$	0.1s – 100s	1, 2, 3
High precision visibility mode (HPVM)	0.01%	$K \geq 5$	$\mathcal{R} \leq 100$	0.01s	1, 3, (4)
High spectral resolution mode (HSRM)	—	$K \geq 4$	$1000 \leq \mathcal{R} \leq 1000$	100s – 4h	3, (1, 2)

Table 3.2: Summary of acquisition modes.

	Fringe detection	Fringe tracking	Exposure time	Individual fringe	Dual feed	Spatial filter	Spectral resolution	Observing modes
1	dispersed		short	yes		X	$\mathcal{R} \geq 70$	IM, HPVM, (HRSM)
2	dispersed		short	no		X	$\mathcal{R} \geq 70$	IM, (HRSM)
3	dispersed	X	any		possible	X	$\mathcal{R} \geq 70$	IM, HPVM, HRSM
4	scanned		short			X	$\mathcal{R} \sim 5$	(HPVM)
5	dispersed		short			no	$\mathcal{R} \geq 1000$	

Acquisition mode #1 is the **AMBER standard acquisition mode** which will be supported in first place. Acquisition mode #2 is the extension of #1 to very faint objects (the fringes are not detected in individual frames). Acquisition mode #3 will be the AMBER standard mode as soon as fringe tracking becomes available. The last 2 modes are potentially interesting modes.

3.7 Observing procedures

For the standard acquisition mode (#1) the following steps will be followed during the observing procedure. We assume that AMBER is already aligned.

- **Initial alignment at the beginning of the night**
- **Initial calibration for a given configuration**:
  - Instrument configuration set-up
  - AMBER instrument calibration
- **Observing cycle**: Fringe check, observation set-up, object/calibrator #1 cycle, object/calibrator #2 cycle , ..., final calibrations. The object/calibrator cycle lasts typically 5 minutes.
- **Data reduction**

3.8 Expected performances

3.8.1 Input parameters

The following characteristics of the VLTI have been chosen. The report AMB-REP-001 justifies all these numbers.

- *Telescope diameter :* $D = 8$ m for the UTs, $D = 1.8$ m for the ATs;
- *Global optical throughput for VLTI:*
  H-K band: $t_{\rm VLTI} = 30\%$
  J band: $t_{\rm VLTI} = 5\%$ (due to the M9 dichroic)
- *Strehl ratio*[1]*:*
  Excellent conditions ($< 20\%$ of time), K band, UT: $SR = 30\%$, AT: $SR = 90\%$
  Average conditions ($< 60\%$ of time), K band, UT: $SR = 10\%$, AT: $SR = 80\%$
- *Coupling efficiency:* $C = 70\%$;
- *AMBER throughput:* $t_{\rm AMBER} = 45\%$;

[1]The numbers come from the simulations made by M. Tallon in AMB-REP-001 report for 31 actuators and a curvature sensor.

Table 3.3: Adaptive optics Strehl ratio at different wavelengths.

	2 UTs			2 ATs		
Seeing conditions	J	H	K	J	H	K
excellent (< 20% of time)	2%	11%	**30%**	71%	83%	**90%**
average (< 60% of time)	0.06%	2%	**10%**	49%	67%	**80%**

- *Number of measurements needed for one visibility measurement:* $n = 4$ for 2 telescopes and $n = 12$ for 3 telescopes ;
- *Detector read-out noise:* $\sigma_d = 10$ e$^-$;
- *Detector quantum efficiency :* $\eta = 0.5$;
- *Elementary exposure time:*
  $\tau = 100$ms for imaging mode
  $\tau = 10$ms for high precision visibility mode
  $\tau = 100$s for high spectral resolution mode

The dependance of the Strehl ratio SR with the wavelength is approximated by the following law:

$$SR(\lambda) = \exp\left(\ln(SR_K)\left[\frac{\lambda_K}{\lambda}\right]^2\right) \tag{3.1}$$

where SR_K is the Strehl ratio at the effective wavelength λ_K of the K band. Table 3.3 gives the Strehl ratio for J, H and K for the two cases considered in this report.

3.8.2 Limiting magnitude formula

The spectrograph is cooled down to 77K and therefore the thermal background is negligible (see AMB-REP-001). To define the limiting magnitude, one takes a $SNR = 5$ for detecting the fringes out from the noise. The SNR formula is then for a photometric limiting magnitude:

$$SNR = \frac{N_*}{\sqrt{\sigma_*^2 + \sigma_d^2}} \tag{3.2}$$

Knowing the read-out noise σ_d and the photon noise $\sigma_*^2 = N_*$, we find that the number of photo-electrons at the limiting magnitude is $N_L = 64$. The limiting magnitudes are then defined by:

$$m = 2.5 \log\left(\frac{E_0\ S\ t_{\rm VLTI}\ t_{\rm AMBER}\ SR\ C\ \Delta\lambda\ \tau\ \eta}{N_L\ n\ hc/\lambda}\right) \tag{3.3}$$

3.8.3 Performances without fringe tracking

We use the previous numbers and equations to compute the limiting magnitudes reported in Table 3.4. One should stress that the Strehl ratio has an important role in the results.

Table 3.4: Limiting magnitudes of the instrument without fringe tracker.

Excellent seeing conditions ($< 20\%$ of time)

	2 UTs			2 ATs		
Observing modes	J	H	K	J	H	K
Imaging	10.3	13.7	**14.2**	10.9	12.6	**12.1**
High Precision Visibility	7.8	11.2	**11.7**	8.4	10.1	**9.7**

Average seeing conditions ($< 60\%$ of time)

	2 UTs			2 ATs		
Observing modes	J	H	K	J	H	K
Imaging	6.5	11.6	**13.0**	10.5	12.4	**12.0**
High Precision Visibility	4.0	9.1	**10.5**	8.0	9.9	**9.5**

If the Strehl ratio is 0.5 instead of 0.1 in K, then the limiting magnitudes increase of almost 1.7 magnitudes, reaching $K \sim 14.7$ in the imaging mode on the UTs. Therefore is it of importance to have a good AO system on the telescopes. We need to get the ESO estimates for the Strehl ratio in order to produce more accurate estimations of the limiting magnitudes.

3.8.4 Performances with on- or off-axis fringe tracking

With fringe tracking, the integration time in the spectral channel can be as long as desirable providing that it is short compared to baseline variations. We think that $\tau = 100$ s is a reasonable number for this mode. We present *SNR* curves for different resolutions on Fig. 3.2. A lost of 0.7 mag must be taken into account when the source is used as a fringe tracking reference itself. Table 3.5 reports the limiting magnitudes for observations of 4 hours with a $SNR = 100$.

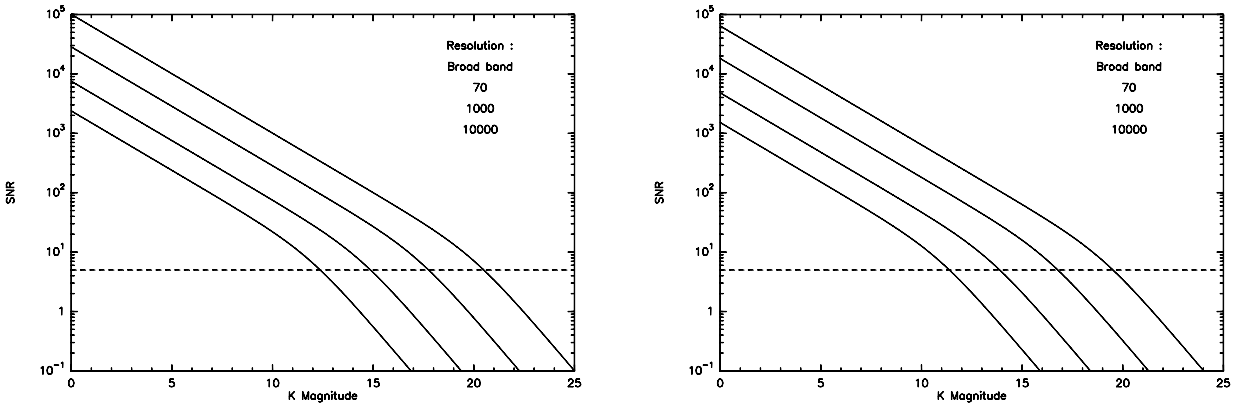

Figure 3.2: Signal to noise ratios in K band for the UTs (left) and the ATs (right) in *High Spectral Resolution mode* ($\tau = 100$ s) (see AMB-REP-002 for details on computation).

Table 3.5: Limiting magnitudes with fringe tracking with the UTs (left) and with ATs (right). Total integration time of 4 hours and $SNR = 100$.

Excellent seeing conditions ($< 20\%$ of time)

	2 UTs			2 ATs		
	J	H	K	J	H	K
No dispersion	17.7	21.1	**21.6**	18.3	20.0	**19.5**
$\mathcal{R} = 70$	15.0	18.3	**18.9**	15.6	17.2	**16.8**
$\mathcal{R} = 1000$	12.1	15.4	**16.0**	12.7	14.3	**13.9**
$\mathcal{R} = 10000$	9.6	12.9	**13.5**	10.2	11.8	**11.4**

Average seeing conditions ($< 60\%$ of time)

	2 UTs			2 ATs		
	J	H	K	J	H	K
No dispersion	13.9	19.0	**20.4**	17.9	19.8	**19.4**
$\mathcal{R} = 70$	11.1	16.2	**17.7**	15.2	17.0	**16.7**
$\mathcal{R} = 1000$	8.2	13.3	**14.8**	12.3	14.1	**13.8**
$\mathcal{R} = 10000$	5.8	10.8	**12.3**	9.8	11.6	**11.3**

Chapter 4

System analysis

We present in this chapter the details of the concept choices which were made in the concept phase (see section 3.5 for a summary). This chapter justifies these choices.

4.1 Preliminary optical lay-out

A schematic view of AMBER is displayed on Fig. 4.1. This scheme will ease the understanding of the system analysis. The different elements are:

1. afocal system used to compress the incoming beams
2. polarization control module
3. differential refraction module
4. spatial filtering
5. beam splitter to separate the photometric and interferometric channels
6. fold mirrors for the photometry
7. cylindrical optics which compress the beams in the y-direction
8. compressor for the photometric channels
9. cold pupil stop
10. filter wheel
11. grating or prisms for low to high dispersion of the interferometry channels
12. chamber mirrors
13. detector
14. flat mirror or low dispersion prism for the photometric channels

4.2 Atmosphere systematics

We have made an initial estimation of the transversal and the longitudinal effects of the atmospheric refraction (see annex E of memo AMB-IGR-003). The first one occurs on each

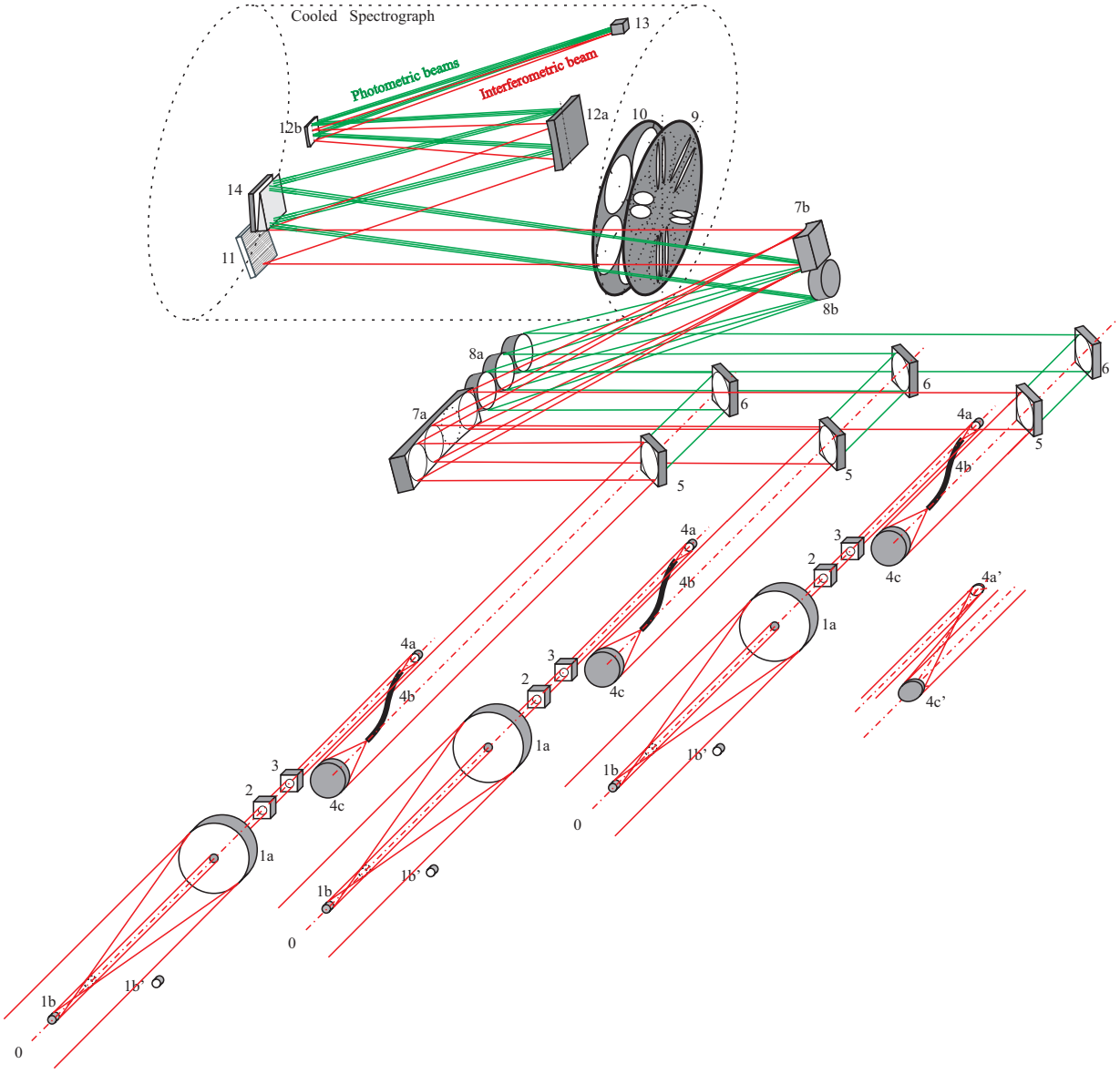

Figure 4.1: Preliminary optical layout of AMBER. See text for details.

beam of the interferometer and consists in its spectral dispersion, measured in an image plane; we call it "atmospheric refraction". The second one is a differential effect, occuring along the optical path before the recombination; we call it "atmospheric dispersion". So, only the latter will depend on the spectral resolution of AMBER.

Both effects depend of course on the refractive index of the air, n, function of the wavelength and of the atmospheric parameters at the ground. For this first evaluation, we have taken mean values of the Paranal for the air pressure, the air temperature and the water vapor-pressure:

$P = 562.55$ mmHg (760 mbar)
$T = 0°$C
$P_v = 0.6$ mmHg (corresponding to 12.5% of humidity at 0°).

The empirical formula used for estimating n is the one of the *Astrophysical Quantities* book. A more precise formula is given by Ciddor (1996), but, for a first estimation, the former is sufficient.

4.2.1 Atmospheric refraction

If z_0 is the apparent zenithal angle, the refraction angle R has the following expression (second order approximation):

$$R = \alpha(1-\beta)\tan(z_0) - \alpha(\beta - \frac{\alpha}{2})\tan(z_0)^3, \tag{4.1}$$

where $\alpha = n - 1$; $\beta = P/\delta r$ with δ the density of air and r the terrestrial radius. With $\delta = 0.00096$ g/cm^3 and $r = 6373.6$ km, a maximal value for z_0 of 60° for the UTs and 30° for some largest ATs configurations, we compare, versus the wavelength, the value of R to the value λ/D on Fig. 4.2. Arbitrarily we have canceled R for the maximal wavelength of each bandwidth.

Let us see Fig. 4.2.b for the J-Band, the UT and 60° of zenithal angle (the worst case!). Let us suppose that the Airy disk at $\lambda = 1.4$ μm is centered on the spatial filter. We can read that at $\lambda_m = 1.1$ μm, the Airy disk is shifted 4.8 times λ_m/D. The coupling will be negligible. Without correction, the whole bandwidth will not be accessible by the focal instrumentation.

In addition to this effects, the refraction leads to different position of the optical axis for different bands. This is especially important between the visible, where the tip-tilt correction is achieved, and the near-infrared where the fringe tracking and fringe detection is done. This has to be corrected and the best way is to do it for all beams before the instruments in the ESO interferometric facility.

4.2.2 Atmospheric differential dispersion

The origin of this effect is the inequality of the horizontal optical paths in the air due to the OPD existing in the vacuum above the atmosphere, this OPD being equal to $B \sin z_p$,

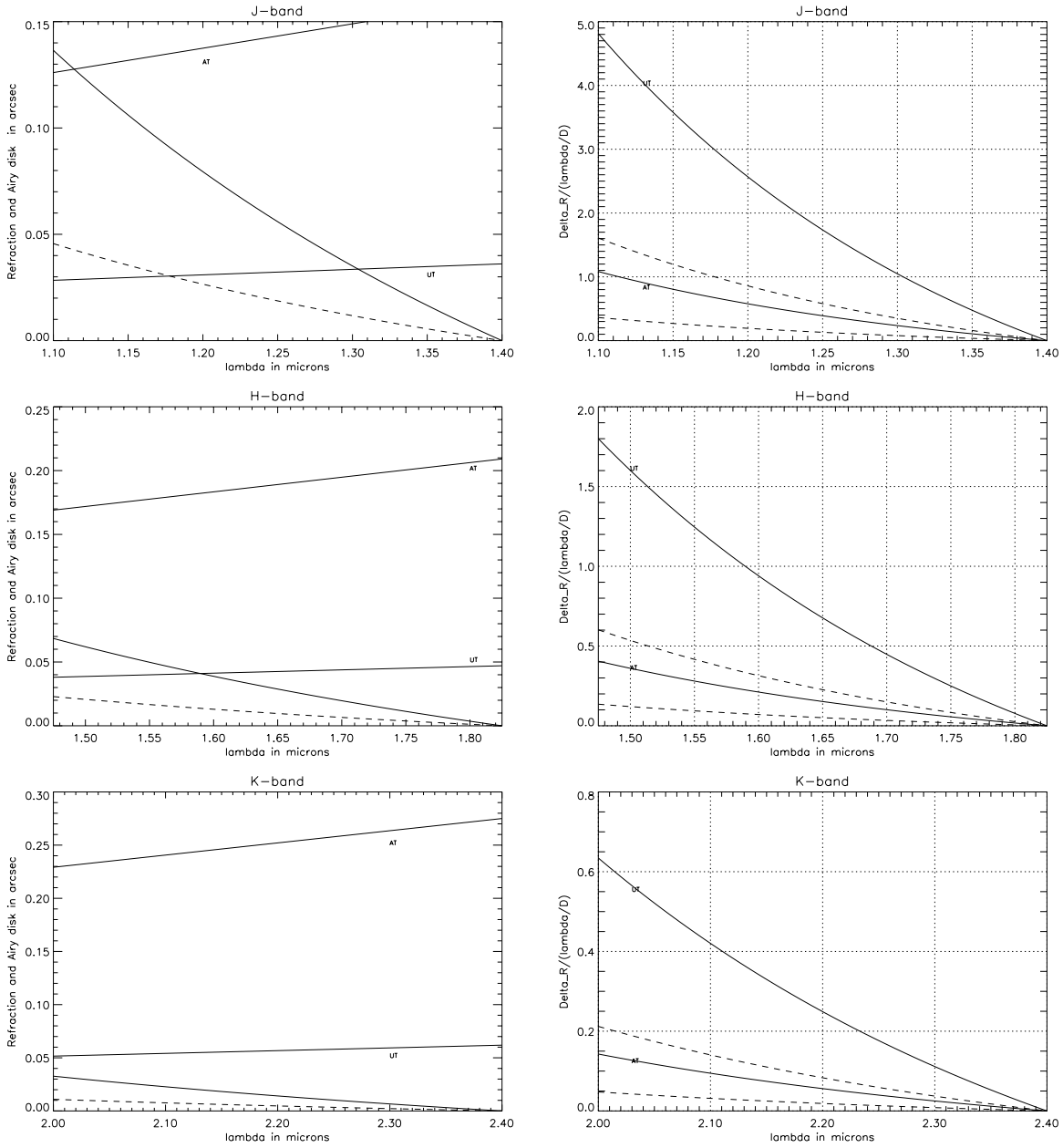

Figure 4.2: a- (left column) Refraction for 8m and 1.8m Telescopes for 2 zenithal angles 60° (full line) and 30° (dotted line). Are also plotted the angular Airy disks (straight lines referred by 'UT' and 'AT'). b- (right column) Shifts, due to the refraction, of the Airy disk versus the wavelength expressed in λ/D unit.

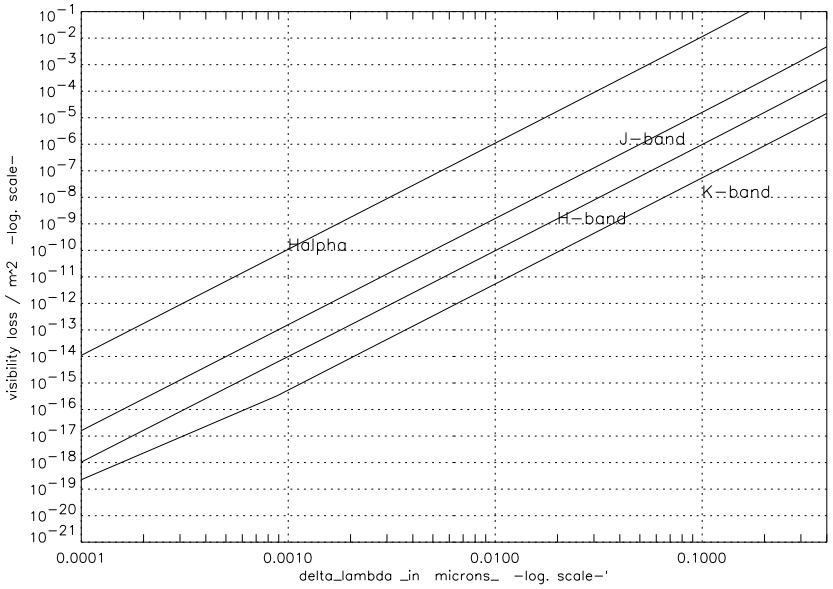

Figure 4.3: Visibility loss per meter squared of air for different spectral bands, versus the spectral resolution

where B is the baseline length and z_p the projection of the zenithal angle on the meridian plane. That means that not more than two wavelengths can arrive phased: the maximal visibility can no longer be equal to 1. The gap to 1 depends of course on the spectral bandwidth.

We show that the visibility V can be written as: $V_0 \simeq (1 - \Delta V)$ with ΔV proportional to the variance of the interference order $\sigma\delta(\sigma)$. The resulting loss is:

$$\frac{\Delta V}{[B \sin z_p]^2} = 2\pi^2 \int d\sigma \left[d - p_a \frac{\int p_a d}{\int p_a^2} \right]^2 , \tag{4.2}$$

with

$$p_a = n\sigma - \int n\sigma \text{ and } d = \sigma - \int \sigma \tag{4.3}$$

$$\sin z_p = \cos\beta_B[-\cos\varphi \sin\delta_o + \sin\varphi \cos\delta_o \cos(H)] - \sin\beta_B \cos\delta_o \sin(H), \tag{4.4}$$

φ is the latitude of the site: $\varphi_{\text{mean}} = -24,55°$,
δ_o is the declination of the object,
H is the hour angle,
where β_B is the angle made by the baseline direction with the North-South one.

For numerical applications, we plot two synthetic graphs for representative cases. Figure 4.3 shows, for each spectral domain, the variation of ΔV with the spectral bandwidth for a $B \sin z_p$ equal to 1 meter. Figs. 4.4 describe the temporal variation of the quantity $(B \sin z_p)^2$, for different B and δ_o for the following baselines:

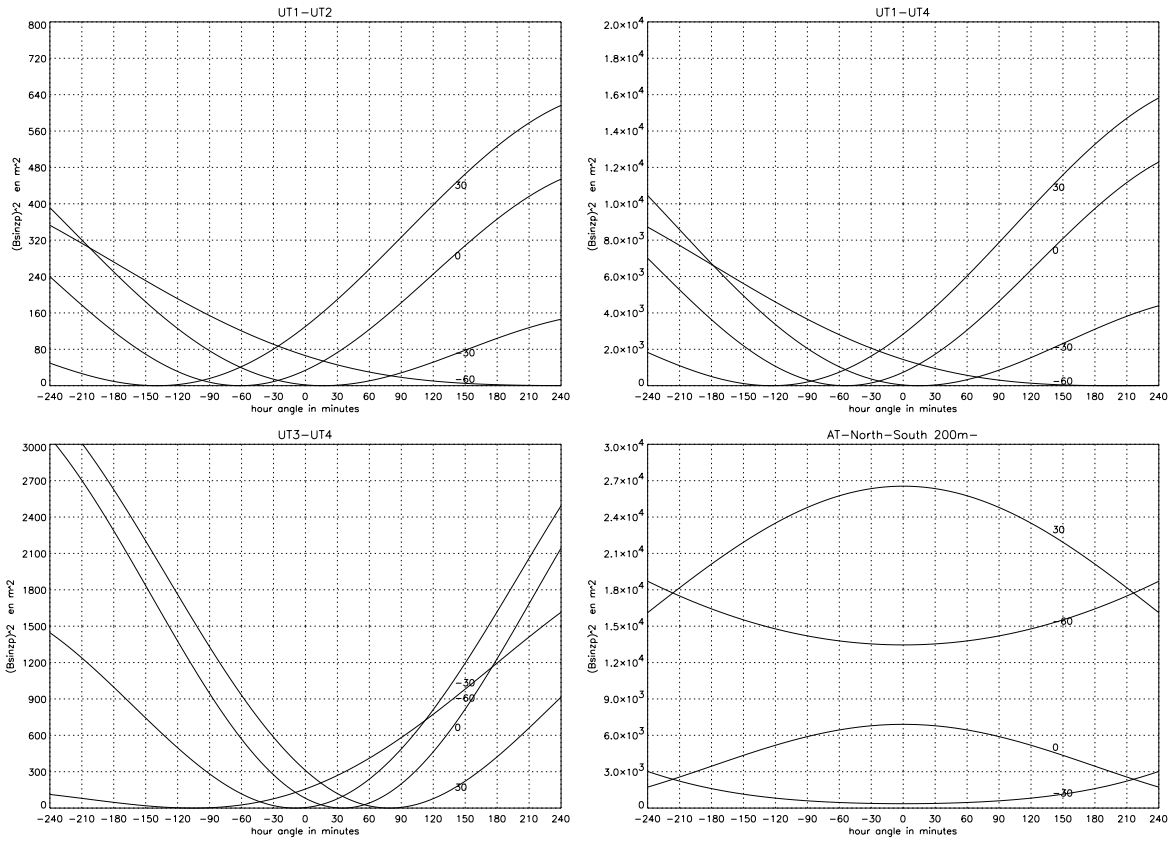

Figure 4.4: Variation of the square of $B \sin z_p$ with the hour angle for different baselines

UT1-UT2 (the first UT-baseline available):	$B = 56.6$ m	$\beta_B = 25.45°$
UT1-UT4 (the largest UT-baseline):	$B = 130$ m	$\beta_B = 59.8°$
UT3-UT4 (the more E-W UT-baseline):	$B = 62.5$ m	$\beta_B = 110.25°$
The largest AT-baseline available (North-South):	$B = 200$ m	$\beta_B = 0°$

The accessible zenithal distances imply that δ_o can vary from about $-84.5°$ to $+35.5°$. I arbitrarily have taken the values $-60°, -30°, 0°, +30°$.

In Fig. 4.3, J-band, and $\Delta\lambda = 0.25$ (Resolvance 5), we can read $\Delta V = 10^{-3}$ m^{-2}. In Fig. 4.4, for the UT1-UT2 baseline, for $\delta_0 = +30°$, at 1 hour after the transit, we can read that $(B \sin z_p)^2 \approx 260$ m^2.

So, the loss of visibility is 26%! During the 30 following minutes, it will increase from 6%. Even if this visibility loss is only a bias, well known and hence which we can take into account, it remains that the interferometric signal is for such cases seriously degraded and that a compensation would be necessary. Other example in this sense: for the whole H-band, the loss of visibility per air meter squared is about 10^{-4}; only for objects passing near the zenith at the transit-time (of δ_o between around $-24°$), and for observations 2 hours before or after the transit long, the visibility loss is less than 1%.

Fortunately, ΔV is rapidly decreasing with $\Delta\lambda$, this is a way to reduce the visibility loss expected for faint objects.

For K-band, and the highest resolution ($\Delta\lambda = .0002$ μm), ΔV/air m^2 $= 1.4\,10^{-18}$ m^{-2}. For the largest baseline, $\delta_0 = -60°$ and 4 hours after the transit-time ($(B \sin z_p)^2 \approx 1.8\ 10^4$ m^2), the loss of visibility is still negligible ($=2.10^{-10}$).

4.2.3 Conclusion

We see that the elongation due to the atmospheric refraction is of the order of 5, 1.8, 0.6 λ/D for the J, H and K bands respectively for the maximal zenithal angle (60°) on the UTs. The conclusion is that this effect is important for the J and H band. It will be nearly negligible for the K band. However, the effects between bands are still large. The adaptive optics system will give a direction at a given wavelength (the one used for image sensing in the lab). The angle between this latter direction and the actual direction at the observing wavelength will vary with time and will imply coupling degradations. We therefore concluded that an Atmospheric Refraction Compensator is needed before AMBER and actually before any instruments which operates at a different wavelength than the image sensor.

Concerning the atmospheric dispersion (cf. Fig. 4.3 and 4.4), its effect is rather negligible except at long baselines, at the H_α wavelength and at low spectral resolution. We recommend to use higher spectral resolution when the effect is no longer negligible since the dispersion decreases with $\Delta\lambda$. We still have to evaluate the impact on faint sources for which we do not wish to disperse the signal.

Some place should be left on the table to place these modules. However, it seems that ESO has already foreseen these compensators in its development plans (see chapter 5).

4.3 Polarization

The expected problems of instrumental polarization have been well identified in the AMB-REP-001 and AMB-REP-002 reports. They will come from a difference between the coatings of two interferometer arms and because of a variation the incident angle of the light on the mirrors.

4.3.1 Polarization control

Normally the VLTI concept is based on symmetric arms to avoid polarization problems. If one has a contrast decrease, one would like to compensate it with a Bravais compensator (with prisms or fibers). The polarization changes will be probably slow. Therefore we recommend to have a passive system which uses the instrument to maximize the instrumental contrast. There are no needs for an active system and a servo-loop. Of course the trade-off must be done between the throughput losses due to additional optics and contrast losses due to uncompensated polarization effects.

VLTI polarization

ESO has studied two different cases: with nominal coatings and with different coatings for UT1 and UT2 (optimized respectively for the IR and the UV!). Only the first case matches the error budget for the polarization, i.e. $\frac{\Delta V}{V} \leq 0.5\%$. There are uncertainties in computing the polarization state of the VLTI in the second case.

Differential aging effects have not been taken in account in the calculations.

Up to now, it seems that the coatings on UT1 and UT2 will be the same ones. A good trade-off could be to have the same coating for the two M3 mirrors which will influence the differential polarization evolution with time conversely to M1 and M2.

Analysis of the AMBER needs

The polarization effects of the VLTI can be separated in two categories:

1. The constant instrumental polarization
   It only induces a constant visibility loss. Whatever the coatings, it can be calibrated thanks to ellipsometric measurements, either in laboratory (which seems to be difficult given the sizes of the mirrors), or on standard polarimetric objects for various star positions. In this case, it implies a specific focal instrumentation (polarimeter).

2. The variable instrumental polarization with time
   This polarization variation with time can occur at a long scale (coatings aging) or at the observing scale (pointing movement). The former is calibrated during each observing run thanks to a polarimetric instrumentation. The latter can degrade the visibility accuracy if the calibrations are not repeated enough.

This section provides the polarization variations that are accepted to reach various visibility accuracies. For a given visibility accuracy ΔV, the following table provides the acceptable error on the flux balance I_1/I_2 and on the phase delay $\Phi_1 - \Phi_2$ between the two interferometric arms. Note that the results concern *only one visibility measurement.* Moreover only mere errors are considered. There are computed with the following equations:

$$V' = 2V\frac{\sqrt{I_1/I_2}}{1 + I_1/I_2} \tag{4.5}$$

$$V' = V\cos(\frac{\Phi_1 - \Phi_2}{2}) \tag{4.6}$$

$$\tag{4.7}$$

where V' denotes the measured visibility for a visibility V which is assumed to be equal to 1.

ΔV	Error on I_1/I_2	Error on $\Phi_1 - \Phi_2$	
10^{-2}	$\leq 32.8\%$	16.2 deg	or $\lambda/22$
10^{-3}	$\leq 9.4\%$	5.1 deg	or $\lambda/44$
10^{-4}	$\leq 2.9\%$	1.6 deg	or $\lambda/225$

Different strategies

The AMBER polarization should be small compared to the VLTI, but the VLTI polarization has a strong impact on the observing procedures. How fast will the polarization states will change within a night or even an hour? The system visibility changes will vary smoothly with time. It probably means that if we want to reach high precision visibility, we will have to switch from the source to a reference sufficiently often. However it is difficult to determine the frequency without input data.

The different strategies are listed below:

1. accept the polarization states as they are provided by the VLTI
2. select one polarization direction with a polarizer but we lose 1/2 of the light
3. use a Wollaston prism but we have losses of $1/\sqrt{2}$ of the light in addition to optical losses
4. use a Bravais prism which compensates the polarization defects but introduces losses and chromatic correction due the optical device

A possibility to compensate the polarization phase delay is to separate the two polarization states and work on them separately. This is a quick-and-dirty way to avoid polarization disturbance.

The solution chosen for AMBER is the solution number 2 if the contrast appears to be too small compared to the expectations because of the polarization.

4.3.2 Polarization measurements

The polarization measurements are not first priorities in AMBER (see chapter).

4.4 Coherence quality control

One aim of AMBER is to detect hot exoplanets (see chapter 2). The scientific requirements to detect 51 Peg companion is to measure visibility variations of the order of 10^{-4} due to different spatial frequencies. Therefore the visibility accuracy must be as accurate as 10^{-4}.

4.4.1 Spatial filter

The spatial filtering is a technique which allows to filter out the incoming signal, leaving only one mode (i.e. the flux in only one direction of one diffraction limited pattern). After a perfect filter, the signal depends ideally on two fluctuating parameters, the amplitude and the phase, and the shape of the output mode, which generally has a Gaussian shape.

The question of the choice between a stop made of a mechanical hole and a single-mode waveguide arose. We have therefore studied the effect of both devices on an incoming corrugated wavefront partially corrected by adaptive optics.

Quality of a hole as a spatial filter

The objective of simulations was to estimate the residual incoherent light that goes through a spatial filter which is a hole. To achieve this we used wavefronts computed at the output of an adaptive optics simulator (from the OSM simulator) and calculated the proportion of coherent light in a hole of radius ρ:

$$\eta(\rho) = \frac{I_c(\rho)}{I(\rho)} = \frac{|\int_{||\vec{r}||<\rho} A(\vec{r})e^{i\phi(\vec{r})}d\vec{r}|^2}{\int_{||\vec{r}||<\rho} |A(\vec{r})e^{i\phi(\vec{r})}|^2 d\vec{r}} \tag{4.8}$$

where $Ae^{i\phi}(\vec{r})$ is the complex electromagnetic field at any point $\vec{r}$ of the focal plane. $I(\rho)$ is the spatial integral of the intensity over the hole and I_c is the coherent intensity integrated over the hole.

The result for one particular wavefront is displayed on Fig. 4.5. The wavefront is representative of the sequence of wavefronts. The average Strehl ratio is about 0.4. Figure 4.6 represents in gray scale $\eta(\rho)$ for successive wavefronts (y-axis). Figure 4.7 displays the proportion of coherent light within of 0.75, 0.5 and 0.25 first zero radius. Finally Fig. 4.8 displays the standard deviation (on the time sequence) of the coherence versus the hole radius.

To summarize for a Strehl ratio between 0.35 and 0.5 obtained by optimizing the adaptive optics parameters corresponding to AMBER current design, a hole radius of half the first zero radius leads to coherence variation of the order of 2% peak to peak between 0.98 and almost 1. This corresponds to a standard deviation around 0.7%. It becomes 1.5%

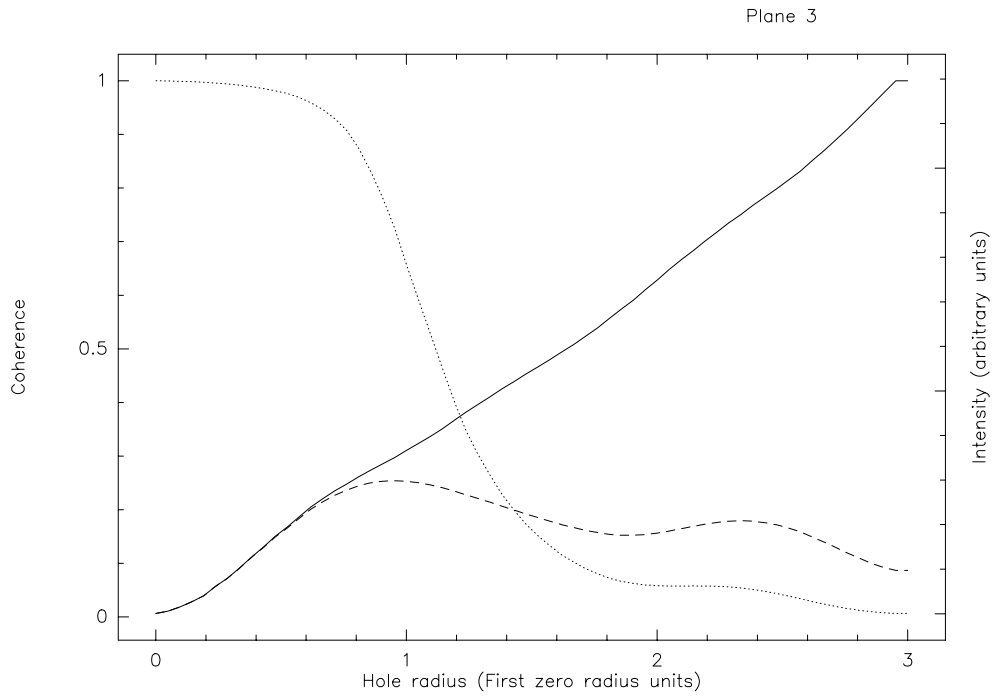

Figure 4.5: Intensity $I(\rho)$ from a particular wavefront integrated over a circular hole of radius ρ (solid line), coherent intensity $I_c(\rho)$ (dashed line) and proportion of coherent light in function of the radius ρ (dotted line). The radius is normalized to the radius of the first zero of the Airy function.

when the hole radius is 0.6 instead of 0.5. The hole radius needs therefore to be very small to achieve a coherence stability at the 1% level with these very optimistic assumptions.

Quality of an optical fiber as a spatial filter

Filtering The computation of the residual incoherent errors after filtering in a fiber is much more complex. However, work made by telecom people on single mode waveguides have shown that the beam is coherent after a propagation on a length of 1000λ, i.e. few millimeters.

Polarization However, optical fibers are very good sensors because they are very sensitive to the environmental context: temperature, pressure, mechanical constrains, etc. The main problem comes from the polarization behavior in the fibers. A way to prevent such effect is to used polarization-maintaining fibers. The core of these fibers are elliptic and have slow and fast axes on which the polarization is maintained (see Reynaud in AstroFib'96). Therefore for AMBER, this kind of fibers are required.

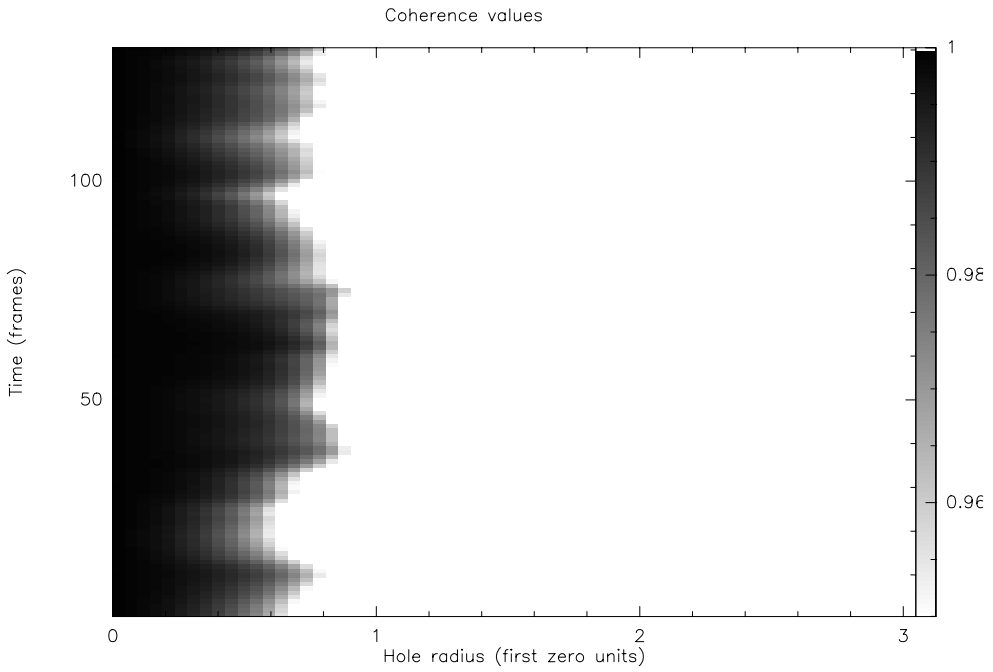

Figure 4.6: Proportion of coherent light in function of the radius ρ (x-axis) and time (y-axis). The radius is normalized to the radius of the first zero of the Airy function. Time between frames is 10 ms.

Transmission Silica fibers are cheap and have behaviors very well characterized at telecom wavelength. However their properties at $\lambda > 2$ μm are not so well understood. The transmission is determined below 2 μm. We have extrapolated the transmission of such fibers to the [2-2.4 μm] domain with a power law. The validity of such extrapolation must be checked but seems sensible.

The transmission curve of silica and the extrapolation is shown on Fig. 4.9. This leads to the following performance per meter of fiber:

Wavelength	$l = 1m$	$l = 2m$
2.4 μm	0.8	0.6
2.5 μm	0.6	0.4

Actual measures of the transmission is being done, but we do not have yet the results.

If the results are not satisfactory with the silica fibers in the K band, we plan to use fluoride glass fibers. They are more expensive and less well known, but their transmission is very good in this domain.

Optimum length and curvature radius It is difficult to compute, however experimental results can be used as reference. These numbers depends strongly on the fiber conditioning. By using liquid with a refractive index matched with the cladding, all the flux from the non-guided modes can be extracted. In these conditions, 10cm is sufficient.

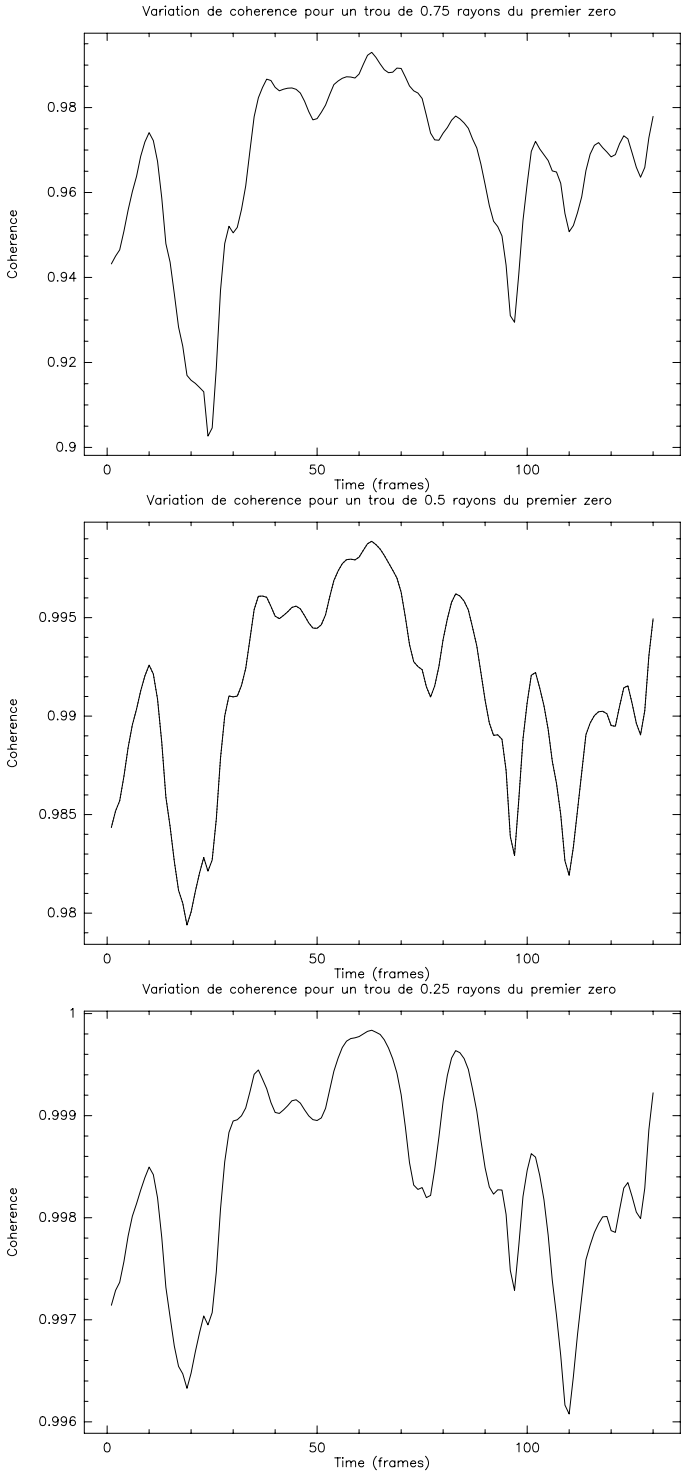

Figure 4.7: Proportion of coherent light in function of time for holes with 0.75 (top), 0.5 (middle) and 0.25 (bottom) first zero radius. Time between frames is 10-ms.

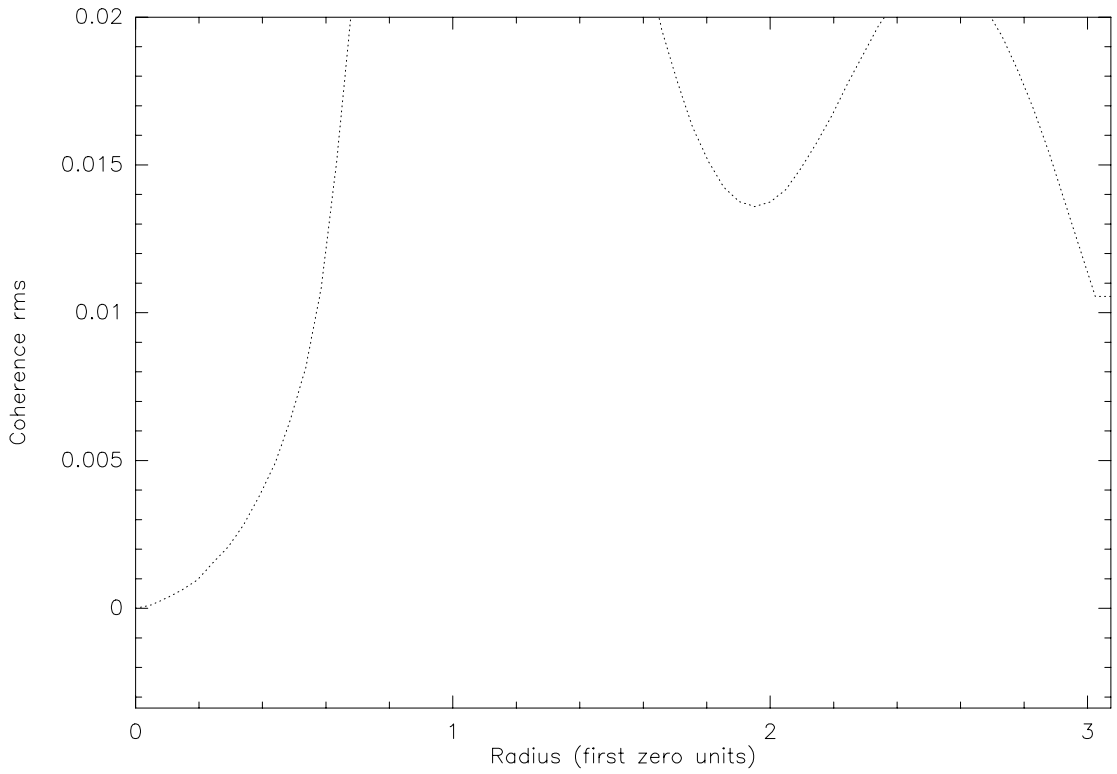

Figure 4.8: Coherence standard deviation computed on the time sequence versus hole radius in units of first zero radius.

The rejection rate could be better than 10^5 (100 dB). With no special care, 1 m of fiber is recommended.

Light scattering in the cladding will never be detected in the core.

The fiber curvature radius is an important parameter to filter the higher modes. The more curved the fiber is, the better the rejection. However it means also that the rejection will be stronger for side wavelengths. The results is then a worse wavelength transmission and a loss of photons. Conversely, the fiber offers a good adaptation with λ if there is no curvature.

4.4.2 Photometry calibration

When the signal is filtered out the output beam is 100% coherent, but the amplitude fluctuates because of the coupling in the fiber. On individual measurement, the visibility contains a term which depends on the level of intensity which is:

$$2\sqrt{I_1 I_2}/(I_1 + I_2). \tag{4.9}$$

By averaging the measures, one can reach rather visibility accuracy (Shaklan & Roddier 1992), but the atmospheric behavior is changing rather quickly and in a non predictive

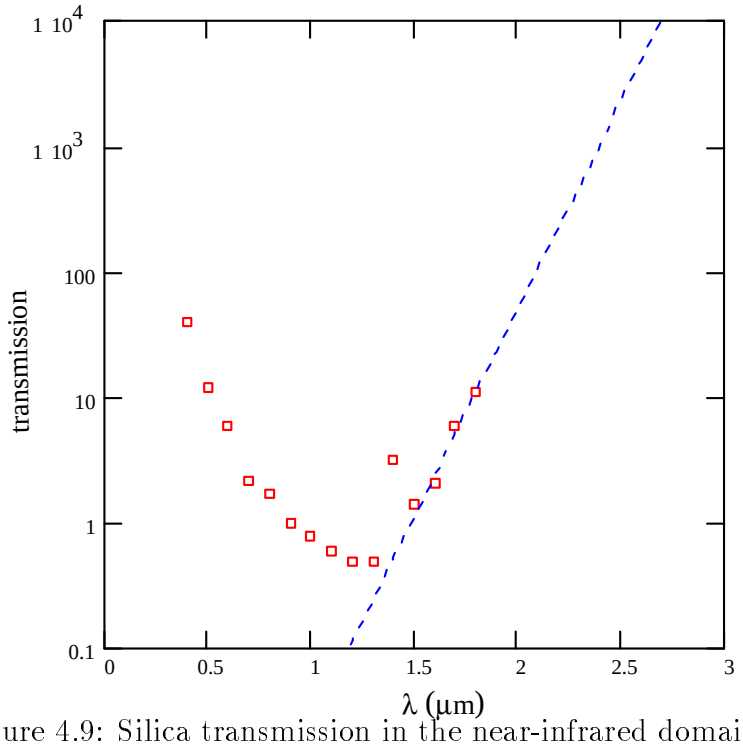

Figure 4.9: Silica transmission in the near-infrared domain.

manner. Therefore to reach an extremely good accuracy, one needs to monitor the photometric fluctuations of each beams (see FLUOR papers). This is done by picking up some flux from each beam. We call these beams the photometric beams, whereas we call the interfering beam the interferometry beam.

Ratio photometry/interferometry channels

A computation has been made to evaluate the best flux ratio between the photometry and interferometry channels (see memo AMB-IGR-004 for further details). Figure 4.10 shows the result of these calculation in one case (the photon noise regime). The ratio 0.65/0.35 is a good trade-off.

Spectral behavior and variation of the coupling

Turbulent coupling Using temporal wavefront provided by OSM ($D = 8$m, f_e=1 kHz, bright star, good seeing, 31 actuators AO) gives the coupling shown fig 4.11. Values before frame 50 (servo rising time) have not been averaged.

Coupling turbulent wavefronts in a fiber modifies the injection $\rho_\lambda = |\Omega_\lambda|^2$ but also the piston $\arg(\Omega_\lambda)$. All the Zernike modes of the incoming phase Φ with rotational symmetry can contribute to the injected piston. Therefore, piston in the fiber is the sum of the classical piston and defocus, spherical aberration, etc... The simulation clearly shows that

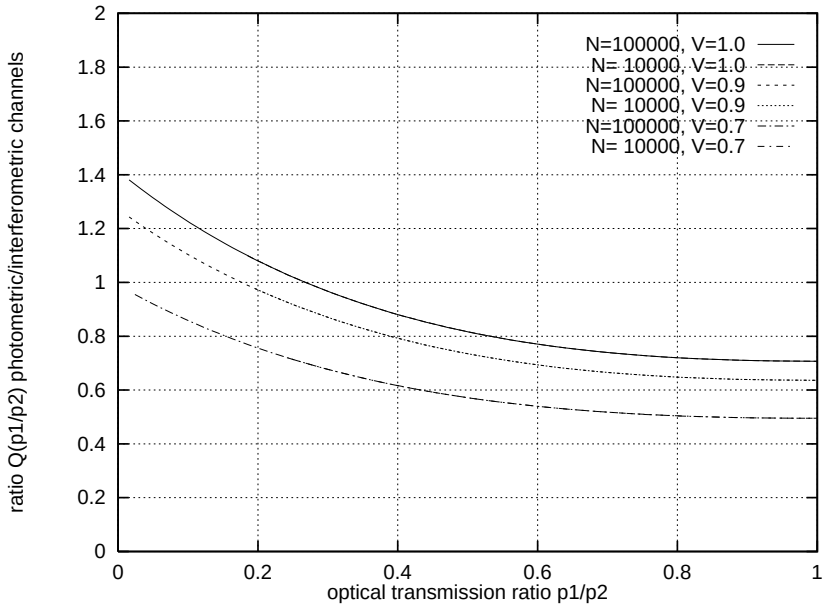

Figure 4.10: Photon noise regime (co-axial beam combination): The optimum photometric / interferometric ratio $Q(p_1/p_2)$ depending on the optical transmission ratio p_1/p_2 for different "true" visibilities. Only those values are plotted where the SNR in the photometric channels was high enough to avoid systematic visibility errors $> 10^{-2}$ and only those with $p_i\,(1-\alpha)\,\overline{N} > 2\sigma_d^2$ and an assumed detector noise of $\sigma_d = 20$ (Photon noise regime).

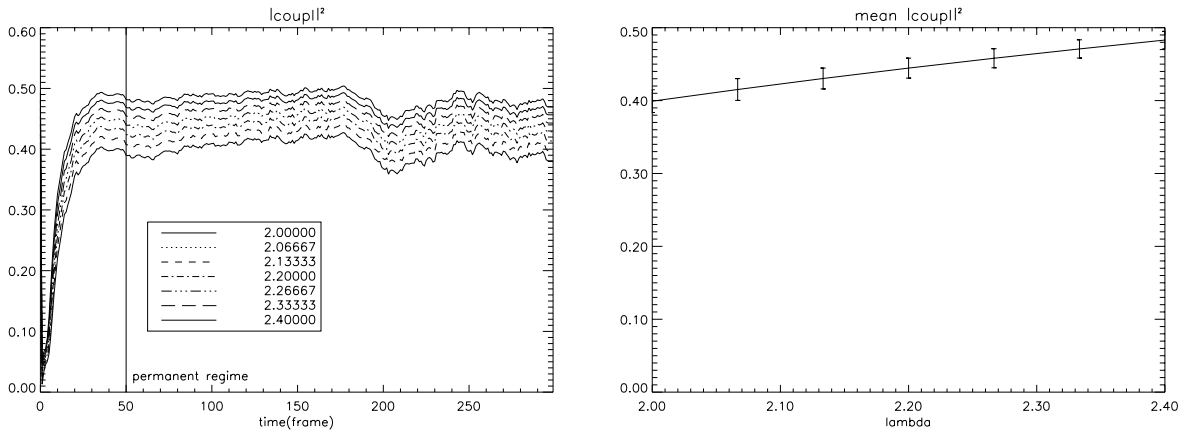

Figure 4.11: Turbulent coupling: temporal (left) and averaged (right).

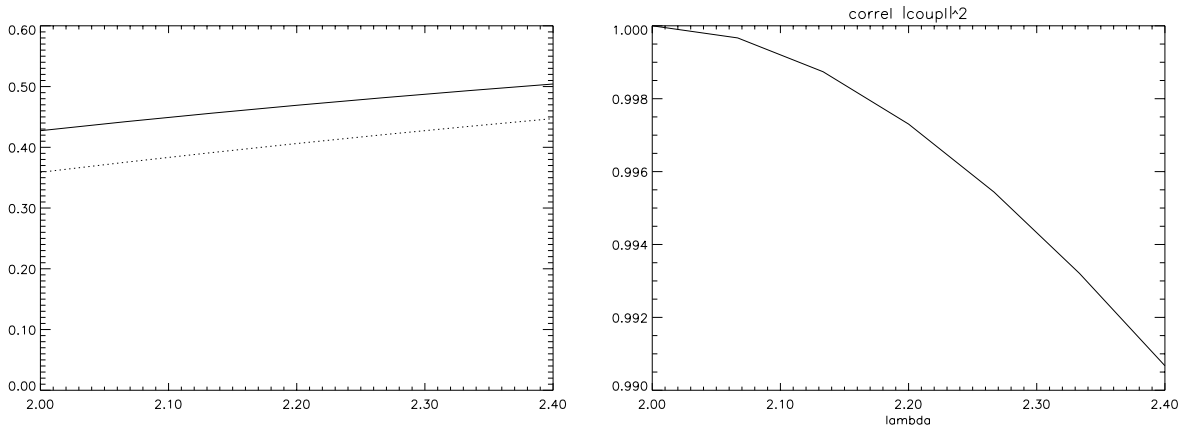

Figure 4.12: Chromatic evolution of the coupling for the 2 extrema frames (left) and mean correlation with λ_r=2.2 μm (right).

even if the piston is removed in the incoming turbulent wavefronts, the coupled piston is non null because of AO residuals.

Chromatic analysis Fig 4.12 shows the coupling the two frames corresponding to the extrema of fig 4.11. The chromatic dependence of ρ is quite linear. The departure from linearity can be computed with the following correlation, plotted fig 4.12 :

$$C(\lambda) = \frac{\left\langle \rho'_\lambda(t)\rho'_{\lambda_r}(t)\right\rangle}{\sqrt{\langle \rho'_\lambda(t)^2\rangle \left\langle \rho'_{\lambda_r}(t)^2\right\rangle}} \text{ where } \rho'_\lambda(t) = \rho_\lambda(t) - \langle\rho_\lambda(t)\rangle\,. \tag{4.10}$$

For the piston, since the atmospheric turbulence is achromatic in OPD, the amplitude of the Zernike coefficients coupled in the fiber is proportional to λ^{-1}, i.e. the same than the classical OPD. The piston coupled into the fiber cannot be distinguished from the classical piston. In fact, the spectral dependence of the coupled piston is not strictly linear, but departure is very low (correlation such as Eq. 4.10 for the piston is better than 99.96 % between λ_{min} and λ_{max}).

Conclusion We have conducted an analytical analysis and simulations to study the spectral behavior and the variation of the coupling of the light in the fibers (see memo AMB-IGR-004 and 005). The objective was to assess the behavior of the complex amplitude of the light $A = \rho e^{i\psi}$ after the coupling. Several conclusions can be drawn from this work:

- A, ρ, and ψ depends linearly on the wavelength λ. A 4 μmcore fiber, the spectral dependence of the coupling is rather small without aberrations. Usual core diameter are closer to 10 μmthan 4 μm. Therefore the spectral dependence should be very small.

- The amplitude ρ and the phase ψ result from the coupling of the Zernike modes because of the spatial filter.
- The piston ψ is affected by other Zernike polynomials than the first one. It depends at first order on the AO residuals.
- The amplitude ρ follows a second order dependence with respect to the AO residuals.

Therefore the spectral dependence of the coupling is deterministic and can be calibrated. The conclusion is that we do not have to disperse the photometric channels. However for safety reason, we recommend a low dispersion mode with ~ 10 spectral channels.

4.4.3 Phase calibration by field inversion

Measuring the variation of the fringe phase as a function of wavelength is of particular interest for several astrophysical programs. One of the most interesting and critical one is the detection of hot massive exoplanets where the value to be measured can be as small as 10^{-5} fringes. Preliminary *SNR* estimates show that for a 5-mag star this very ambitious result can be achieved in about 7 hours of observation if one is only affected by photon and detector noise. However this kind of accuracy requires an extremely good calibration and stability of the instrumental function. The measured function $\phi(\lambda)$ is the sum of the astrophysical information with an instrumental function:

$$\phi_{m+}(\lambda) = \phi_i(\lambda) + \phi_*(\lambda) \tag{4.11}$$

One way to calibrate the instrumental function is to inverse the field direction on each telescope. The astrophysical contribution is reversed while the instrumental function remains unchanged if the field inversion has been fast enough:

$$\phi_{m-}(\lambda) = \phi_i(\lambda) - \phi_*(\lambda) \tag{4.12}$$

One of the advantages of this method for the calibration of the phase variation is that it does not cost observing time. If the field inversion is common to several instruments it permits to measure accurately the variation of the phase between the instruments. AMBER would like the field inversion to be included in the VLTI facilities.

The simplest way to perform the field inversion would be to have a field compressor which switches from a Cassegrain set up (no field inversion) to a Gregory set up (field inversion) without changing the optical axes nor the compression ratio. If the beam compressor is an on-axis mounting this operation can be performed by moving only the divergent secondary (when you insert a divergent secondary in a Gregory set up you switch to a Cassegrain set up). If the field compressor is an off-axis device then the two mirrors must be moved in order to keep the optical axes in the same place. For an on axis beam compressor going from 80 mm to 18 mm whe will have an increase of the central obscuration resulting in a light loss of 3%. If the pupil plane is different from the plane of the obscuration produced by the beam compressor, the lattest will produce a field dependant vigneting whose effects have to be analysed. Doing the field inversion with an additional system would cost three more mirrors.

Table 4.1: OPD maximum RMS fluctuations

Baseline B	40	100	200
0.66" seeing (50%)	18	39	69
0.5" seeing (20%)	14	30	53

Table 4.2: OPD jitter in different time bins

Time length	10ms	100ms	1s	10s
B=40m	0.03	0.33	3.0	11
B=100m	0.04	0.37	3.5	18
B=200m	0.04	0.39	3.8	22

4.5 Optical path difference

There are different needs for an adjustable optical path difference:

- adjustment of the zero optical path difference between two incoming beams
- to scan the complete fringe coherent envelope
- to center the fringe packet on the white-light fringe

4.5.1 Zero OPD

The instrument will be designed in order to have an optical depth difference between two beams to be close to zero. However, like optical alignments are not always perfect, we expect to have to zero the OPD when we align the optics. The adjustment will be of the order of 1 mm. This can be achieved with a translation stage.

4.5.2 OPD modulation

The coherence length depends on the spectral resolution: $\lambda^2/\Delta\lambda$. The scan mode is foreseen only in broad band. With a broad-band filter, the resolution is of the order of 5, so the fringe packet will at maximum of 10 fringes, i.e. at max 25 μm. The scan speed is determined by the time spent on the fringes. One foresees to spend at maximum 10ms on one fringe in K, so the scan speed must be of the order of 250 μm/s and at maximum 1mm/s.

However, we must take into account the effect of the atmospheric piston in addition. The scan length will then be increased, but not the speed.

4.5.3 OPD centering

When the fringe tracker will not be available (at the beginning of the operation for example), we wish to have the possibility to center the fringe packet on the detector.

Atmospheric piston

Memo AMB-IGR-003 contains some details on the computation of the piston power spectrum. The OPD RMS variations in an infinite time length and point-like aperture with a Kolmogorov atmosphere are reported in microns in Table 4.1.

However, since the aperture are not point-like, the fluctuations are filtered out. The gain is small at most 2% for the UT with a 40-m baseline. This effect is therefore negligible. If the value of the outer scale of turbulence is finite, then the fluctuations can decrease. This effect can go from 30% up to 75%.

The fluctuations in a finite time bin are always smaller than the one given above. For the following values ($V = 10$m/s, $D = 8$m, $B = 40$m, $L_0 = \infty$, $r_0 = 0.19/0.26$m), one finds that the standard deviation of the differential piston in microns for 10ms, 100ms, 1s, 10s are reported in Table 4.2.

These numbers are similar to those used by ESO in its error budget. In conclusion, it seems that the length of the OPD scan should be smaller than 70 μm. This number is consistent with piston found on IOTA and PTI.

OPD centering in the dispersed fringe mode

When we operate AMBER in the dispersed fringe mode, the spectral resolution will always better or equal to approximatively 100. This means that the coherence length will be greater than 100λ. At 2.2 μm, the coherence length will be of the order of 200 μm. When looking at Table 4.2, we see that the atmospheric piston will never be greater than 22 μm. The fringe packet will never be at a distance greater than 10 fringes from the white-light fringe within 10s, and 2 fringes within 1s. Therefore one can specify a fringe centering algorithm working between 0.1 and 1Hz in order to center the fringes. The stroke will never be larger than 70 μm at maximum.

OPD scan efficiency in scan mode

In order to lose statically less than 10% of the scans, one needs to explore 4.8σ. Therefore a OPD scan of 300 μm would be recommended for the OPD scan device. However if AMBER or the VLTI provide a kind of fringe centering then this specification can be relaxed down to 50 μm.

4.5.4 How to perform OPD in AMBER

As we say previously, we will need to have an OPD adjustment in AMBER to obtain the zero OPD. This can be achieved with a translation stage, since no real-time motion is required.

In scan mode, we need modulate the OPD. The specifications are a maximum of 300 μm, with a speed between 250 μm/s and 1mm/s. This can be achieved by the VLTI delay lines. AMBER will request an OPD modulation of that type for a given time.

In dispersed fringe mode, the centering can be done within a frequency between 0.1 and 1Hz and on length lower than 22 μm. We must see if this must be done with a piezo or a simple translation stage.

If the fringe tracker is working, the numbers are even more relaxed.

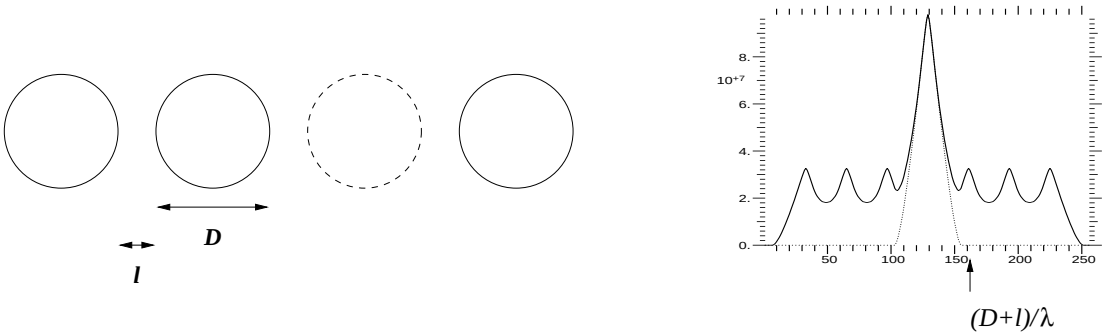

Figure 4.13: Sub-pupil location. Left, the sub-pupils have a diameter D and are separated by the distance l. Right, in the Fourier space, the fringe peaks are located respectively at $(D+l)/\lambda$, $3(D+l)/\lambda$ and $3(D+l)/\lambda$.

Table 4.3: Spacing between the sub-pupils in the different bands.

Wavelength coverage	λ_{eff}	$\Delta\lambda$	l/D
J	1.2	0.2	0.17
H	1.6	0.3	0.19
K	2.2	0.4	0.18

4.6 Beam combination

The beam combination is multi-axial using a non-redundant 1-D array. Therefore the fringes are coded on one direction and one can disperse in the other direction. The fringes are coded spatially and modulated by the impulse response of each beam. The beam exiting from the fiber has a Gaussian profile, therefore the modulation will be Gaussian. In fact the Gaussian will be truncated and the modulation will also be convolved to an Airy pattern.

Since we are operating AMBER in a non-monochromatic fashion, one needs to separate the sub-pupils in order to avoid a kind of cross-talk between the different baselines. The fringe peaks are located respectively at $(D+l)/\lambda$, $3(D+l)/\lambda$ and $3(D+l)/\lambda$ (see Fig. 4.13) for each wavelength. Because of the detector sampling, the power spectrum is multiplied by a "shah" function. At the central wavelength, the detector samples the maximum of the fringe peaks. For adjacent wavelength, it samples a part of the fringe peak. If we want to avoid contamination of one baseline by another wavelength, one needs to separate the sub-pupils by a length l so that $l/D = \Delta\lambda/\lambda$. Table 4.3 reports the values of l for broad band leading to a value of 0.2.

In order to reduce the number of pixels, we compress the beams in the direction perpendicular to the fringe coding. If x is the number of pixels per fringes at the highest spatial frequency, the compression factor is $(1 + l/D)xn$, where n is the number of sub-pupils

interval. With 2 beams $n = 1$, with 3 beams $n = 3$. Therefore with $x = 4$ pixels per fringes, the compression factor is 4.8 for 2 beams and 14.4 for 3 beams.

4.7 Spectral dispersion

4.7.1 Interferometry channels

For scientific reasons (see chapter 2), the requirements are: $\mathcal{R} \sim 5$, 70, 1000 and 10000. For operation at the highest resolution in the K band, the spectrograph must be cooled down to $-40°$C.

4.7.2 Photometry channels

The conclusions of paragraph 4.4.2 on fiber coupling shows that the dispersion of photometric channels does not need to be high. The requirements are $\mathcal{R} \sim 5$ and 70.

4.8 Detection

The performance of AMBER at the limiting magnitude is severely constrained by the read-out noise (see AMB-REP-001). In order to have the best performance, we decided to choose the best detector in terms of read-out noise at the time being. This detector is the HAWAII detector from Rockwell with a read-out noise less than 10 e^-. More details about the detector are given in section 6.4.

Concerning the optical requirement on the focus of the light on the detector, we are constrained to one pixel. As a matter of fact, if we consider the signal S_0 and the read-out noise r, then the ideal signal to noise ratio would be $\mathrm{SNR}_0 = S_0/r$ on one pixel. If a fraction f of the light is leaking on x pixels, then the signal to noise would be: $\mathrm{SNR}_1 = (1-f)S_0/r$ if we use only the brightest pixel and $\mathrm{SNR}_2 = S_0/\sqrt{xr^2}$ if we use all the x pixels. We see that $\mathrm{SNR}_1 > \mathrm{SNR}_2$ if $f > 1 - 1/\sqrt{x}$.

When $x = 2$, we see the SNR is better when taking into account only 1 pixel than 2, if f is smaller than 30%. Therefore the requirements is to concentrate the light one one pixel rather than spreading out the signal.

4.9 Acquisition modes

We have defined 5 different contexts for observations on AMBER sorted by order of importance, the first one being the most important or expected to be the most frequent context and the last one having the lowest priority (see also Table 3.2)

1. Dispersed fringes without fringe tracker on sources brighter than the magnitude limit.

Fringe coding: dispersed fringes

Fringe tracking: absent

Exposure time: short compared to the atmosphere turbulence

Fringes detected in individual exposure: yes

Dual feed: no relevant

Spatial filter: fiber

Spectral resolution: > 70

2. Dispersed fringes without fringe tracker on sources fainter than the magnitude limit.

   Same as case 1, except for:

   Fringes detected in individual exposure: no

3. Dispersed fringes with fringe tracker.

   Same as case 1, except for:

   Fringe tracking: present

   Exposure time: any

   Fringes detected in individual exposure: not necessary

   Dual feed: yes if the tracking source is off-axis

4. Scanned fringes without fringe tracker.

   Same as case 1, except for:

   Fringe coding: OPD temporal modulation

   Spectral resolution: low (wide-band)

5. Non-filtered mode.

   Same as case 1, except for:

   Spatial filter: removed

4.10 Data reduction

4.10.1 Visibility estimation

Generalization of the ABCD method

AMBER beam combination use a multi-axial scheme which spatially codes the interferometric information. The interferometric information is restricted to basically one fringe and

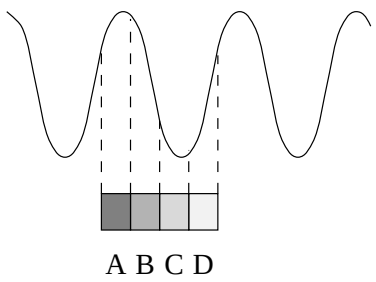

Figure 4.14: Representation of ABCD and a simple interferogram.

therefore that is why we have adapted the ABCD algorithm used in the coaxial scheme with a temporal coding. We recall here the basics of the ABCD algorithm in order to generalize it to the AMBER case.

In the coaxial combination scheme with two beams of equal intensity I_0, the interferometric signal $I(\delta)$ is given by:

$$I(\delta) = I_0 \left(1 + V \cos(\frac{2\pi}{\lambda}\delta + \Phi_0)\right) \tag{4.13}$$

where V is the visibility amplitude, δ is the optical path difference and Φ_0 is the sum of the object phase and the instrumental and atmospheric phase difference.

The ABCD algorithm is based on the measurement of interferogram flux during a scan of a quarter of wavelength (see Fig. 4.14). With 4 measurements (from A to D) we scan a complete fringe. Then we define the quadratures X and Y and the number of photons N as follows:

$$\begin{aligned} X &= A - C = \tfrac{\sqrt{2}}{\pi} NV \cos\phi \\ Y &= B - D = \tfrac{\sqrt{2}}{\pi} NV \sin\phi \\ N &= A + B + C + D. \end{aligned} \tag{4.14}$$

We obtain therefore an estimation of the square visibility:

$$V^2 = \frac{\pi^2}{2N^2}(X^2 + Y^2) \tag{4.15}$$

and the phase:

$$\phi = \arctan\frac{Y}{X} \tag{4.16}$$

For AMBER, we would like to generalize this simple scheme to the spatial coding of the fringes (see Fig. 4.15) where the fringes are modulated by a envelope.

Linear algebra

The intensity of the k-th pixel can be written:

$$i_k := \overline{N}\, p_1 \cdot a_k + \overline{N}\, p_2 \cdot b_k + \overline{N} \cdot 2\sqrt{p_1\, p_2} \cdot [V \cdot \cos\phi \cdot c_k - V \cdot \sin\phi \cdot d_k], \tag{4.17}$$

where

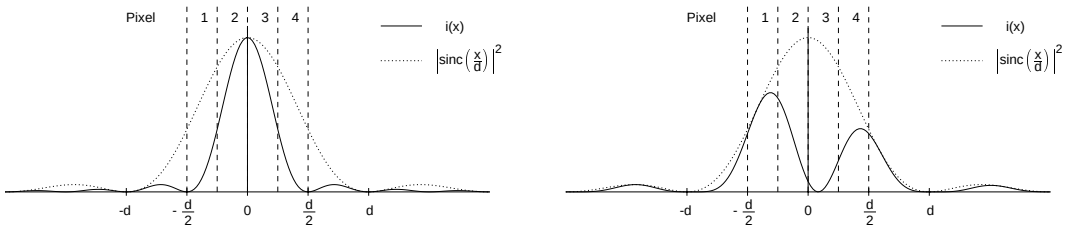

Figure 4.15: Two Amber interferograms sampled with 4 pixels and different phases: $\phi = 0^o$ (left) and $\phi = 150^o$ (right).

- $\overline{N}$ denotes the average number of photons in the interferometric channel,
- p_1 and p_2 are the transmission coefficients of apertures 1 and 2, respectively
- V is the object visibility, and
- Φ is the object Fourier phase plus atmospheric and instrumental phase.

and where a_k, b_k, c_k and d_k are coefficients which depends on the k-th pixel. Therefore, we can write Eq. 4.17 on the form of the multiplication of a M$\times$4-matrix A_{kj} with a vector of dimension 4 (where M is the number of interferometric pixels used to derive the fringe parameters):

$$A_{kj} \cdot x_j = i_k. \tag{4.18}$$

where the vector X is

$$X = (x_j) = \begin{cases} \overline{N} \cdot 2\sqrt{p_1\, p_2} \cdot V \cdot \cos\phi \\ \overline{N} \cdot 2\sqrt{p_1\, p_2} \cdot V \cdot \sin\phi \\ \overline{N}\, p_1 \\ \overline{N}\, p_2 \end{cases} \tag{4.19}$$

and the matrix A is a M$\times$4-matrix of coefficients $(c_k, -d_k, a_k, b_k)$.

In order to sample the interferogram with as few as possible pixels in order to minimize detector noise, the output pupils are located as close as possible. Such an interferogram cannot be evaluated directly in the Fourier plane. But the determination of the fringe parameters requires the knowledge of the coefficients c_k, d_k, a_k and b_k to solve the above system of linear equations.

The coefficients c_k, d_k, a_k and b_k have to be determined before or during the science measurement depending on their time stability (for example, the values of the coefficients depend strongly on the positions of the two Airy disks on the detector; hence also a good reason for the fibers as spatial filters). The measurement can be performed by illuminating the spatial filters, for example the fibers, with the same plane light wave. The input intensity at each fiber has not to be the same, but they should be approximately equal in order to have nearly equal quality measurements of the coefficients. We need to measure the

intensity distribution from each fiber separately in the image plane of the interferometric channel, and, the interference pattern with zero phase and 90° phase between the inputs.

The linear estimator is given by:

$$V \cdot e^{i\phi} = \left(\frac{x_1 + i \cdot x_2}{2\sqrt{x_3 x_4}} \right). \tag{4.20}$$

The quadratic estimator is given by:

$$|V|^2 = \left(\frac{< |x_1|^2 > + < |x_2|^2 >}{4 < x_3 x_4 >} \right) \tag{4.21}$$

However, this estimator is biased by the noise in each individual frames and therefore we should compute the biases coming from the photon-noise and the read-out noise in order to subtract them.

4.10.2 Data reduction steps

The permanent characteristics of AMBER are assumed to be known. For example the shape of the fiber field has been calibrated in the lab, or the transmissions are known.

The product of the observation is a set of intensities observed at a given time. These intensities contain:

- the dispersed fringes
- the photometric channels
- the calibrations

The final product is a set of calibrated visibilities independent of any instrumental effects indexed by the universal time and given with the associated uncertainties.

The following steps must be followed (see also Fig. 4.16):

1. Signal cleaning
2. Visibility estimation
3. Correction from instrumental effects
4. Averaged visibilities and uncertainty estimation
5. Calibrated visibilities and quality checks
6. Beam shape correction

Signal cleaning

The signal is cleaned from the detector characteristics: offset (sky), gain (flat-field), other. We obtain clean intensities.

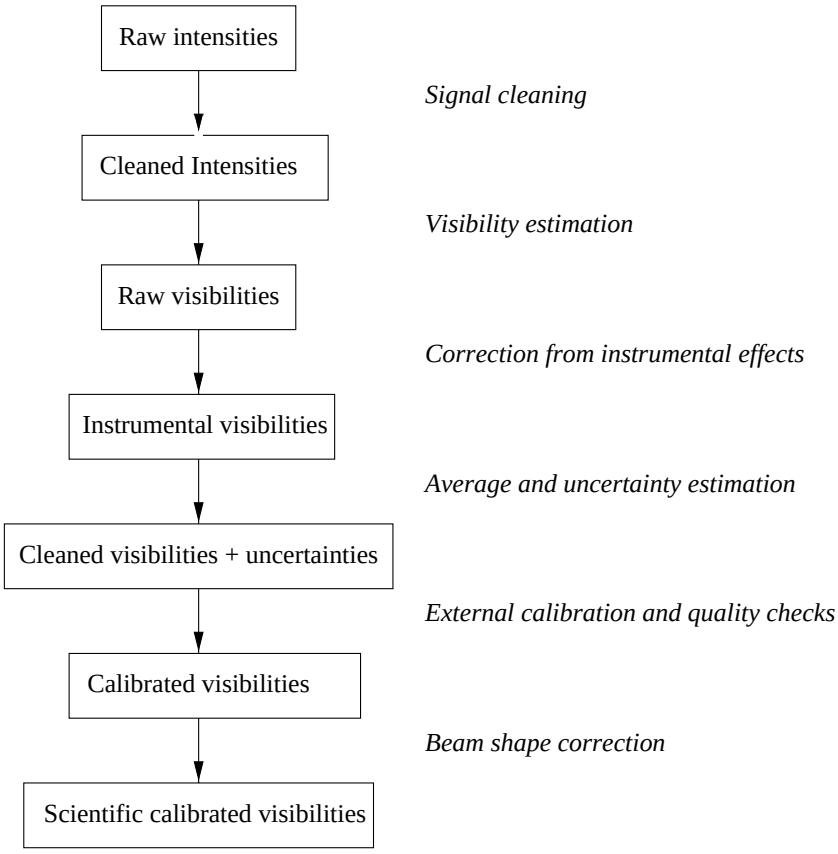

Figure 4.16: Data reduction steps

Visibility estimation

- visibility estimation through linear algebra (ABCD matrix):
  - linear estimator
  - quadratic estimator
- corrections from the photometry fluctuations
- Estimator biases for the quadratic estimator: correct from the biases due to the noise. For example, the signal from a non-coherent source (e.g. off fringes) will give a non-zero visibility.
  - read-out noise bias
  - photon-noise bias

We obtain raw visibilities.

Correction from instrumental effects

This step consists in correcting all the biases introduced by the instrument or the operating procedure.

Spectral calibration: corrects from the spectrograph answer

Jitter correction: corrects from the loss of contrast due to fringe jitter during the elementary exposure. A good criterium is the phase difference between two consecutive exposures.

Dispersion correction: corrects from the dispersion within a spectral channel.

Polarization correction: if we have a good model of the polarization within the VLTI. The correction is function of the angle of incidence on the optics.

OPD shift correction: To correct the visibilities of fringes which are not well centered. The criterium is the estimated phase shift.

We obtain therefore visibilities as much as possible independent from the instrumental effects. We also derive the associate internal errors

Averaged visibilities and uncertainty estimation

We group the visibilities by time bins in order to estimate averaged visibilities. We compute the associated uncertainty. To estimate this uncertainty, one way is to compute histograms and compute the full width at half maximum. If the histogram is non-Gaussian then the statistical bootstrapping technique can be used. Comparison with the internal error computation is useful to understand the instrumental effects.

Calibrated visibilities and quality checks

However we have not corrected from possible remaining constant contrast losses. To estimate the instrumental contrast, we correct the calibrator visibilities from their intrinsic visibility (for partially resolved objects). Then we fit a polynom of low order to the instrumental transfer measurements in function of time. This leads to the estimation of the instrumental transfer function for each object measurement and therefore to the calibrated visibility and the associated error.

Few quality checks can be performed to estimate the quality of the data:

- visibilities vs. Strehl ratios of the AOs
- visibilities vs. source fluxes
- visibilities vs. source flux uncertainties
- etc...

At the end we obtained calibrated visibilities with associated errors.

Beam shape correction

However the measured visibilities correspond to the average of the *true* visibility over the spatial frequency domain covered by the interferometer. For objects partially resolved by one of the telescope (size greater than the beam size), we must correct from this. We need to estimate the beam shape and to measure a map at the resolution of the telescope.

A map obtained by NAOS, the adaptive optics system at the focus of UT1, will be able to give informations on the spatial distribution of the object at the resolution of individual apertures[1] and might be useful in this *deconvolution* process.

4.10.3 Simulations

Figures 4.17 to 4.19 show preliminary applications of the above fringe parameter estimators to simple simulated AMBER interferograms. The projected interferograms for each spectral channel were generated from two 1-dimensional rectangles as telescope apertures touching each other in the output pupil plane (interferograms similar to those of Fig. 4.15). The object visibility was set to $V = 1$. The ratio between photometric and interferometric channel, i.e. photometric/interferometric, was set to 0.3 and one fringe in the interferogram was sampled with 6 pixels. An equally distributed differential piston and varying intensity at the output of the spatial filter (fiber) was simulated. Different photon noise and readout noise of $20e^-$ was introduced to the interferograms.

The bias-free visibility was estimated with the linear and quadratic estimator as described in section 4.10. Figure 4.17 shows simulated AMBER interferograms with readout noise of $20e^-$ and photon noise of N = 100 000, 25 000, 8000 and 4000 photons. Figure 4.18 shows the bias-free visibilities reconstructed with the linear estimator for 160 different interferogram realizations.

For comparison of the linear and quadratic estimator, Fig. 4.19 shows the reconstructed bias-free visibilities for each of 10 spectral channels over the K band (here the differential piston was simulated as statistically independent between the spectral channels which is not realistic, of course, but is useful in order to see the noise for the quadratic estimator). The results of the quadratic estimator are the averages over 160 interferograms, whereas the results of the linear estimator are direct from 1 interferogram. The standard deviation of the visibility reconstructed by the linear estimator is close to the theoretical predictions plotted in Fig. 4.20.

4.11 Observing procedures

For the standard acquisition mode the following steps will be followed during the observing procedure. We assume that AMBER is already aligned.

[1] We can also removed the spatial filter and use the AMBER detector.

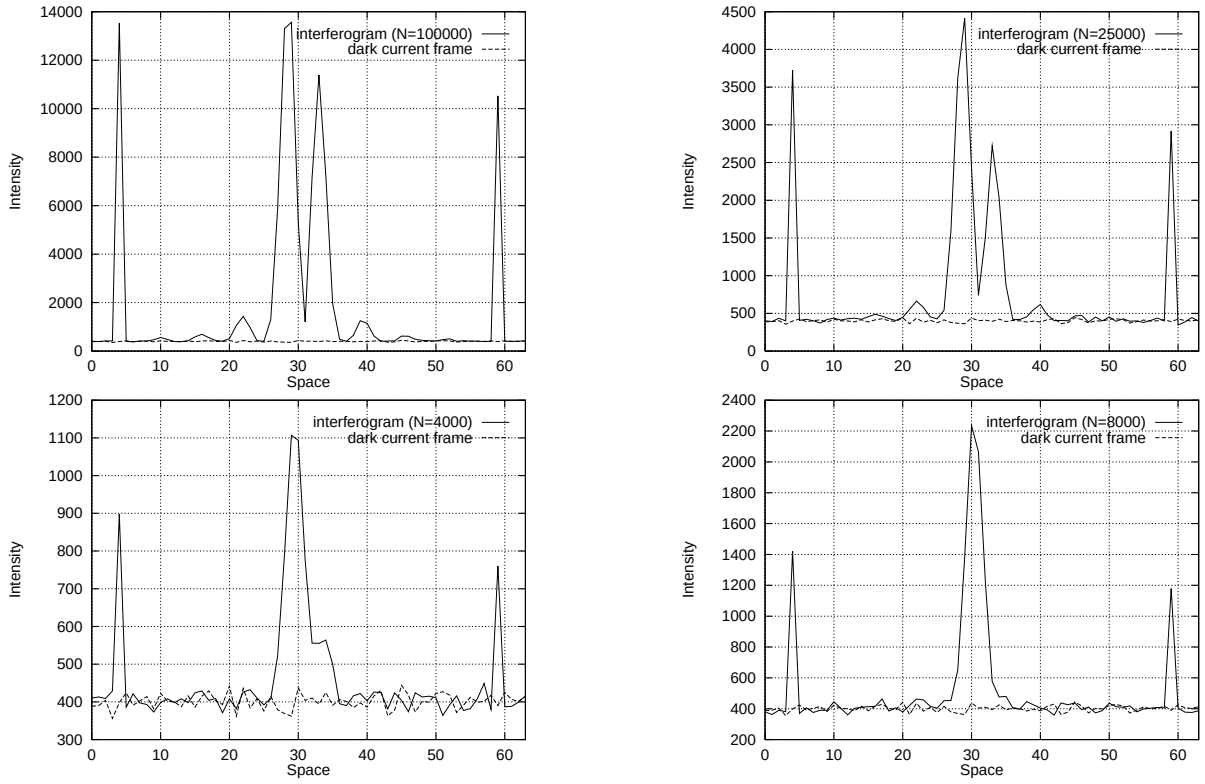

Figure 4.17: Two-beam-AMBER interferograms with sampling of 6 pixels/fringe at different photon noise and a readout noise of $20e^-$ (object visibility V=1, photometric beams at pixels 5 and 60, intensity ratio photometric/interferometric channel = 0.3).

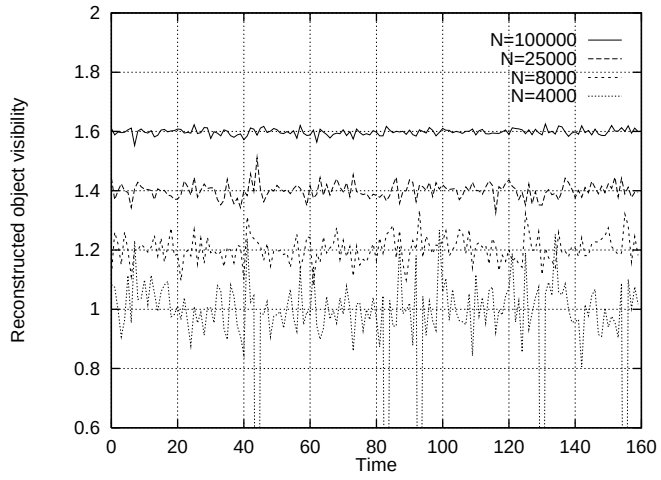

Figure 4.18: Reconstructed visibilities (original V=1.0) with the linear estimator from 160 different interferogram realizations (the y-axis numbers 1.6, 1.4, 1.2 and 1.0 correspond to visibility value 1.0).

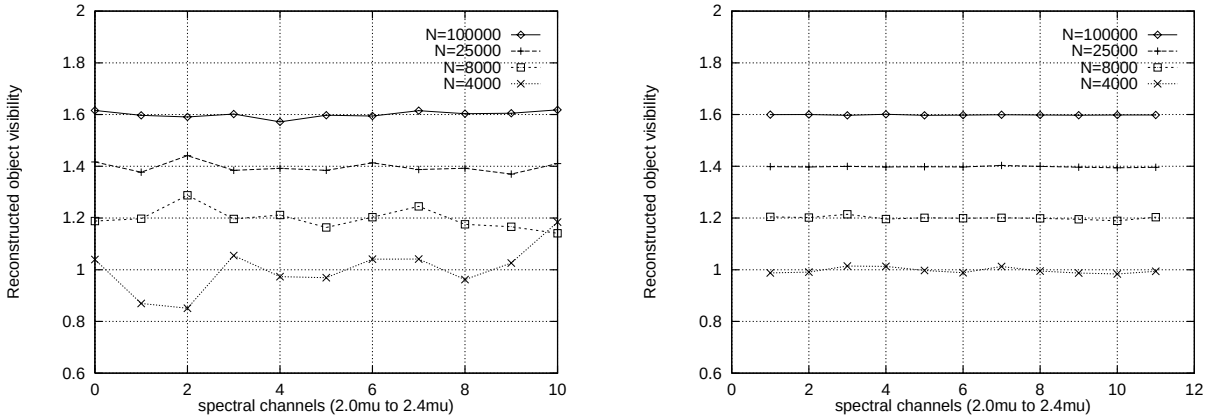

Figure 4.19: Visibilities (original V=1.0) reconstructed by the linear (left) and quadratic (right) estimator (the y-axis numbers 1.6, 1.4, 1.2 and 1.0 correspond to visibility value 1.0). Details are given in the text.

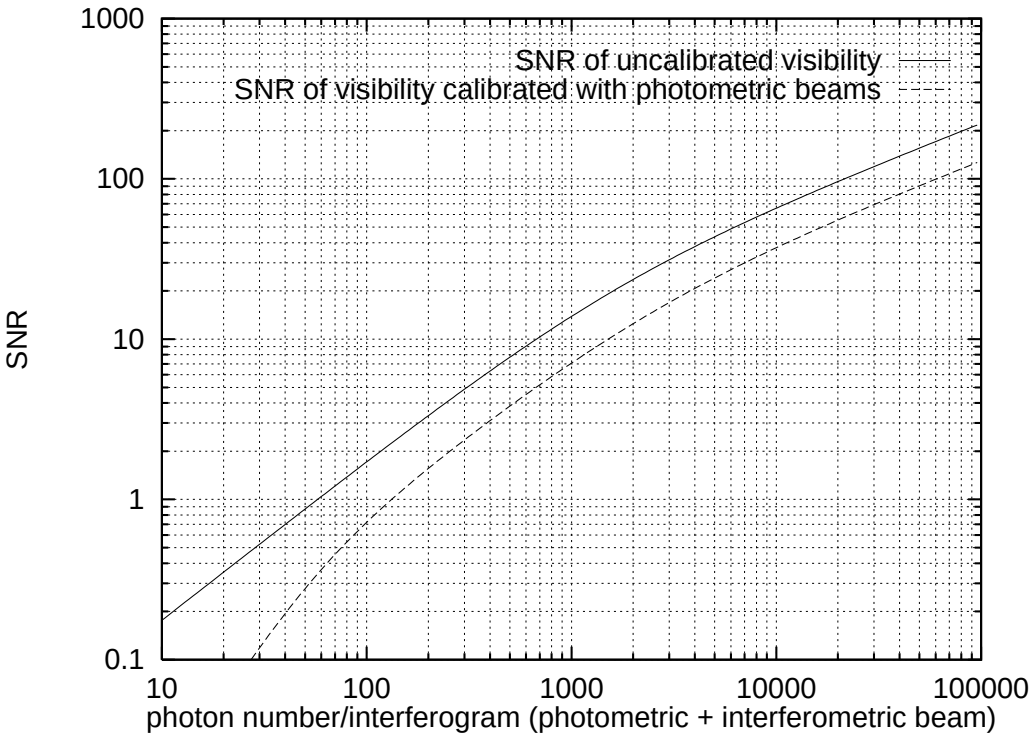

Figure 4.20: SNR of the visibility derived from two-beam-AMBER interferograms with and without photometric calibration. Readout noise of $20e^-$ and an unresolved star were assumed. The intensity ratio photometric/interferometric beam was assumed to be 0.7 (i.e. optimum in the photon noise regime for nearly unresolved objects). The optical transmission ratio (i.e. between the two spatial filters) was assumed to be ideal, i.e. 1.

4.11.1 Initial alignment at the beginning of the night

We initialize the VLTI with the parameters relevant to AMBER, check the VLTI alignment, move every AMBER devices to `HOME` position, check AMBER internal alignment, co-alignment between AMBER and VLTI and that the VLTI reference light arrives to AMBER detector.

4.11.2 Initial calibration for a given configuration

Instrument configuration set-up

We set up the band of observation (J, H, or K), the spectral resolution and the central wavelength (when needed at high spectral resolution).

AMBER instrument calibration

- Detector: bias, read-out noise, ADU/e^- conversion factor
- For each beam (other beams occulted by shutters): dark current (no light on), gain at low spectral resolution (with black-body source on), gain at high spectral resolution (with white light source on)
- move the OPD compensator to match the zero OPD using internal fringes. The source is a white light source which serves as a reference for ZOPD for all VLTI instruments (TBC).
- calibrate the fringe estimator matrix (cf. section 4.10) with the same white light source:
  - For each beam (other ones are stopped): background (light off) and foreground (light on) measures.
  - For each pair of beam (other ones are stopped): fringe measures at about zero phase and 90 degree phase.
- Spectral dispersion calibration: wavelength / pixel calibration (spectral lamps on or Fabry-Perot)

4.11.3 Observing cycle

Description of the cycle:

1. Check fringes on a known star with an acquisition
2. Observation set-up
3. Object/calibrator cycle #1:

   (a) Calibrator #1 cycle
   (b) Object cycle
   (c) Calibrator #1 cycle
   (d) Object cycle

4. Object/calibrator cycle #2:
   (a) Calibrator #2 cycle
   (b) Object cycle
   (c) Calibrator #2 cycle
   (d) Object cycle

5. etc ...

6. Final calibrations

The following sections give further details on the different steps.

Acquisition

We set the exposure time, get the star coordinates, point the VLTI (telescopes and delay-lines), request to close the servo-loop of the VLTI AO, point AMBER (e.g. move the ARC to the corresponding position), optimize the signal on the detector (injection in fibers), search for fringes, move the delay lines to center the fringes and enter in the centering loop.

Observation set-up

We set the neutral density (needed if bright star to avoid saturation), the integration time (number of elementary exposures) on source and for sky, the frequency of source cycle (source/sky) and the frequency of object/calibrator cycle .

Source cycle

The source cycle is aimed either for the object cycle or the calibrator cycle.

1. background calibrations: measure the background during the transition object – reference star (dark and sky).

2. object: search for fringes, enter the centering mode, and get N exposures (or up to final integration time).

4.11.4 Data reduction

The data reduction steps are detailed in section 4.10.

4.12 Observing in other ontexts

In other contexts, the observing procedure is changed according to the following steps.

4.12.1 No fringes detected in individual frames

We group the individual frames in blocks of M frames. We used the quadratic estimator to compute the visibility and phase of fringes over a block. The same number of frames must be used in the blocks of the calibrators even if we detect fringes in individual frames. The centering is made after completion of each block and no longer at the frame level (section 4.11.3) .

4.12.2 Fringe tracking

We do not separate fringe tracking on-axis and off-axis except that in the last case, we need to enter the off-axis reference coordinates in the initial observation set-up. We use also the concept of elementary exposures (frames) which are limited in time by the detector saturation. Concerning the data reduction, one can use either the linear estimator or the quadratic estimator, depending on the quality of the fringe tracking during a frame.

We center the fringes by using the AMBER internal OPD compensator, since the delay lines are linked to the fringe sensor unit. This OPD compensator must also correct from the OPD due to the differential dispersion between the two different operating wavelengths of AMBER and the fringe tracker (if any).

The data reduction must incorporate additional corrections computed from the residual errors given by the fringe sensor and from the offset command sent to the delay lines.

4.12.3 Scanned fringes

This is similar to the FLUOR mode. All procedures will be adapted from the FLUOR observing procedures and data reduction programs.

Chapter 5

VLTI interfaces

This chapter is a review of the environment information needed by AMBER as well as the interfaces with the VLTI which have to be discussed with ESO. It is particularly important to freeze the optical interfaces rapidly to clear the way for the AMBER design.

In addition some AMBER requirements are common to others instruments and we propose that some devices are included in the VLTI facilities. Within this context, AMBER requirements are specified.

5.1 Environment

- Operation temperature in the focal lab: 15.0° ± 0.1°
- Spatial temperature homogeneity: $\Delta T \leq 0.22$°C PTV
- Diurnal temperature variation : $\Delta T \leq 0.02$°C PTV
- Vertical temperature gradient : $\Delta T / \Delta z \leq$ -0.04/+0.00°C/m
- Humidity: ♠ **(TBD ESO)**
- Altitude: ♠ **(TBD ESO)**
- Sismicity: there are frequent micro-seismic events which affect the fringe contrast. The recorded data must be flagged with information coming from a seismic monitor. Frequency and format: ♠ **(TBD ESO)**

5.2 Infrastructures

The infrastructures interfaces concern the interactions between AMBER and the VLTI lab. They include:

- Laboratory space: 7 x 20 m^2
- Access means: 2.4 x 2.9 m^2 (exception: 6 x 3 m^2)
- Overhead crane in lab: 5 Tons capacity

- Integration room available next to the lab
- 4 SCP connections available with:
  - 400 V, 3-phases, 50 Hz
  - 230 V UPS, 50 Hz
  - Liquid cooling (5 kW each)
  - Compressed air
  - LAN, time bus
  - Fast link
- Electromagnetic environment: ♠ **(TBD ESO)**
- Nitrogen and vacuum equipment availability: ♠ **(TBD ESO)**
- AMBER heating: ESO must define the dissipation tolerated in the focal lab ♠ **(TBD ESO)**. AMBER will modelize the heating levels and cycles compatible with the 10^{-3} requirement on visibility accuracy

5.3 Optical interfaces

They include optical interfaces (beam size, position, ...) as well as the requirements of some modules eventually provided by ESO.

5.3.1 Input beams

Characteristics

- Absolute position / AMBER table: ♠ **(TBD AMBER/ESO)**
- Space between two beams : 100 mm is the minimum set by ESO. Actual spacing is ♠ **(TBD AMBER/ESO)**
- Optical axis:
  - 1 140 mm from the lab floor
  - ♠ **(TBD AMBER/ESO)** from the table top
- Diameter: 18 mm

Beams compressor

A compression of the 80 mm incoming beam is mandatory for AMBER. The 18 mm beam proposed by ESO and accepted by MIDI is acceptable for AMBER although it might complicate the field inversion device (see below). We think that removable beams compressors

Table 5.1: Summary of input beam characteristics

Type of aperture	Beam diameter		Use of beam compressor
	Delay lines	Instrument	
Siderostats	80 mm	18 mm	X
UTs	80 mm	18 mm	X
ATs w/o BE[1] (AMBER)	18 mm	18 mm	
ATs w BE[1] (MIDI)	80 mm	18 mm	X

BE: beam expander which expands the AT beams from 18 mm to 80 mm

at the VLTI lab entrance (i.e. common to all the instruments) are the preferable solutions ♠ **(TBD ESO)**.

Note that with ATs and AMBER adaptive optics, AMBER needs to expand the beams from 18 mm to 55 mm (for the bimorph mirror) and then to compress the beams from 55 mm to 18 mm. These functions will be realized by AMBER but space has to be foreseen for that.

Field inversion

The requirements are:

- Applied only to the science beam. The sensors on the reference beam do not see it
- Removable (if not included in the beam compressor)
- Pupil position: in the plane where the Gregory mirror of the beam compressor intercepts the incoming beam.
- Inversion frequency: f $\leq$ 0.016 Hz
- Inversion duration: $\leq$ 1 s
- OPD variation at inversion: $\leq$ 1 μm ♠ **(TBC AMBER)**
- stability of OPD variation at inversion: if there are variations of the OPD at each field inversion, the final result will be affected by the difference between the total OPD drift for all "field up" measures and the total OPD drift for all "field down" measures. It should be easy to remove this in the data processing if this OPD drift difference is smaller than a fringe at the shortest wavelength. This yields:
- OPD drift difference: 1 μm ♠ **(TBD AMBER)**

Beam extraction

All the sensors are on the reference beams. If there is a reference star, all the scientific flux is used by the instrument, else half of the flux is used for the sensors (this separation is included in the "star separator" in the telescope).

The spectral ranges used by AMBER depend on the instrument configuration.

1. Phase 1: AMBER with the UTs: K, H and J bands
2. Phase 2: AMBER with the ATs:
   (a) AMBER must receive the R, I, J, H, K, L, M bands
   (b) Wavefront sensor in the focal lab fed by the visible but a band around H_α or by 50% of the visible. It would be efficient if this wavefront sensor also serves for the image sensing for tip-tilt correction

5.3.2 Beam quality

Guiding

- Guiding: $\pm$ 0.015" pour V=20 (K0 type)

Pointing

- Slewing time $\leq$ 3 minutes to point anywhere in the sky coverage.
- Pointing time for a 5 degrees angular movement (the nearest bright reference star): $\leq$ 1 minute♠ **(TBC ESO)**

Wave Front Error (WFE)

- WFE for each beam: 40 nm RMS
- Differential WFE between two beams:
  - UT: 170 nm RMS
  - AT: 160 nm RMS

Jitter

- Internal OPD stability for any pair of beams:
  - blind mode: 106 nm @ 2.2 μm with an exposure time of 48 ms
  - Fringe tracking mode: $\leq$ 70 nm RMS over 3 minutes

Adaptive Optics

- Strehl ratio: ♠ **(TBD ESO)**
- Piston generated by the bimorph mirror: by nature a bimorph mirror supported on three fixed points introduces a piston. After a calibration, it should be possible to compute this piston from the commands applied to the mirror and to compensate for it in the OPD controler. Therefore the VLTI needs:

- Fast Link between the wavefront sensor computer and the OPD controler. ♠ **(TBD AMBER and ESO)**

Polarization

The VLTI error budget assumes a visibility loss less than 0.5% for $\lambda \geq 1$ μm due to polarization effects of the Coudé trains (excluding dichroics).

This implies that at least all the M3 mirrors have the same coatings.

- Polarization state: ♠ **(TBD ESO)**

Atmospheric refraction

An atmospheric refraction correction is required for AMBER in the spectral bands from R (around Hα) to H (and perhaps K - ♠ **(TBC AMBER)**). In addition, an inter-bands correction is mandatory:

- between the tip-tilt sensor and the instruments
- inside AMBER if observations at simultaneous spectral bands are foreseen

Thus we propose a general removable corrector for atmospheric refraction provided by ESO and working from the R to the K bands (it should then correct also the refraction between the image sensor and MIDI ♠ **(TBD ESO)**. AMBER can help defining its specifications ♠ **(TBD AMBER)**.

Atmospheric dispersion

AMBER needs an inter-bands atmospheric dispersion correction only. This function is included in the AMBER OPD controller.

5.3.3 Field rotation

For AMBER such a device could have some use only for the non filtered mode with spectral dispersion. We have decided that such a mode has the lowest priority. If for other reasons a field rotator is present at the telescope level, it would very efficiently ensure the field inversion function if the field rotation can be performed in seconds.

5.3.4 Pupils

- Pupil longitudinal position:
  - in the inversion plane if any
  - in the ATs adaptive optics plane if any
- Pupil longitudinal stability: $\pm$ 15 cm

- Lateral pupil jitter:
  - 20 μm RMS in 100 ms
  - 100 μm RMS in 1 s
  - 250 μm RMS in 10 s
  - 400 μm RMS in 30 minutes

5.3.5 Optical path difference

Delay lines

- Stroke: 60 m
- Operation: in air @ 15°C
- Accuracy:
  - $\pm$ 50 μm for 60 m
  - $\pm$ 1 μm for 3 m
- Guidance accuracy:
  - $\pm$ 1 750 μm for 60 m
  - $\pm$ 250 μm for 3 m
- Mechanical speed: $\pm$ 5 000 mm/s or 0.5 μm/s **???**
- Spectral band: optimized for [1 - 20] μm
- Modes: blind and fringe tracking
- OPD jitters:
  - 14 nm RMS in 10 ms @ visible wavelengths
  - 50 nm RMS in 50 ms @ near-infrared wavelengths
  - 225 nm RMS in 300 ms @ infrared wavelengths
- OPD resolution: $\leq$ 20 nm RMS
- WFE (without tilt): 40 nm RMS
- Tilt: 1.5"
- Input for FSU/OPD controller in fringe tracking loop
- Dual feed for phase referencing/astrometry facility
- Field of view on the sky: $\geq$ 2" (i.e. 300" instrumental field of view)

OPD scan

AMBER foresees to use the VLTI delay lines for scanning the fringes. ♠ **(TBD ESO)**. The scan law has to be defined. A typical requirement will be triangle functions with:

- stroke: 300 μm
- speed: 500 μm/s
- linearity: linearity defects smaller than the atmospheric piston

♠ **(TBD AMBER)**.

5.3.6 Fringe tracking

- Tracking accuracy: 33 nm RMS
- Poor fringe tracking: ♠ **(TBD ESO)**

5.3.7 PRIMA

- Beams separation: ♠ **(TBD ESO)**
- Residual aberrations: ♠ **(TBD ESO)**
- Residual OPD: ♠ **(TBD ESO)**

5.3.8 Simultaneous observations with MIDI

5.4 Mechanical interfaces

They define the hardware interface between the VLTI lab and the AMBER instrumentation whose mechanical specifications are:

- AMBER table provide by ♠ **(TBD ESO)**
- AMBER dimensions: ♠ **(TBD ESO)**
- AMBER weight: ♠ **(TBD ESO)**

5.5 Software interfaces

They concerns:

- Commands from AMBER to VLTI
- Warning signals from VLTI to AMBER
- Informations of the VLTI data base (VLTICS) to AMBER

The software interfaces includes :

- List of commands
- Commands parameters
- Exchanged data (returned values and error codes)
- Data format

AMBER will need the following environmental data from:

- seeing monitor
- weather station
- wavefront sensor
- seismic monitor

Chapter 6

Optical bench

This chapter describes the optical set-up of the experiment and gives additional elements about the spectrograph and the detector

6.1 Beam quality control

This describes all operations affecting each individual beam before the beam combiner:

- Beam inputs
- Polarization filter
- Spectral band separation
- Atmospheric refraction compensators
- Dispersion compensator
- Spatial filter
- Setting the zero OPD
- Spectral band combination
- Non filtered mode

This operations are illustrated in Fig. 6.1 showing the implementation of the optical elements realizing this functions.

6.1.1 Beam inputs

The beam compression and possibly the field inversion are performed by the VLTI beam compressor when the UTs are used. This device is a pair of off axis confocal mirrors combined in an afocal system. They must be off axis because the central obscuration of the beam is used by ESO to propagate metrologic light. The beam characteristics are:

- Beam diameter: 18 mm

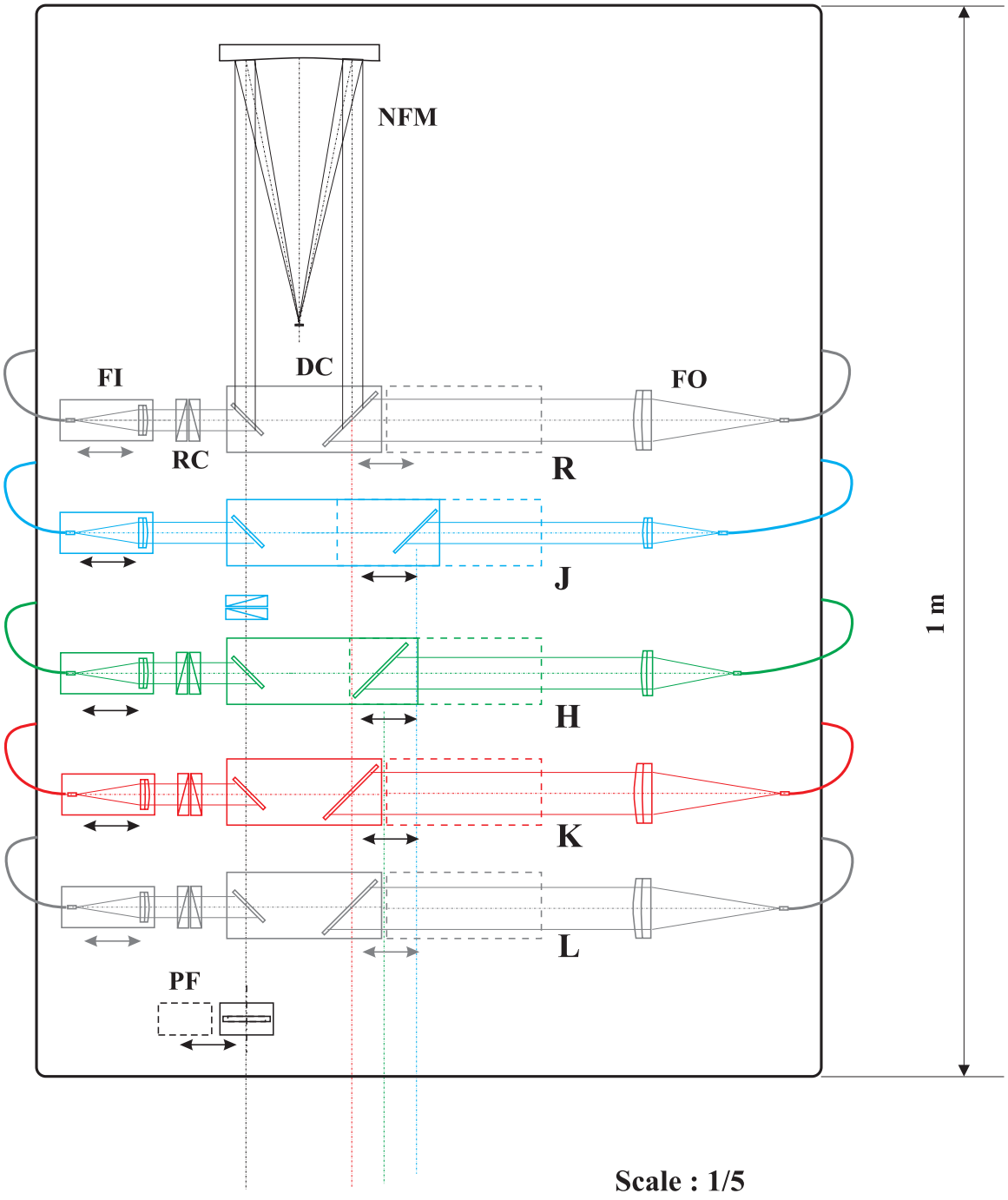

Figure 6.1: Optical processing of individual beams. FI: fiber inputs; RC: refraction correctors; PF: polarization filter; DC: dichroic plates; FO: Fiber outputs; NFM: non filtered mode activated when all dichroics are off. Space is reserved for R, J, H, K and L bands. In the first phase only K, H and J will be implemented, in this order

- Zero OPD plane: at the input of the instruments (MIDI, FSU, AMBER) three beams separated by 100 mm ♠ **(TBC ESO/MIDI)** will be at the same OPD
- Pupil position: at the input of MIDI. Pupil position and field affect the size of the optics. We have assumed that there is at maximum 3 m of the input of the AMBER beams
- Field: for single mode optics we consider 3 λ/D, for non filtered modes we use 2 arcseconds

6.1.2 Polarization control

A polarization plate can be inserted in the beam to select the polarization corresponding to the fiber polarization axis. A study is being made to see if a single plate can perform correctly from the R to the K band.

6.1.3 Spatial filter

We have seen that an efficient spatial filtering requires single mode fibers. A fiber cannot be single mode over bandwidths much larger than this of an atmospheric photometric band. This implies splitting the bandwidth before the fiber. Seen from the detector inside the spectrograph all fiber outputs must be superimposed or at least separated by less than the equivalent of a few pixels. Also, the non filtered mode, where the spatial filters are bypassed works in white light. This two points imply that the bands are combined again in a single beam before entering the beam combiner.

Spectral band separation

In the first phase of AMBER, we implement the K, H and J bands. Later on, the R and the L band will be implemented and space reservations must be made for this. The bandwidth separation is made by a set of dichroics as shown in Fig. 6.1. If the dichroics are fixed this will degradate the transmission for the down stream bands. We therefore will install the dichroics on movable translation plates which extract the band from the beam. When not all dichroics are "in", one given fiber will receive wavelengths for which it is not single-mode. This problem is solved by the band selection filters at the spectrograph input. Removing a dichroic will slightly shift the axis of the beam which will not affect the location of the beam focus on the fiber input. Parallelism and mechanical support of the dichroic plates are specified in order to avoid a tilt of the beam producing a shift of the focal point by more than 0.1 μm ♠ **(TBC AMBER)** If the preliminary mechanical study shows that removing and then inserting the dichroics without affecting the coupling factor in the fiber is too difficult or expensive, a solution with fixed dichroics can be selected to the cost of efficiency for the down stream bands.

Single mode fibers

For each photometric band we use a polarization maintaining single mode fiber. The length is of the order of 1 m ♠ **(TBC AMBER)** in order to have a good rejection of incoherent modes. From R to H we use silica fibers. An experimental measurement is in progress to check that we can use one meter silica fiber in the K band (see section 4.4.1). In L, it will be necessary to use fluoride glass fibers. Each fiber is fed by a doublet. The input fiber head is mounted on a $x-y$ mount with piezoelectric actuators and is moved to maximize coupling efficiency in presence, for example of image motion introduced by the variable difference in atmospheric refraction between the bands. The output fiber head is also mounted on an $x-y$ plate and moved in order to ensure the superposition of the images coming from the different telescopes on the same point on the detector. The preliminary mechanical study will tell if this plate needs to be remotely actuated or is stable enough to be adjusted only before observing periods. The input and output fiber heads are adjusted in rotation in order to co-align the polarization filter, the orientation of the polarization maintaining fiber and the lines of the grating in the spectrograph.

Setting the zero OPD

This done by translating the ensemble input fiber head + doublet with an accuracy better than $\lambda/4$ for the shortest wavelength i.e. 0.2 μm. The stroke depends on the accuracy on the mechanical set up and the fiber length.

Differential refraction correction

We need a correction of the differential atmospheric refraction inside the R, J, H and possibly K band in order to avoid a substantial loss in coupling efficiency. We also need to correct the differential refraction between the central wavelength of the fringe sensor and the central wavelength used in AMBER. If we want to observe in several spectral bands simultaneously we also need to correct the differences between the bands. Ordinary Risley prisms cannot work efficiently for more than one spectral band. This is why we display in the figure one Risley prism per spectral band. The J prism is common to the J spatial filter and to the non filtered mode. The differential refraction between different spectral bands of AMBER (or of the FSU) is corrected by moving the fiber input head in x and y with an accuracy of 0.1 μm ♠ **(TBC AMBER)**. The possibility to use a single refraction corrector from the red to the infrared is being studied and we are discussing with ESO if this task can be performed at the VLTI level.

Differential dispersion correction

We have seen that it does not affect the quality of the spatial filtering and is really needed only in the R band. It will therefore be included in the future visible spectrograph.

Band combination and pupil configuration

The possibility to have all fibers outputs positioned at the focus of a single collimator by means of a V-groove plate is still being considered but such a solution has some drawbacks. The main problem is that the pattern of output fibers must be identical for all beams with a very high accuracy. Other problems are the necessity to have a good optical quality of the collimator in a larger field and the absence of modularity.

This is why we are studying a set of dichroics similar to the one used before the fiber inputs as shown in Fig. 6.1. The output dichroics are on the same plate than the input ones and therefore are removed from the beam in the same conditions. The drawback of this solution is that it might increase the number of actuators and decrease the throughput. A clear advantage is the possibility to implement the spectral bands at different epochs. An even greater and in our mind decisive advantage is that this system permits to re-configurate the output pupil in each spectral band in order to have a sampling of the fringes almost independent from the spectral band without having to actively adjust the focal length of the chamber inside the cooled spectrograph. The focal length of each doublet is selected in order to have a diameter of the collimated beam proportional to the central wavelength of the spectral band i.e.:

- Beam diameter in K: 40 mm
- Beam diameter in H: 30 mm
- Beam diameter in J: 20 mm
- Beam diameter in L and R: 40 mm (use of specific spectrographs)

The beam diameter in K has been selected to permit a maximum spectral resolution of the order of 10000. The configuration of beam sizes and locations as a function of wavelength is discussed again below.

6.1.4 Non filtered mode

When all dichroics are removed, the beam goes through a cat's eye optical device sized to permit a two arcseconds field to be transmitted. The mirror in the focal plane transports the pupil to the entrance of the spectrograph. One or more field diaphragms or slits are installed in this focal plane. The output beam diameter remains 18 mm, which permits full access to all the $u - v$ information given by individual telescope pupils. There is no geometry adaptation with wavelength which means that in non filtered mode the sampling will be critical in the J band. If the preliminary mechanical study shows that we must use fixed dichroics then the cat's eye for the non filtered mode will be installed on a movable plate which can be inserted before the first dichroic and still have the same exit axis than the output beams from the fibers.

6.2 Beam combiner

The combination of three beams is displayed in Fig. 6.2 up to the first cylindrical mirror.

The beam combination is realized by:

- The fiber output (head and dichroic) is set in order to position each image and pupil in a specific place
- The beam splitters BS change the beam separation in order to have a compact non redundant pupil configuration.
- The geometrical location of each plate for beam quality control is defined in order to have a zero OPD before the first cylindrical mirror. The offset depends from the distance of beams at the entrance of MIDI and the FSU. For the drawing we have based the computation on a 100 mm distance between the input beams of the FSU and MIDI.
- The cylindrical optics expand the image (compress the parallel beam) in the direction of the output baseline.
- The pupil mask at the entrance of the spectrograph redefines the pupil in the case of filtered beams with Gaussian profile
- The spectrograph chamber superposes all the parallel beams in a common focal image.

6.2.1 Output pupil geometry

Figure 6.3 shows the geometry of output beams as a function of wavelength for three telescopes. The largest pupil pattern corresponds to the largest wavelength used in the spectrograph, i.e the K band. The smallest is for the J band. The future R and possibly L bands will have geometries identical to the K band since they will use specific spectrographs and detectors. In non filtered mode, the pupil size is reduced to 18 mm and located in the center of the K band pupils.

As shown in Fig. 6.1, the pupil reconfiguration is obtained by:

- Selecting the focal length of the output doublet to change the diameter of the collimated beam.
- Offsetting the dichroic plate to change the axis of the output beam

6.2.2 Cylindrical optics

The cylindrical optics and the spectrograph entrance are set as shown in Fig. 4.1. For two telescopes the ratio of focal lengths between the two mirrors is 4.8. For three telescopes it is 14.4. Adapting AMBER for three telescopes requires only the installation of a third beam control plate, a change in the cylindrical optics and the use of a specific pupil mask at the spectrograph input. With the cylindrical mirrors set up for three telescopes, if only

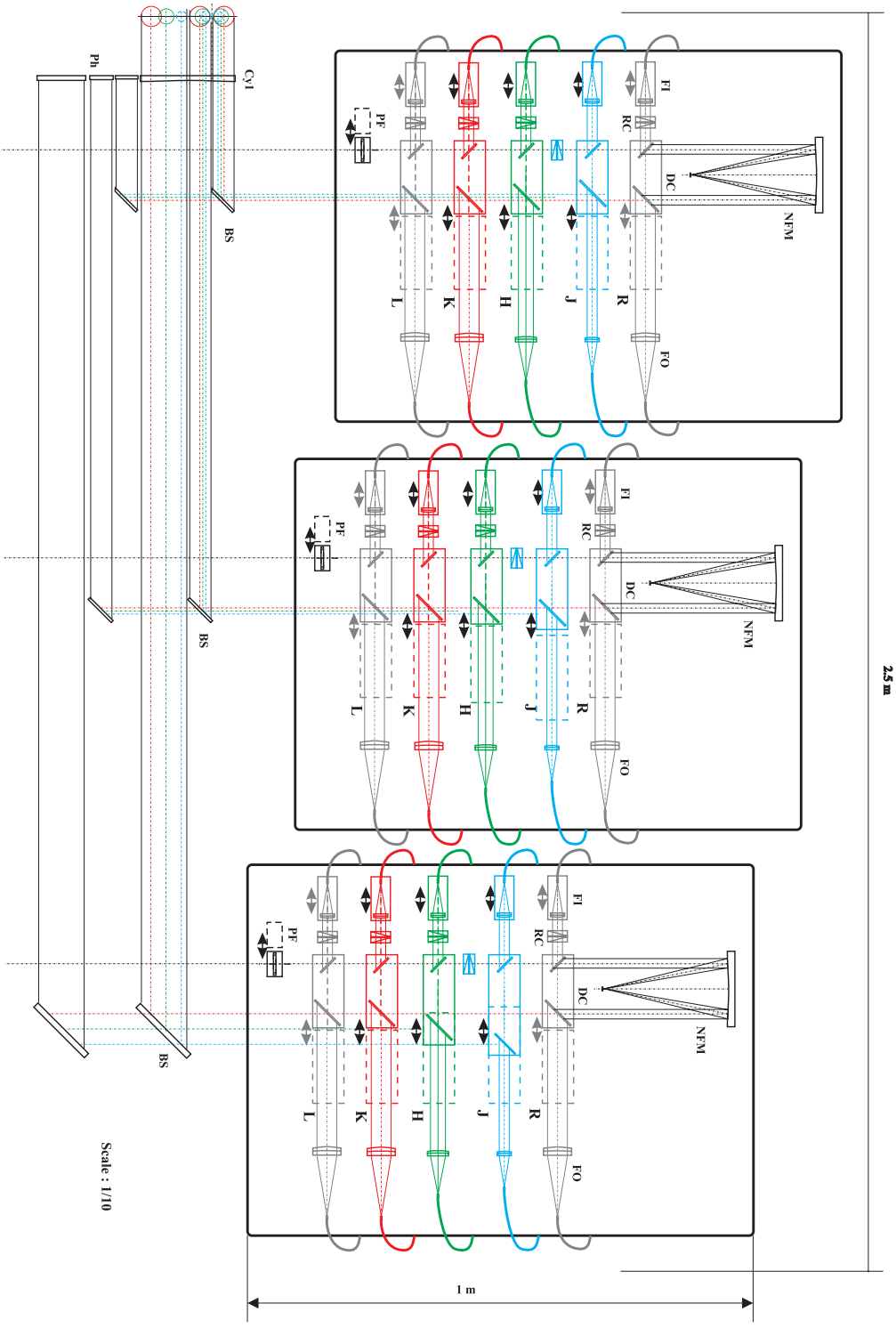

Figure 6.2: Combination of three beams. Cyl is the first cylindrical mirror. The OPD between beams is zero before Cyl. Ph are the flat mirrors transmitting the photometric beams. After this mirror, the second cylindrical mirror and the spectrograph are set up as shown in Fig. 4.1

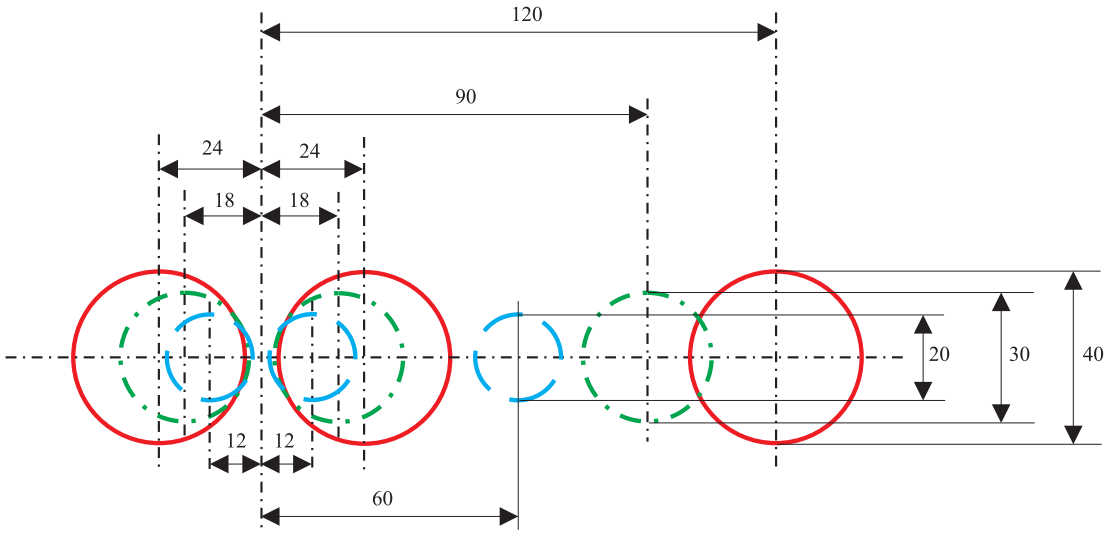

Figure 6.3: Pupil geometry as a function of wavelength. The largest full line drawing is for K, the smallest dashed one for J and the dash dotted for H

two telescopes are used we will be using three times more pixels than necessary, leading to a loss of 0.6 magnitude. We are studying a system where the two telescope cylindrical mirrors can replace the three telescopes system at any moment. This requires two motors to insert the mirrors in the beam and probably remotely controllable adjustments on the orientation of one movable mirror and on the translation (focus) of the other. This movable system can be installed some time after the beginning of operation with two telescopes. The characteristics of the mirrors are as follow:

- Cy1 for two telescopes: l=200 (in the direction of the curvature), h=55, f=1000
- Cy2 for two telescopes: l= 50, h=55, f=208
- Cy1 for three telescopes: l=200, h=55, f=1000 (can be the previous one slightly tilted)
- Cy2 for three telescopes: l=14, h=55, f=70
- angle with the beam 19 (axis of spectrograph beam 400 mm above axis on beam combining table)

6.2.3 Photometric beams

The beam splitters transmit one third of the light to the photometric beams which are relayed inside the spectrograph by plane mirrors of useful diameter 50 mm. It has been shown that the separation between photometry and interferometry can be made after the second cylindrical mirror, immediately before or after the spectrograph entrance. The impact of this on the global design still has to be evaluated.

6.3 Spectrograph

At the present date, the optical design is based on the following input parameters:

Detector:
Hawaii 1024×1024 with 18.5 μ pixel size

Spectral coverage:
K+J+H in order of importance (i.e. 1-2.5 μ)

Spectral resolutions:
interferometric beam

- in K band: 10000 / 1000 / 100 / no dispersion
- in H and J band: about the same than K (but less priority)

$\Rightarrow$ This implies at least 4 positions for the changeable device on the beam:

- grating 500 g/mm ($\mathcal{R} = 10^4$),
- grating 100 g/mm ($\mathcal{R} = 2 \times 10^3$),
- prism for resolution of 50,
- mirror;

photometric beams

- no dispersion/slightly dispersed (about 50)

$\Rightarrow$ this implies 2 positions for the changeable device on the beam

Input pupil:

- interferometric beam: because of anamorphosis we assume (for the first approximation design) a 20×40 mm rectangular input (to be replaced by the actual size and form of the pupil image whatever smaller than the assumption above)
- photometric beams: no anamorphosis, we assume a circular input with 40 mm diameter

Sampling on detector:

- spectroscopic channel: about 2 pixels for spectral element
- photometric channel: 1 pixel for resolution element

Camera focal length: fixed to 370 mm (2 pixels for spectral element at 2 μm)

Aberrations:
PSF degradation less than 5% (TBC)

Input field:
object only on axis (zero amplitude field)

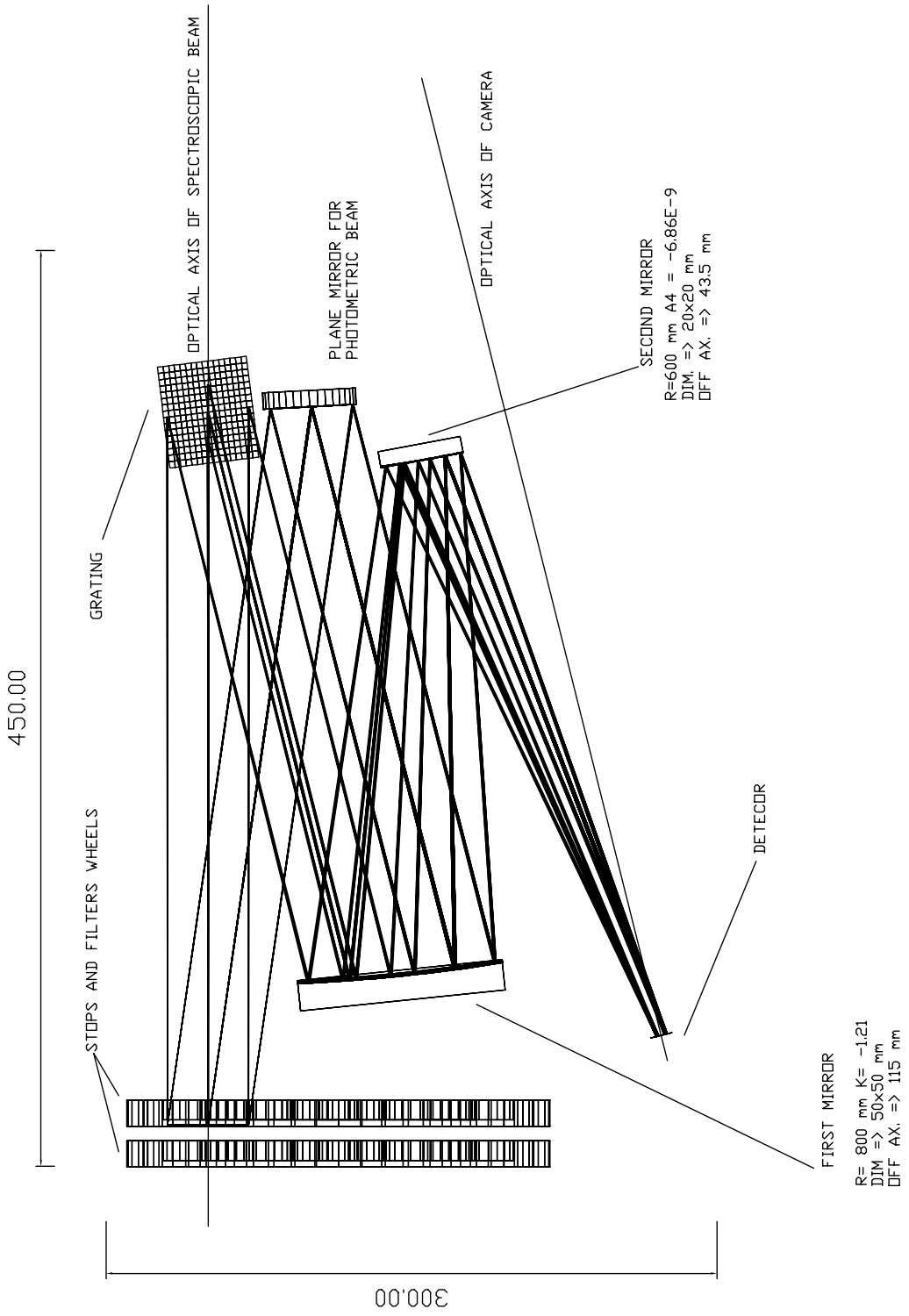

Figure 6.4: Spectrograph preliminary design

Stability:

better than 10^{-4} (to be better defined, according to the value assumed for the opto-mechanics)

Accessory:

Wheels for filter and pupil mask selection (two for spectro-channel and one for photo channel)

The Arcetri Observatory is equipped to perform full tests on the assembled spectrometer (but without the detector), in the field of vacuum, cryogenic functionality, and optical alignment. Some partial tests can be performed with the detector, according to the availability of a suitable detector or of a detector operating in visible, by exploiting the large spectral response of reflective optics.

6.4 Detector

6.4.1 Hardware description

Since 1995 the MPIfR used an infrared camera for speckle observations at different telescopes in Chile and Russia. At the end of 1997, they started to develop a new electronics for their infrared speckle cameras. The first camera is equipped with a NICMOS-3 array. The second camera is presently built and has a HAWAII array. The only change will be the reprogramming of the 68HC16 micro-controller and the Xilinx XC4010 LCA.

Mechanical layout

There are 5 electronic boards which sit in individual chambers of a metal case, milled out of a solid block of aluminum. This ensures optimum decoupling and isolation across the boards and to the outside. The five boards are:

1. a sequencer, generating the clock pattern
2. a clock driver board
3. a preamplifier + signal filter for each quadrant
4. a 14-bit ADC for each quadrant
5. a TAXI link with fiber optic converter for data transmission.

All signals from and to the multilayer electronic boards go via coax cables (including the data lines) or filtered feedthroughs (for power, etc.).

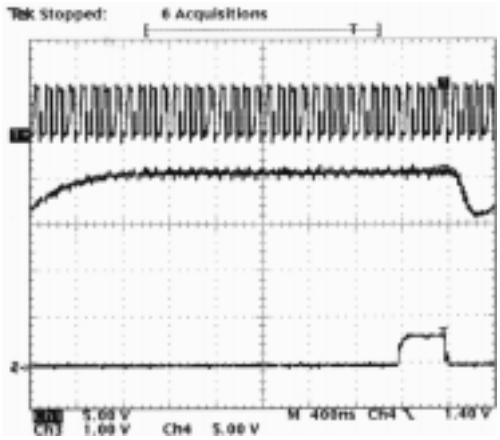

Figure 6.5: Video signal settling

Signal filtering

Speckle interferograms are obtained by short exposed images (a few 10 to 100 ms).The detector is read out fast (250 kHz pixel clock) as hundreds or thousands of images have to be recorded to reconstruct diffraction limited images. In this mode the limiting sensitivity of the camera is dominated by electronic noise (readout-noise) from the output transistor of the detector. After amplification the analog signal is A/D converted. In addition, a low-pass filter is required in front of the ADC to limit the signal bandwidth and reduce the noise. Very often low order low-pass filters are used for this purpose. The cutoff frequency has to be carefully selected. A low cutoff frequency gives a better noise reduction, but the settling time may get so long that it leads to an additional signal error which is larger than the resolution of the ADC. We tried to overcome this antagonism in the following way: every pixel is sampled several times, the number depending on the ADC sampling rate and pixel clock frequency. A combination of an analog + digital filter is applied to calculate the mean value of the different samples. With this technique, theory says that a factor of ~ 1.6 in noise reduction is gained over simple, first order low-pass filters. The bandwidth of the analog / digital filter can be changed by software and easily be optimized to the actual pixel clock frequency.

Preamplifier and ADC

The preamplifier has a gain of 16. A special analog filter sets the 3 dB bandwidth to ~ 6 MHz and the 10 dB bandwidth to ~ 8.5 MHz. The settling time for a 1-bit ADC accuracy is 150 ns. Despite of this fast signal response the settling time of the detectors is much longer, i.e. 2.5 μs for the NICMOS-3 array. That means, for a 250 kHz pixel clock (4 μs period) 1.5 μs are left to filter and convert the signal (cf. Fig. 6.5).

The ADC has 14-bit resolution at 10 MSPS, 90 dB SFDR ($>$ 100 dB with dithering) and $0 - 5$ V input range. 16 samples per pixel are taken and averaged, resulting in a total

Camera	RON [e^-]
MPIfR Bonn, new electronics	28
MPIfR Bonn, Infrared Labs electronics	46
MPIA Heidelberg (MAGIC)	35
MPIE Garching (SHARP)	50
University of Hawaii	53
Arcetri	45
Steward Observatory, Tucson	28 – 39

Table 6.1: Readout noise of other cameras

resolution of > 16 bit. The signals from the four quadrants are sampled in parallel. The digital ADC outputs are multiplexed and converted into a serial data stream, which is sent via a fiber optic cable to the DSP system for display and storage.

6.4.2 Preliminary results

The results from this electronics with the NICMOS3 detector are presented in annex A of the memo AMB-DET-004. We present here the comparison with other electronics.

We measured the readout noise and the conversion factor with the *old* electronics from Infrared Labs at 0.8 V bias voltage. Here the RON was $45 - 47$ e^-(instead of 31 e^-) and $k = 9.33 \ldots 9.70$ e^-/ ADU. These measurements were made under the same conditions, so they are directly comparable with the new electronics. We gained a factor of $\sim$1.5 in noise reduction. This is nearly the theoretical number given above (see signal filtering). Table 6.1 shows the readout-noise of other NICMOS3 cameras, found in the literature.

6.4.3 Detector specifications

The specifications for the detector are summarized in Table 6.2.

6.4.4 Observing modes

The observing modes and their characteristic parameters displayed in Table 6.3. The different image sizes, the need for photometric channels, the readout speed and other restrictions (detector, optics, cold stops) strongly influence the locations of the sub-array, which have to be read on the detector. For example, the separation of the photometric channels depends on the quality of the optics. Even for diffraction limited images, the separation should be a few Airy disk diameters to avoid crosstalk.

The maximum pixel clock of the HAWAII array is given to < 1 MHz in the data sheet. We do not have any experiences up to now whether this is achievable with a readout noise of < 10 e^-. Therefore a pixel clock frequency of 800 kHz (1.25 ms) was used for all calculations with an expected readout noise of 10 e^-.

Table 6.2: Detector specifications

Detector type:	Rockwell HAWAII ($HgCdTe/Al_2O_3$)
Number of pixels:	1024×1024 in 4 quadrants
Pixel size:	18.5 μm $\times$ 18.5 μm
Wavelength range:	0.8 μm - 2.5 μm
Readout noise:	9 e^- 800 kHz
Cooling:	liquid nitrogen (78 K)
Delivery time:	9 months
Electronics:	MPIfR described in § 6.4.1
Observing modes:	scan mode, 12×1 pixels, 350 frames/s 2 ms
	dispersed fringes, 12×25 pixels, 80 frames/s 10 ms
	spectral mode, 12×1000 pixels, 0.96 frames/s 1000 ms
	(large field, 1024×1024 pixels, 0.75 frames/s 1000 ms)
Sequencer:	clock pattern generation with Xilinx programmable gate array
	100 kHz to 1 MHz pixel clock frequency
	correlated double sampling
	multiple non destructive readout for noise reduction
	flexible sub-frame readout to achieve high frame rates
	simple control via RS 232
Preamplifier:	one for each quadrant, wide band , low noise,
	$>$ 88 dB dynamic range
	analog filter bandwidth set to 6 MHz
Analog/digital:	14-bit resolution
converter	10×10^6 samples/s
	90 dB spurious free dynamic range
	16 samples/pixel averaged for noise reduction
Data transfer:	max. data rate: 6.4 MB/sec (detector limited)
	fiber-optic interface

Table 6.3: Observing modes and their characteristic parameters

Modes	Image size [pixels]	Photometric calibration channels [pixels]	Exposure time
Scan mode	12×1[a]	3×1[a]	2 ms
Dispersed fringes	12×25	3×10 (dispersed)	10 ms
Spectral mode	12×1000	3×100 (dispersed)	1 s
Large field	$1024 \times \{1\|25\|1000\}$	-	1 s

[a] 12×3 option: reading 3 lines with vertical binning for SNR improvement

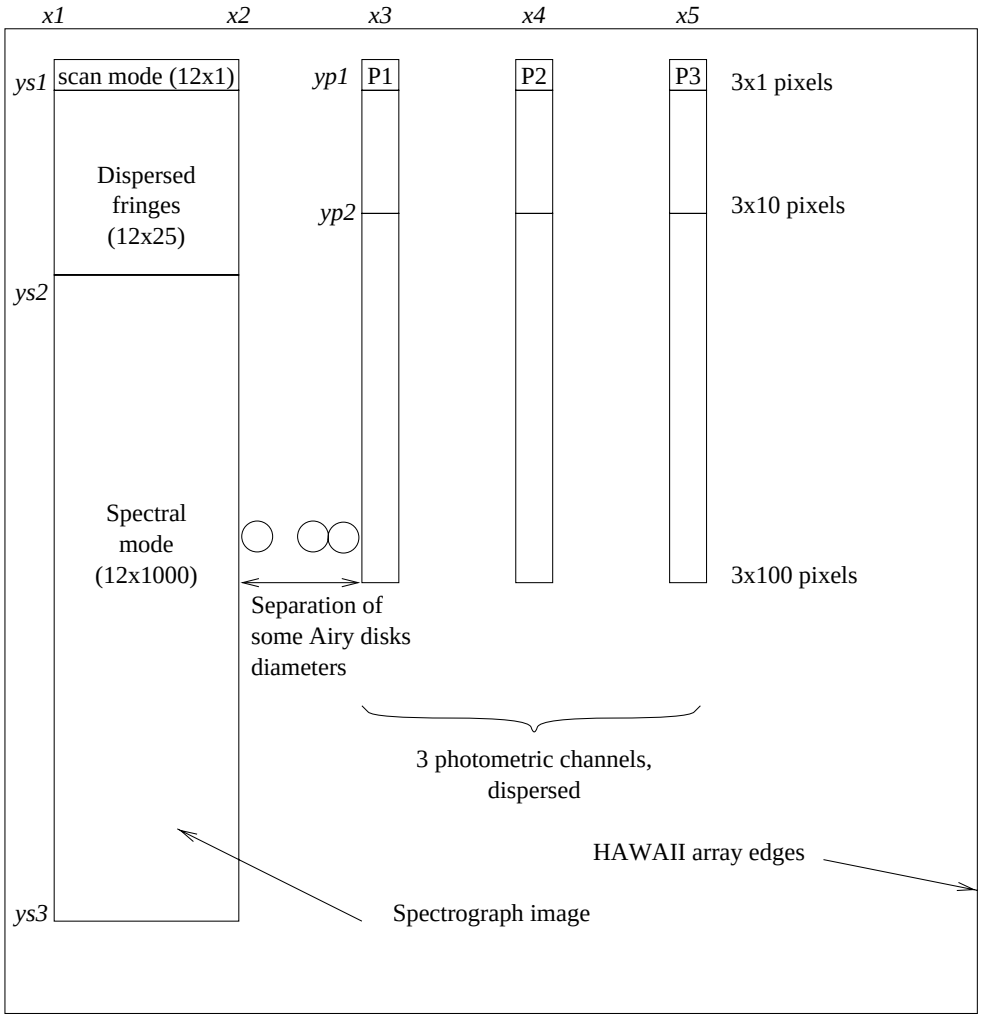

Figure 6.6: Sub-array locations on the HAWAII detector

For the different observing modes the **maximum frame rate** was calculated with the parameters given in Table 6.2. The sub-arrays should start a few lines and columns away from the detector's top left edge. These unused pixels should reflect mechanical adjustment tolerances in the optical trains. $x1$, $ys1$ and $yp1$ are set to 10 (see Fig. 6.6). The separation between the photometric channels is set to 10 pixels.

When using the HAWAII array the following frame rates (compared to the PICNIC array) can be achieved:

	PICNIC	HAWAII
scan mode (2 ms exp.):	326 fps	358 fps
dispersed fringes (10 ms exp.):	44 fps	79 fps
spectral mode (1 s exp.):	0.94 fps	0.96 fps
large field (1 s exp.):	0.88 fps	0.75 fps

If it turns out that the readout noise is too high, the pixel clock frequency can be reduced for example to 400 kHz (2.5 ms). Then the maximum frame rates would be:

Scan mode	279 frames/s
Dispersed fringes	66 frames/s
Spectral mode	0.93 frames/s
Large field	0.6 frames/s

For long exposures and when reading large areas of the detector a shutter is recommended. The opening and close times are about 5 ms for an electro-mechanical shutter with 25 mm aperture.

Chapter 7

Instrument control

7.1 Software functional analysis

The Software package dedicated to the control and use of AMBER has been at the very first stages of the project, partitioned in two main assemblies: OSM (Observing Support Module) and ICM (Instrumental Control Module). This scheme roughly corresponds to a vertical stratification of the functions to be implemented by the soft, from the fine control of hardware elements to the post-processing of scientific data produced.

7.1.1 Software use cycle

For the high-level software of AMBER (ICM+OSM), the following contexts of use are identified, with specific requirements and constraints:

- phase 0: conceptual design of AMBER
- phase 1: preparing an observation proposal
- phase 2: preparing the observation
- phase 3: managing the observations
- phase 4: maintenance of AMBER
- phase 5: off-line reduction

phase 0: conceptual design of AMBER This phase only exists in the first period of the project (ending after the final commissioning). The software (OSM) shall provide simulation tools to assist/validate the conception of the whole system, the preparation of the first observing programs, the definition of observing and reduction procedures.

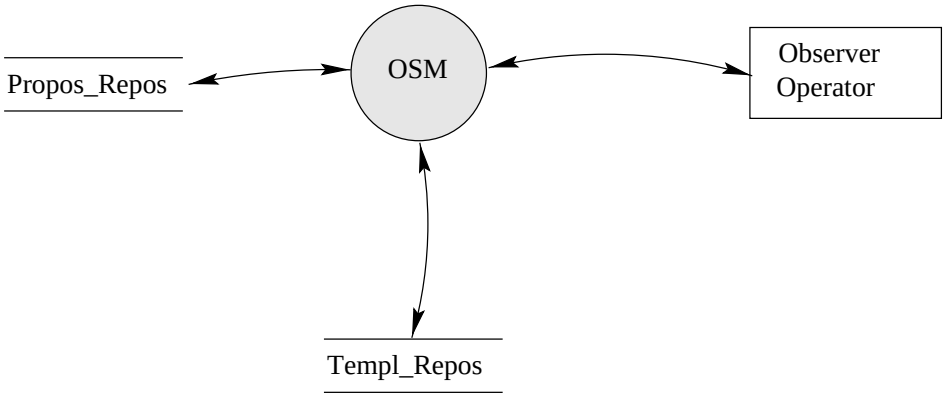

Figure 7.1: Context Diagram for OSM phase 2

phase 1: preparing an observation proposal In this phase, the observer cares about the interest of a scientific program and how to get interesting information with AMBER. The purpose is to define all the observational parameters (but not the operational parameters).

The observer is supposed to know about interferometry, about what AMBER can do (with the support of OSM), but not technically how to do it.

In order to build a proposal, some helpful materials will likely be supplied:

- user manual
- a software tool box: typically some simulator developed during the previous phase. The list of provided tools will grow as the experience on the instrument increases (object observability, expected SNR, u-v coverage, ...)

phase 2: preparing the observation The actual preparation of the observation means the production of 'scripts' to be executed by the instrument itself, on the basis of predefined proposal.

These scripts may be some classical observing modes (= predefined 'templates') in which case OSM proposes such a template list to the user, accepts the parameters values and generates the corresponding script. It may also be a new/specific sequence of actions, in which case OSM only proposes such a script editor, together with syntax verification function.

The user is either an astronomer (who has defined the proposal) defining such a script and/or an operator present at the time of observation, translating a proposal into observation script, or modifying a prepared observation script to fit the current conditions of observations.

The operator is this definition cares about providing the requested data, assuring their good quality, but not about the scientific program. He handles the execution of observation and the latest phase of preparation. He is not allowed to change the scientific program,

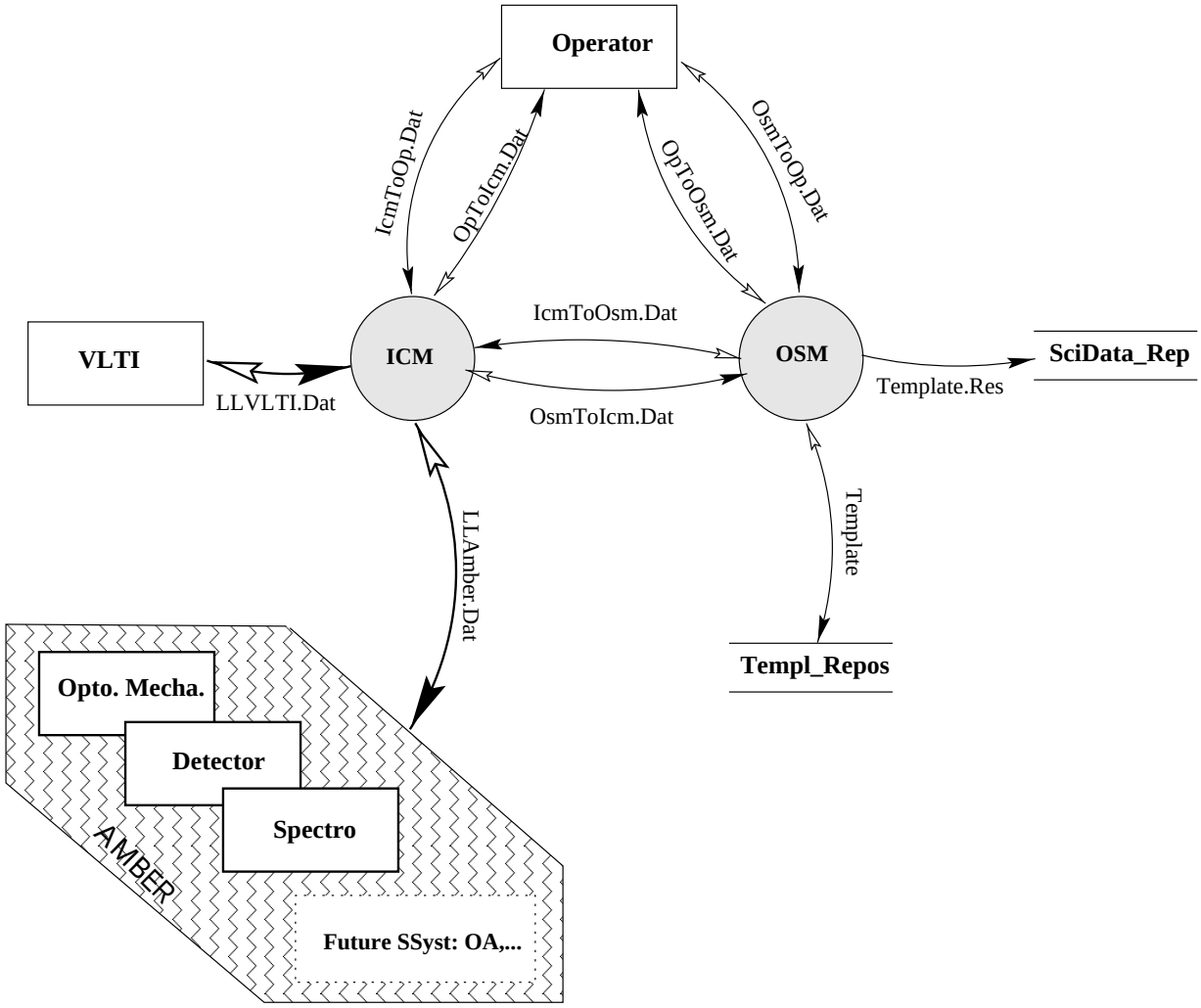

Figure 7.2: Context diagram for observation phase.

but some parameters of the templates, and he handles all scheduling constraints. He is supposed to know about AMBER (same knowledges as the observer + commands + error reports meaning).

phase 3: managing the observations In this phase, OSM and ICM are in close interaction. OSM interacts with

- the user (operator), to accept the execution of prepared scripts, to provide useful information on the current observation (mainly quick look analysis derived from on-line reduction: see AMB-OSM-005)
- ICM to transmit the corresponding observation execution request, access to obtained data and environment data that will be on-line reduced and saved.

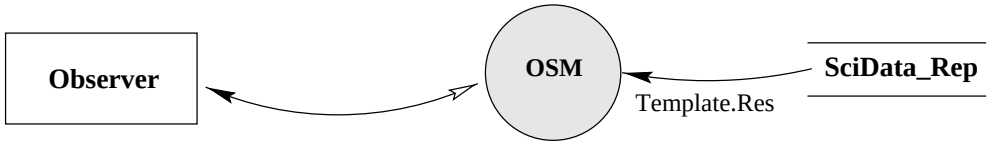

Figure 7.3: OSM during off-line Reduction Phase

phase 4: maintenance of AMBER . Instrument maintenance: corrective and preventive maintenance, test of components, check-up, ...

phase 5: off-line reduction OSM calibrates the produced data, which means here to derive object complex visibilities and phase closures, depending on the projected baseline, on the object, on the wavelength, on the date (...) but not depending on the instrument. The uncertainty on these visibilities should also be estimated.

Some calibration could have been performed in the observation context when providing on-line reduced data. Because of on-line time constraints and since the whole set of data scientifically related to an object is not available on-line, we have to consider a off-line context of use of OSM.

No clear time constraint is identified here. Longer computation time may be acceptable if they allow finer estimations.

On top of that, the user will further proceed to data analysis which are not specific to AMBER but possibly common to any interferometric instrument. In the future, it would be useful to gather some very often or systematically used procedures. This in particular could include object model fitting or image restoration.

This work is an interesting extension of primary OSM functions. This is not a requirement of OSM as described here (i.e. relevant for the AMBER first operation years) but may be added to the OSM reduction tools.

7.1.2 Operating modes

Both ICM and OSM can operate in two main modes corresponding to different users (see below) and thus to different functionalities .

Engineering Mode it concerns the instrument and commissioning teams. For instance this mode gives the ability, in phase 2, to edit "by hand" a whole template ready to run, to build sequences and settings values, instead of using the proper GUI to set some values on pre-defined templates, as this would be the case in the Service Mode (see below)

Service Mode this is the standard mode. Visiting astronomers have only access to this mode.

7.1.3 The user

This paragraph distinguishes different kind of users:

Observer in the classical sense, the scientist using AMBER at its highest level. For instance, in phase 2, the observer has only access to OSM, not to the basic commands of ICM. The Engineering Mode is not allowed. In the first times, he would be a member of AMBER team or with similar knowledges.

Operator , he effectively manages the instrument, controls the execution using OSM, or drives directly through ICM his main operating tools. He has access to all OSM and ICM commands, not to the internals of the software themselves.

Developer/Maintainer of the software. Super-user, root user.

In this taxonomy it is clearly stated that privileges for using the instrument are highly organized in hierarchy. Conversely, skills levels are supposed to be proportional to privilege level.

User	Phases					
	0	1	2	3	4	5
Observer		x	x			x
Operator			x	x		
Developer/Maintainer	x	x	x	x	x	x

7.2 Control software

7.2.1 Scope

The main task of ICM is to operate the instruments in phases 3 and 4, i.e. to give instructions to the different subsystems to achieve the action requested by the user.

7.2.2 Functional analysis

This section describes the full range of functionalities of ICM, as stated in the memo AMB-OSM-011 and displayed on Fig. 7.4.

ControlSpectro

The ControlSpectro function is devoted to the control of the spectrograph in all phases.

* select the spectral resolution (0-100-1000-10000) through gratings and prisms selection

* select the central wavelength

* manage position of slits, filters and masks

* send back housekeeping (temperatures, locks, ...)

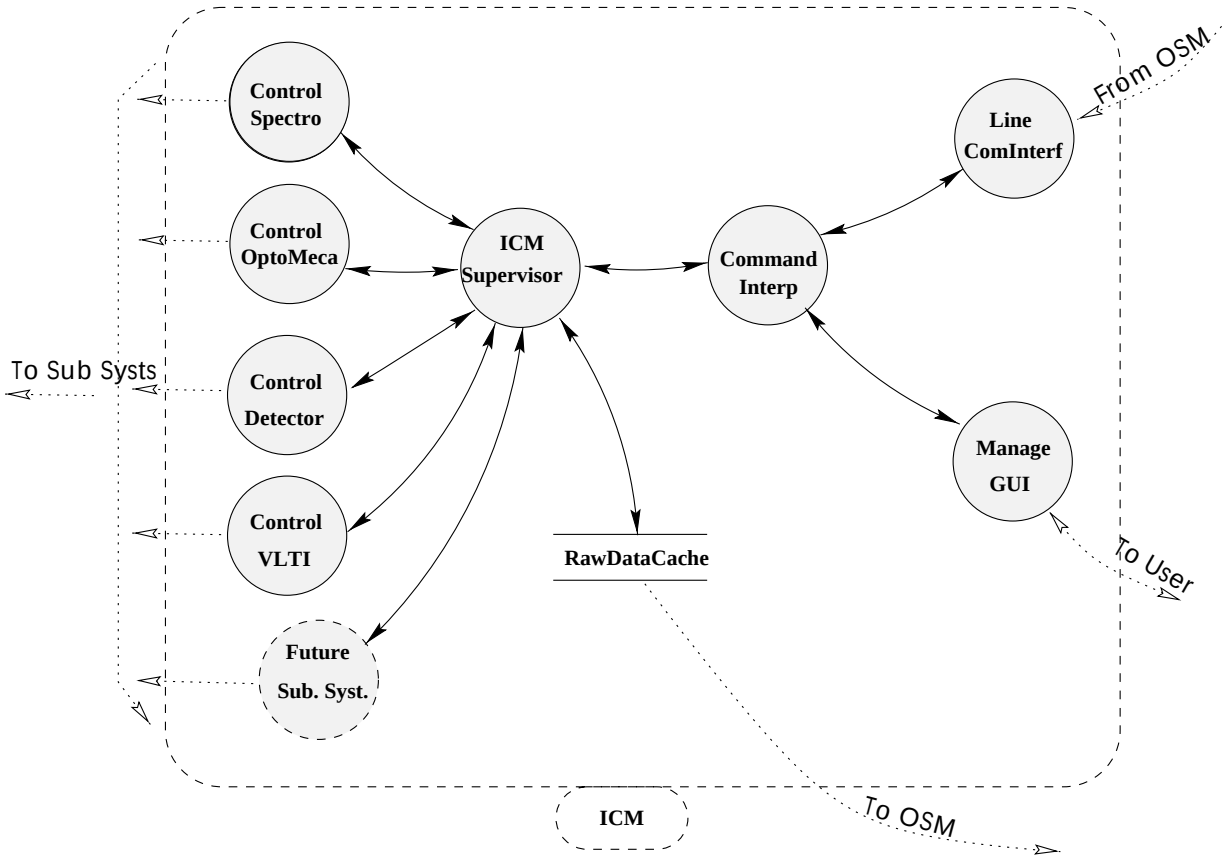

Figure 7.4: Oversimplified scheme of systems functions of ICM. For the sake of simplicity, no external data flow is represented

ControlOptoMeca

The ControlSpectro function is devoted to the control all the low-level control mechanisms.

A first list of intermediate level systems is given below for AMBER working in K,H,J spectral bands and with 3 telescopes. This list has been established that in operation phase it must be possible to check and correct the adjustment of the instrument from the control computer.

* insert shutters and fold mirrors for calibration beams (1 motors per beam)

* insert polarization filter (1 motor per beam)

* insert dichroics for band selection (1 motor per beam per band)

* input fiber heads motion (2 piezos per beam and per band)

* zero OPD set up (1 piezo per beam and per band)

* atmospheric refraction compensators (2 motors per beam and per band)

* beam combiner: superposition of images of output fiber heads (2 piezos per band and per beam)

* selection of 2 or 3 telescopes configuration: selection and adjustment of cylindrical optics: 4 motors

* switch between spectrograph and test detector: 1 motor

* read check up detectors (1 single pixel detector per beam + 1 single pixel detector conjugated with the spectrograph)

This leads to about 9 motors and 15 piezos per beam + 5 motors in beam combined part. This corresponds to 49 actuators and 3 probes with two telescopes and 77 actuators and 4 probes with three telescopes. This should be top values. Some actuators might be partially redundant such as the x-y motion of input fibers and the refraction compensators, or the fact that we might be able to have a single refraction compensator for all bands. Others might be replaced by fixed adjustments after the preliminary mechanical study, such as for example the output fiber heads. The low values would typically be: 5 motors and 9 piezos per beam which yields 29 actuators and 3 probes with 2 telescopes and 47 actuators and 4 probes with 3 telescopes.

ControlDetector

* Records images and sending to ICM (ICM has in charge to record data for functional aspects) ¡1Mb/s

* drive shutter

* pre-reduction data

* Detector configuration

* log book

* flag over acquired data

ControlVLTI

This function is devoted to the interface with the VLTICS software.It must:

* request the set up of the interferometer

* collect environmental data (seeing, sismicity, weather...)

* inform VLTI about instrument status

* request OPD motions (through a fast link ?)

* request field inversions (through a fast link ?)

* make recorded data visible by the VLTI ?

MonitorStatus

Central monitor of ICM. Manages the other soft components.

ManageGUI

Manages the GUI interface with the operator in order to get input commands and display status information and raw data (QLA) in a proper format.

LineComInterf

Manages the line interface to present a connection socket to both OSM and VLTICS. Receives a command flow from OSM, in a script language and returns status information and raw data.

CommandInterp

Command interpretor. Converts high level language commands into basics, simply executable by a terminal computing process.

ICM Supervisor

Manages the state of the systems and coordinates all the sub-tasks.

RawDataCache

Data cache for temporary storage, mainly for raw data coming from detector.

7.3 Scientific software OSM

7.3.1 Scope

The main tasks of OSM are described AMB-OSM-004 and the previous report AMB-REP-003, namely to support the user to :

i design AMBER

ii prepare AMBER observations

iii operate the observations according to the scientific purposes

iv calibrate the produced data

The corresponding functional analysis is presented in AMB-OSM-011. The next section presents an internal analysis of OSM with interfaces and attributes.

Note that much more detailed information on OSM can be found in successive OSM memos relative to OSM meetings or specific studies (number 001 to 011).

7.3.2 Organization

Internal system functions

Figure 7.5 describes the internal structure of OSM, designed to satisfy the external functions as stated in the previous section (see amb-osm-011 for more details).

External interfaces

The OSM, if this description is validated, interacts only with

- the user: observer or operator, depending on the context
- ICM in phase 3. (in particular, the interface with OSM-ICM includes OSM needs for information concerning the VLTI status and environment conditions)

This has to be validated by ESO.

System attributes

See amb-osm-011 for a preliminary description. Maintainability, adaptability and other constraints on the development are however still to be precised, in agreement with the global decisions for the AMBER about operation plan and delivery to ESO.

7.3.3 Work status

We present here some indications about the work already done in OSM group and scheduled further developments.

Simulation of the instrument

A complete numerical simulation of the whole instrument (+ astronomical source and atmosphere) has been defined and is under final integration (see amb-osm-007). It has been realized in order to be easily modified (with independent modules) for up-graded versions, and re-usable in the final OSM.

The two main parts :

- production of realistic data,

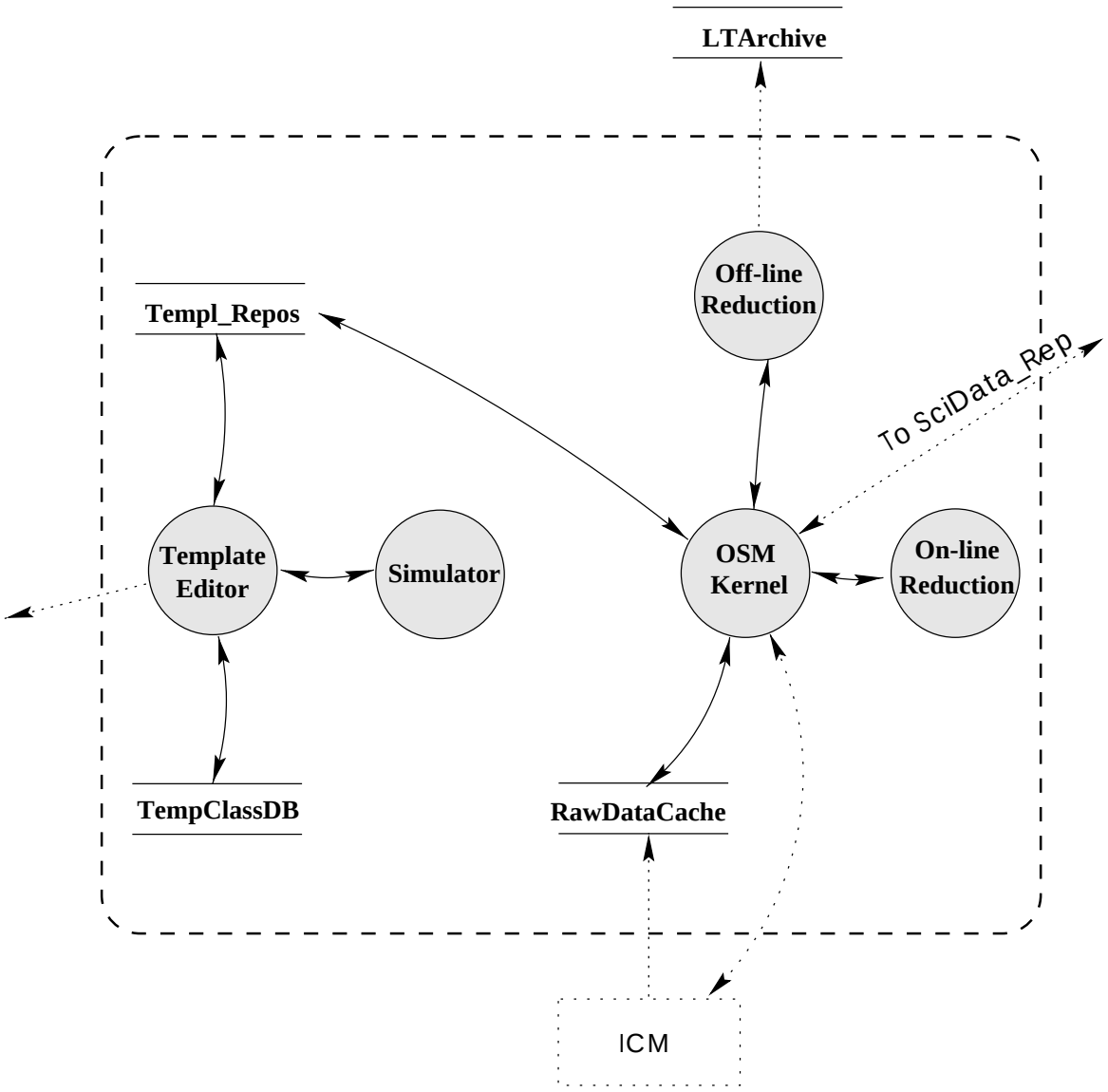

Figure 7.5: Simplified scheme of system functions of OSM.

- calibration of data,

should be integrated by the end of the year.

This part is a critical step for further developments of the project: phase 0 task of OSM, definition and validation of observing and calibration procedures, development of simulator and calibration tools of the final OSM.

Definition of final product

Preliminary and detailed design of OSM The presented functional analysis of OSM is a significant part of the design of OSM. The actual content of data to be exchanged is to be precised. In particular, the list of high-level commands to ICM will be defined together with ICM and the interferometric group, on the basis of the analysis of typical observing procedures. Also, the list of useful information from the VLTI is under definition.

Software and hardware solution For OSM, basically, hardware means consist in a work station and an archiving system. Some solutions are under evaluation and shall be decided accordingly to budget/compatibility constraints.

The software development implies a software platform (for interfaces, displays, interpretor), and simulation/calibration procedures. The choice is made to use as procedures only compiled routines (Fortran or C) in order to assure: computing efficiency, suitability for various contexts, no need for specific licenses, ... The GILDAS platform is proposed as an environment to manage these procedures, commands, displays, scripts, ... It offers already many tools directly suitable to our purposes, fulfills the functional requirements. This choice also has to be validated under budget(time and human)/compatibility constraints.

7.4 Control hardware

7.4.1 General architecture

The architecture of the control hardware follows the General ESO guidelines as described in the document VLT-ESO-15400-0886 or in Verola's presentation in the Kona SPIE meeting in 98. This architecture is presented in figure 7.6.

We analyzed several solutions having in mind the following constraints:

- We must communicate with the VLTI and therefore have an interface with the VLTI CS compatible with the VLT software.
- We have time and budget limitations. This is an incentive to use as much as possible hardware and software well mastered in our Institutes.
- The instrument must be operated far from the Institutes where it was built and after typically 2003 the number of nights of operation should be quite high (more than 100 per year). Therefore the instrument must be easily operable by ESO and should therefore comply with a fair range of its standards.

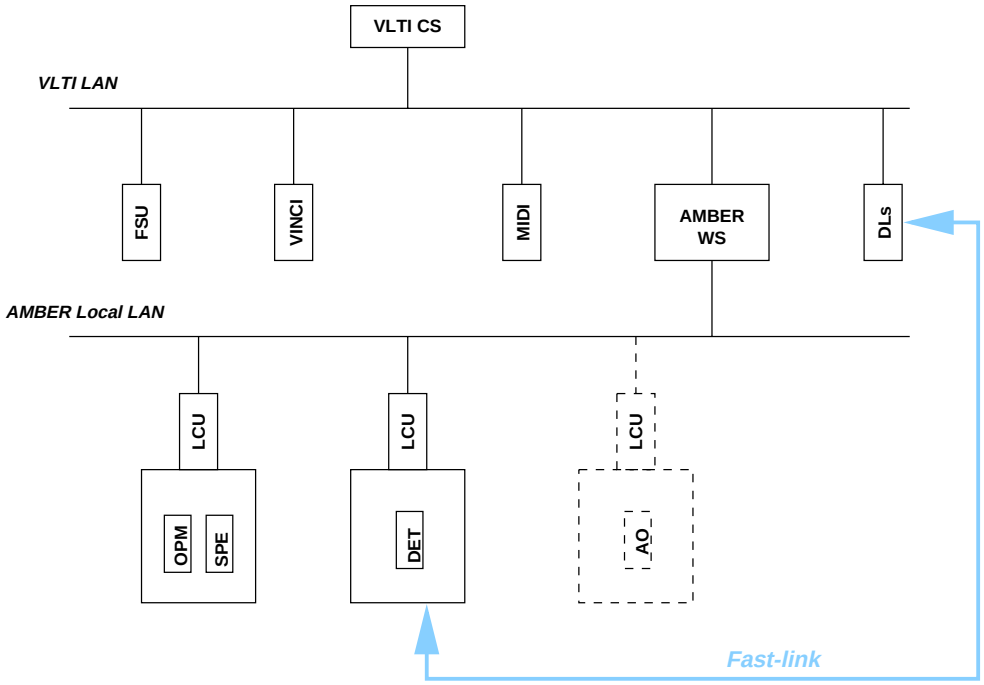

Figure 7.6: ICM general hardware architecture

- The selected architecture must ease the collaboration between the four Institutes in charge of the development, manufacturing and integration.
- The system should be easy to maintain at Paranal. To achieve the reliability and ease the maintainability, the system must be as homogeneous as possible.

To achieve the architecture described on Fig. 7.6, we must specify the following items from the high level control to the low level control.

- workstation (WS) and operating system
- communication software
- communication network between WS and LCUs (LAN)
- local unit control (LCU) CPU
- LCU software
- communication between CPU and boards
- actuator or sensor control boards
- connection between the boards and the actuators or sensors

7.4.2 Solutions

Three solutions have been considered:

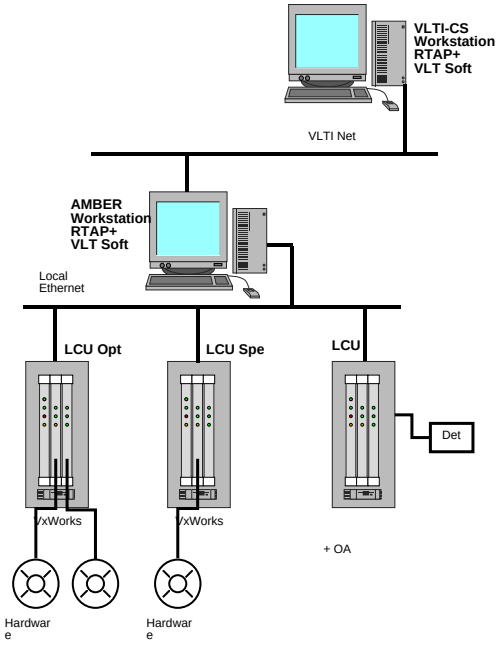

Figure 7.7: ESO fully standard solution for ICM hardware architecture

- full compliance with ESO standards
- fully institute-based solution
- solution complying with ESO standards but with derogation for some subparts.

Full compliance to ESO standards

This solution is represented in Fig. 7.7 and follows the ESO recommendations for the control hardware and software.

Workstation/OS: HP/HPUX or Sun/Solaris

Communication software: RTAP

LAN: Ethernet

LCU CPU: VME CPU board (one LCU per subsystem: OPM, SPE, DET)

LCU software: VxWorks

LCU bus: VME backplane

Control boards: from "ESO catalog" (MACCON for 4 motors, etc...)

Connection: radial: between each actuator/sensor and the control rack

The local control is achieved with a VME bus. The detector is controlled by a FIERA like controller (Beletic et al. 1998).

The advantages of such a solution are multiple. The instrument can be fully operated and maintained by ESO as soon as the tests are over and the optimum operation procedures have been established (which will take some time after the first successful and efficient scientific observations). It also has the following drawbacks:

- It is expensive. We will have between 40 and 60 actuators or sensors in a three beam experiment. The typical cost in the ESO catalog is of the order of 10 kDM per actuator. The typical cost for industrial standards is lower than 2 KDM per actuator. The difference can easily reach 500 KDM.
- For some subsystems, the ESO standards cannot be used without a risk of loss of performance (or the need for new development). This is especially the case for the detector electronics. For other parts, such as for examples piezo actuators, the solutions available in the ESO catalog seem quite inefficient.
- All four institutes must invest in ESO compliant workstations, software licenses and personnel training. This implies again an extra cost and some of the Institutes have stated that the manpower they have available for AMBER is not compatible with this.

Such a solution would need to accept the extra cost for hardware and a quite heavy help from ESO software engineers. Even if such a collaboration between the AMBER consortium and ESO can be established, the delay implied by its set up would make it very difficult to complete AMBER for 2001.

Institute-based solution

Each Institute develops its subsystem its own way. There must be a structure to interface the subsystems and to interface with ESO. The compatibility with ESO is reduced to the correct definition of this interface. Figure 7.8 represents the solution proposed by the LAOG which is based on the CAN bus technology (see AMB-ICM-xxx memos).

Workstation/OS: PC/Linux

Communication software: PVM (Parallel Virtual Machine)

LAN: Ethernet

LCU CPU: PC104

LCU software: Linux/PVM

LCU bus: CAN field bus (twisted pair)

Control boards: CAN node with a micro controlers (e.g. XEVA)

Connection: circular, between nodes.

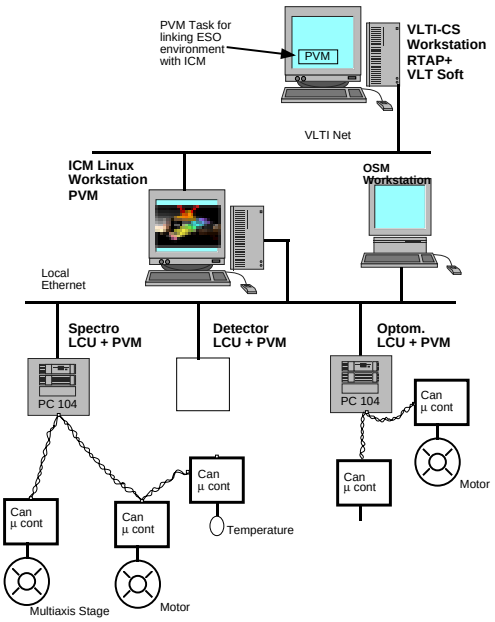

Figure 7.8: Institute-based solution for ICM hardware architecture

The communication software is not the standard VLT / VLTI communication software (RTAP) and therefore an interface must be installed. This is done by installing a PVM process, which is a public domain software, on a VLTI workstation. The PVM process can talk with the CCS software (Communication Control Software).

For some subsystems, VME CPU boards and VxWorks could be used and control actuators and sensors through serial lines like in the PFSU developed by OCA for ESO. A specific interface is developed between the VLTI workstation and the AMBER workstation. The detector electronics head is the one developed by the MPIfR (see chapter 6). The control computer is a PC under Linux equipped with DSPs.

CAN is a field bus which works in a distributed I/O environment. It has been developed for the automobile industry where it appears as being "the solution" to control actuators and sensors distributed in space. It is now proposed on almost catalogs of all manufacturers. It is based on a "Ethernet like" approach where each actuator or sensor is connected to a node of a network materialized by a pair of twisted cables. This permits a strong reduction of the quantity of wires distributing the power and the information in the instrument and can therefore increase the reliability and decrease the power dissipation.

Table 7.1 compares the power and the mass of the CAN solution compared to the VME solution. The numbers comes from the NAOS instrument for the VME bus. Table 7.2 gives elements for a cost comparison between CAN and VME buses. This elements show that this solution is quite worth considering in a context where cost and the dissipation of power are critical elements.

Table 7.1: Mass and Power comparison between VME bus and CAN bus (10 nodes).

VME-based			CAN-based		
Type	Mass (kg)	Power (W)	Type	Mass (kg)	Power (W)
VME LCU	30	200	PC 104	1	10
Cooled Rack	30	0	CAN nodes	5	5
Total	60	200	**Total**	6	15

Table 7.2: Cost comparison in kDM for the control of 20 motors between VME- and CAN-based solutions.

Item	VME-based	CAN-based
Workstation	35	6
Comm. soft. license	60	0
LCU	30	3
LCU soft. license	30	3
Control board 20 motors	30	3
Total	185	15

The main advantage of such a system is that it minimizes the workload on the Institutes and the hardware cost. Also the use of a field bus can have specific technical advantages. The main drawbacks of such a solution are that we are really very far from ESO standards. If the interface is correctly defined, this might not affect that much the operation of the instrument. But the maintenance of AMBER and its future check ups and evolutions will require heavy implication of the consortium. Also, the harmonization of the work between the Institutes might be more difficult.

Proposed solution

The chosen solution is characterized by a high level of compliance with ESO standards and derogation for some subparts.

Figure 7.9 summarizes the base of a possible trade off between the compliance to ESO standards and the Institutes time, manpower and cost constraints:

Workstation/OS: HP/HPUX

Communication software: RTAP

LAN: Ethernet

LCU bus: VME backplane

LCU software: VxWorks

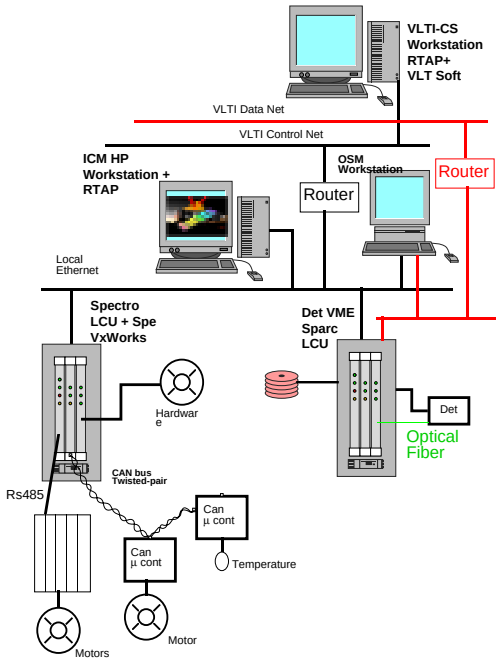

Figure 7.9: ESO compliant solution for ICM hardware architecture

Down to this point, we are fully in the ESO standard environment. The instrument can have one single LCU controlling the subsystems, including possibly the detector (see below). The subsystems can be controlled through institute-based solutions. Several possibilities are considered:

* ESO standard boards will be installed for some applications (digital I/O).
* the VME back plane receives a board controlling a field bus (PROFI bus or CAN bus). A driver for the field bus is developed on the LCU and the local control is done in distributed nodes.
* the VME back plane receives boards controlling the sensors and actuator boards through serial lines. Drivers for these boards are developed on the LCU.

A field bus or a set of boards on a RS485 serial bus control all the actuators and the sensors for a subsystem such as the opto-mechanics for example. The subsystem can also be controlled by a PC computer activating the same field bus or serial line. The main advantages of this trade off is that we have a system which is compliant with ESO standards to a large extent but at a reduced cost. In particular it is not mandatory that all Institutes invest in workstations, software licenses and people training. This is particularly important for the MPIfR and OAA teams who have no experience with VxWorks and VME systems and have manpower limitations.

The decision between field bus and boards on a serial line will be made during the preliminary design phase. It will depend on an analysis of power dissipation, packaging

and wiring problems and of the relative workloads.

7.4.3 Detector control

The detector case needs some further analysis. The detector subsystem contains:

- Detector electronics (clocks and biases to drive the detector + analog / digital signal conditioning like low noise, high speed amplifiers and ADCs.
- High speed data transfer from camera electronics to storage computer
- On-line image processing and display
- Data storage
- Camera control software

The MPIfR has developed and tested an efficient system based on a Linux PC + DSP (see section 6.4) which has all the required performances and features a high level of on-line processing. In any case the detector electronics cannot be built to ESO standards without having a strong risk of performance loss and without a completely new design. For the local control unit, two possibilities can be considered:

- The full MPIfR system is used and appears has a black box controlled directly by the instrument LCU through a serial line or through the instrument LAN. In this case the workload on the MPIfR is minimized and we benefit from all the on line tools they have developed. The operation of the instrument by ESO will not be affected by this structure. The maintenance is ensured by remote diagnostic tools and a set of spare parts. This option is clearly preferred by the AMBER consortium.
- If the first solution appears impossible to accept for ESO, a subpart of the FIERA development can be used for controlling the detector, handling the data and providing a limited set of on line functions. In this case only the functions necessary for the instrument integration and check up will be implemented at detector level. The more advanced estimators for the quality of the data will be implemented on the OSM work station, which has a direct access to the storage disk and can run a fixed subset of the OSM software slightly off line. The extra hardware cost has to be estimated. The main concern of the MPIfR team in this hypothesis is the extra work. The solution seems too need a relatively high level of manpower support from ESO during the development phases (ESO person spending time in Bonn "translating" software for the FIERA machine), the global integration phase in Grenoble and the operations in Paranal.

7.4.4 Summary

To summarize, the proposed solution is

- compliant with ESO standards down to LCU level,
- makes the subparts affected by derogation to the standards transparent for the ESO operator,
- reduces the workload for the Institutes and permits then to use solutions in which they have excellent experience and training and therefore avoids extra delays,
- reduces the total coast of the control system,
- permits future subparts fully compliant with ESO standards,
- should not affect the maintainability at Paranal if the necessary spare parts are provided and the devices used are based on industrial standards.

Chapter 8

Assembly, integration and tests

8.1 Laboratory integration phases

The *passive* integration of each sub-system (i.e. the assembly and the qualification tests of the sub-system alone) concerns the group of the AMBER consortium which is responsible for it. For each sub-system, this integration phase includes:

- the tests of each component or elementary part of the sub-system
- the sub-system internal alignment (with or without simulators from others sub-systems)
- the check of the sub-system requirements

The *active* integration of AMBER (i.e. the assembly and the qualification tests of the global instrument) is managed by the System Engineer and the Integration Manager. This phase includes:

- alignment of each sub-system with others
- tests of the Instrumental Control Module (ICM) with all elements and a VLTI simulation software that mimics the VLTI behavior.
- evaluation of AMBER performances

8.2 Site tests and final commissioning

After shipping to Paranal, AMBER is tested in the same conditions as in lab. After validation, the different interfaces with the VLTI are validated.

Using the test siderostats, the whole observing procedure is tested and validated. Finally some technical time will be requested to validate the instrument in the final configuration.

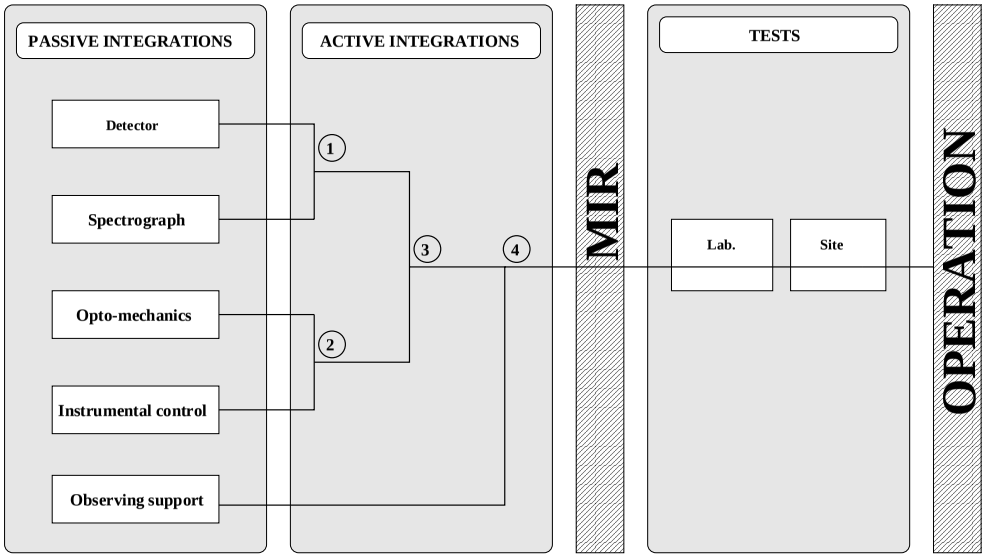

Figure 8.1: Assembly, Integration and Tests phases of AMBER.

8.3 INT phases

The Assembly, Integration and Tests (INT) phases are given in Fig. 8.1.

The active integrations consist in several steps (See number in Fig. 8.1):

1. The spectrograph and the detector are integrated and tested together.
2. In parallel, the opto-mechanics and the instrumental control are integrated and tested together. The proper drive and control of the opto-mechanics by the software is checked.
3. The two previous assemblies are integrated and tested together.
4. The Observing Support (OSM) is integrated and tested with the whole instrument. The proper processing and execution of templates generated by OSM are checked.

Only the tests of the global instrument AMBER are presented in Fig. 8.1. They consist in laboratory tests for qualifying AMBER as an instrumentation and in site tests when AMBER is set in the VLTI environment . The second part obviously includes a integration phase (alignment with the VLTI, ...).

8.4 Test plan

Test plans are established for each sub-system and for the global instrument AMBER. Each of them is established in parallel with the global system analysis by the System Engineer, the Integration Manager and the sub-systems coordinators.

In the following, an *elementary part* denotes a single component for the sub-system test plan or a sub-system for the AMBER global test plan. By the same way, a *global system* corresponds either to a sub-system or to the global instrument AMBER.

Each test plan includes:

- the **integration steps**.
  All the tasks from the first one (requirement test of an elementary part) to the last one (global qualification) are sequentially described. The required manpower, duration and tools are specified. The works which have to be achieved before the beginning of each task are identified.

- the **alignment procedures**.
  All the procedures to properly align each elementary part and then the global system are detailed. Each of them are sequentially described and the required tools are identified.

- the **test procedures**.
  All the procedures to check the requirements of all elementary parts (filters throughput, detector read-out-noise, ...) and all global systems are given. The required tools are identified.

- the **calibration procedures**.
  All the procedures to calibrate the global system (spectral calibrations, shape of the fiber field, ...) are given. The required tools are identified.

- the **performances evaluation procedures**.
  All the procedures to quantify the global system performances (calibrated instrumental contrast, visibility accuracy, ...) are given. The required tools are identified.

8.5 INT Tools

They include:

- the **alignment tools**.

- the **test tools**.

- the **calibration tools**.

They can be:

- standard tools provided with AMBER (spectral sources or Fabry-Pérot for spectral calibrations , laser sources for alignments, ...)

- standard tools specific to laboratory integration phases and provided by the consortium institutes (dark body for detector qualifications, micro-alignment devices, ...). Some of them are required at Paranal.

- tools specific to AMBER laboratory integrations and developed by the AMBER consortium (simulators of few AMBER sub-systems for passive integration phases, simulator of VLTI for active integration phases, ...). Some of them can be required at Paranal.
- tools provided by ESO at Paranal for align AMBER with the VLTI, for calibration facilities, ...

8.6 INT documents

For each sub-system and the global instrument AMBER, reference documents (integration manuals, tests documents, ...) are provided after major integration phases.

Chapter 9

Management, schedule, cost

9.1 Management

9.1.1 AMBER consortium

AMBER is being studied and will be built by a consortium of European Institutes:

- Laboratoire d'Astrophysique, Observatoire de Grenoble (LAOG), Grenoble, France
- Observatoire de la Côte d'Azur and Université de Nice - Sophia Antipolis (OCA / UNSA)[1] , Nice, France
- Osservatorio Astrofisici di Arcetri (OAA), Firenze, Italy
- Max Planck Institute für Radioastronomie (MPIfR), Bonn, Germany

Other institutes provide the help of individual experts and consultants but will not build or integrate sub systems of AMBER. They are:

- Centre de Recherche Astrophysique de Lyon (CRAL), Lyon, France
- Institut de Recherche en Communications Optiques et Micro Ondes, (IRCOM), Limoges, France
- Office National de d'Études et de Recherches Aerospatiales (ONERA), Paris, France
- Observatoire de Paris (OdP), Meudon, France
- Institut d'Astrophysique de Paris (IAP), Paris, France.

The Directors of main institutes and the Sponsoring Agencies (INSU in France) are represented in an AMBER Steering Committee who follows the project with a particular

[1] Two laboratories constitute the Côte d'Azur pole: the *Département Fresnel of the Observatoire de la Côte d'Azur* and the *Unité Mixte de Recherche en Astrophysique 6525 of the University of Nice - Sophia Antipolis*. The geographical proximity between the laboratories and the very well established collaboration make it possible to manage their contribution to AMBER as this of a single Institute.

attention to the budget and manpower problems. The agreement describing the contributions of the various Institutes and their share of the AMBER results is finalized at this level as well as the Memorandum of Understanding between the AMBER consortium and ESO.

9.1.2 Structure of the AMBER consortium

Direction group

Principal Investigator: Romain Petrov (Nice)
Project Scientist: Fabien Malbet (Grenoble)
Chairman of the Science Group: Andrea Richichi (Firenze)
Co-investigator: Karl-Heinz Hofmann (Bonn)
Project Manager: Pierre Antonelli (Nice)
System Engineer: Serge Ménardi (Nice)
Integration Manager: Karine Perraut[2] (Grenoble)

The four Co-Is, each one representing one area (Petrov, Nice; Malbet, Grenoble; Richichi, Firenze; Hofmann, Bonn) meet to discuss political and coordination aspects and particularly to prepare the work of the Steering Committee on the agreements between the AMBER consortium and ESO.

A particular attention is given to a good communication between Nice and Grenoble. The PI Romain Petrov shares its time equally between Nice and Grenoble with typically a systematic presence in Grenoble two days per week, in addition to his other professional travels. This in reinforced by regular meetings of the Direction Group, of the Project Manager with the subsystem coodinators and of the ICM group members. In addition frequent video conferences are set up.

Expert groups

Two groups of experts assist the PS and the Chairman of the Science Group in defining the instrument operation modes and scientific program:

- the Interferometry group (IGR), and
- the Science group (SGR).

Subsystem groups

The design, development, integration and commissioning of the instrument has been divided between working groups: Observing Support Module group (OSM), Instrument Control group (ICM), Optics and Mechanics group (OPM), Detector group (DET), Spectrograph group (SPE), Integration group (INT). They are directed by the Project Manager who is assisted by the System Engineer and the Integration Manager:

[2] Pierre Kern after NAOS

- Project Manager: Pierre Antonelli
- System Engineer: Serge Ménardi
- Integration Manager: Karine Perraut[2]

The Project Manager organizes regular meetings with the System Engineer, the INtegration Manager and the subsystem leaders.

9.1.3 Composition of the groups

Interferometry Group (IGR)

The IGR is a group of experts in optical Interferometry who assist the PS in defining some instrument specifications and observing procedures using the experience gained on existing optical interferometers and other high angular resolution techniques.

- Cassaing (ONERA)
- Coudé du Foresto (OdP)
- Forveille (LAOG)
- Hofmann (MPIfR)
- Mourard (OCA)
- Reynaud (IRCOM)
- Tallon (CRAL)

Science Group (SGR)

The Science Group contributes to the choice of the order in which the various possibilities offered by the concept will (or will not) be implemented. It is in charge of refining and preparing the program specifically permitted by AMBER with the VLTI. It has to work on the selection of observing targets, the feasibility analysis and have to push as far as possible the preparation of the contribution of AMBER measurements to the understanding of the source models.

- Foy (CRAL)
- Fraix-Burnet (LAOG)
- Monin (LAOG)
- Petitjean (IAP)
- Lopez (OCA)
- Stee (OCA)
- Weigelt (MPIfR)

Observing Support module (OSM)

The Observing Support Module (OSM) provides the software to

- prepare the observation through feasibility estimates and the definition of observing sequences from predefined templates.
- transmit the high level orders to the instrument control (send the template and check very high level tests of completion and monitor the quality of the data which is being recorded).
- reduce the data down to calibrated measurements with their error bars.

- Mouillet (LAOG) – **Coordinator**
- Sacchettini (LAOG)
- Duvert (LAOG)
- Monin (LAOG)
- Forveille (LAOG)

This people have AMBER as their first scientific priority in the critical period for AMBER (from now to the beginning of 2002). They are responsible for its software. Other contributors to the software have been identified. The OSM group will subcontract to them specific parts of the software but will be responsible for issuing the specifications, integrating it in the OSM structure and making sure that the tests and the documentation are homogeneous.

Other contributors:

- Hoffmann (MPIfR)
- Aristidi (UNSA)
- Mege (LAOG)
- Carbillet (OAA)
- Thiébaut (CRAL)

Instrument Control module (ICM)

It provides the hardware and the software for the control of the instrument, i.e. the interpretation and the execution of the high level orders sent by OSM, the control of the subsystems (OPM, SPE, DET) down to the electromechanisms and the sensors, the interface with ESO and the recording of the data produced by AMBER flagged by VLTI and environmental information.

- Le Coarer (LAOG) – **Coordinator**
- Sacchettini (LAOG)

- Petmezakis (LAOG)
- Dugué (OCA)
- Agabi (OCA)
- Mars (OCA)

Michel Sacchettini who is a software engineer participating to OSM and to ICM will be in charge in a first phase of a top down functional analysis of the software with a particular attention to the interface problems between OSM and ICM (definition of the exchanged data and their format). He will also be in charge with the harmonization of the software development and documentation standards.

This Group has members in Nice and in Grenoble and has particularly close ties with the OPM group based in Nice. Etienne Le Coarer gives a particular attention to the communication and coordination between Nice and Grenoble. This implies regular (monthly) visits to Nice, regular group meetings in Nice and Grenoble, strong contacts with the detector and spectrograph groups and weekly video conferences.

Optics and Mechanics group (OPM)

- Robbe (UNSA) – **Coordinator**
- Rebattu (OCA, mechanics)
- Glentzlin (OCA, mechanics)
- *Optical Engineer* (to be hired at OCA)
- Bresson (OCA, optics)
- Kamm (OCA, electronics)

It is critical to reinforce this group with an optical engineer, at least for the critical period December 98 December 99. INSU has made available an AFIP[3] in Nice for this position.

Detector group (DET)

The detector group is in charge of the detector from the chip to the data storage. It provides the simple[4] data processing functions necessary for the instrument adjustment and check up. All this is made in the MPIfR in Bonn.

- Beckmann (MPIfR) – **Coordinator**

[3] An AFIP is a position which must be provided by internal mobility in the whole CNRS. This position is open since December 1, 98 and applications can be received until the end of January.

[4] If the current discussion about the degree of respect to ESO standards permits us to keep the detector control architecteure developed in Bonn (Linux PC + DSP) the real-time processing at detector level can provide advanced evaluation of the data quality including calibrated measurements

- Geng (MPIfR)
- Heiden (MPIfR)
- Solchscheid (MPIfR)

A punctual help can be provided by Grenoble on the interface between the FIERA SUN SPARC computer (see 7.2) and the detector head (Petmezakis, Grenoble) if this device is needed.

Spectrograph group (SPE)

The spectrograph group is in charge of the cooled optics and their electromechanisms. They also provide the cryostat in which the detector will be eventually installed. This module is provided by the OAA in Arcetri.

- Lisi (OAA) – **Coordinator**
- Gennari (OAA)
- Baffa (OAA)
- Comoretto (OAA)

Integration group (INT)

The integration group is in charge of defining and realizing the tools for the global integration, test and performance evaluation of AMBER. Therefore, it will be in charge of the final integration. tests and performance evaluation in Grenoble. It is not yet clear which part of integration tools (Optical devices, simulation software, VLTI simplified simulator,...) will be manufactured at subsystem level and which part is built specifically by the integration group and therfore imply an extentension of its manpower.

- Kern (LAOG) – **Coordinator** after end of NAOS
- Perraut (LAOG) – **Coordinator** before end of NAOS
- Delboulbé (LAOG)
- Magnard (LAOG)
- + members of the other subsystems

9.2 Schedule

9.2.1 Milestones

November 1996: French "National program for high angular resolution astrophysics" establishes a working team to select the concept of a near infrared and red focal instrument for the VLTI. *See report AMB-REP-001 in March 1997.*

April 1997: Working group includes A. Richichi from OAA and M. Schöller from MPIfR.

June 1997: Osservatorio Astrofisici di Arecteri (OAA) joins the AMBER consortium.

July 1997: ISAC review of the instrument at ESO. *See report AMB-REP-002 in July 1997.*

January 1998: Max-Planck Institute für Radioastronomie joins the AMBER consortium.

January 1998: Review of the VLTI instrumentation by the Steering Committee of the VLTI tripartite agreement. *See report AMB-REP-002 in January 1998.*

September 1998: Final concept review (FCR) meeting in Nice.

January 1999: Conceptual design review (CDR) at ESO. See report AMB-REP-004 in January 1999 (this report).

September 1999: Preliminary design review (PDR).

January 2000: Final design review (FDR).

March 2001: Manufacturing and Integration Review (MIR). All subsystems integrated and tested.

July 2001: Acceptance review. AMBER integrated and tested, its performance measured in laboratory.

September 2001: Reception of AMBER at Paranal.

November 2001: Laboratory and siderostat tests completed at Paranal.

December 2001: start commisioning / observations with the UTs.

July 2002: start commisioning / observations with the ATs.

End 2002: ESO operation of mode 1 (2 telescope interferometer in spectral channel).

Mid 2003: ESO operation of mode 2 (differential observations).

Early 2004: ESO operation of mode 3 (phase closure).

End 2004: Handover to ESO.

9.2.2 General timetable

GENERAL TIMETABLE																
	1998				*1999*				*2000*				*2001*			
Concept, potential performances, specifications	xxx	xxx	xxx	xxx	x											
Final Concept Selection : 3-9-98			**fcr**													
Concept Design Revue at ESO : 28-1-99					**cdr**											
Detailed management plan				x	xxx	x										
Preliminary design, detailed budget and schedule				x	xxx	xxx	xxx									
Preliminary Design Revue : september 99							**pdr**									
Chip order for the detector : september 99							**o**		**de**	**ds**						
Order spectrograph optics and cryostat							**o**									
Detailed design						x	xxx	xxx	xxx							
Final Design Revue : February 2000									**fdr**							
Manufacturing								xxx	xxx	xxx	xxx	xxx	xxx			
Subsystems integration and tests												xxx	xxx	xxx		
Manufacturing and Integration Revue : April 2001														**mir**		
General integration and tests, performance measurements														xxx	xxx	
Acceptance : September 2001															**Acc**	
Shipment to Paranal															x	x
Tests at Paranal in lab and with the siderostat																xxx
Observing with the Uts : December 2001																**Obs**

9.2.3 Optomechanics (OPM)

Optomechanics	*1998*				*1999*				*2000*				*2001*			
Interfaces and set up in the VLTI focal lab				x												
Precise specifications and budget for optomechanical tolerances				x	x											
Preliminary optical study				x	x	x										
Preliminary mechanical study					x	x	x									
Detailed optical design							x	x								
Detailed mechanical design							x	x	x							
Manufacturing and integration of the OPM									x	x	x					
Full test of OPM and of the control software											x	x	x			

9.2.4 Instrument control (ICM)

Instrument control	*1998*				*1999*				*2000*				*2001*			
Hardware and software architecture for the instrument control (ESO compatible)				x	x											
General functional analysis of the software (ICM+OSM)				x	x											
Preliminary study of the instrument control hardware and software					x	x	x									
Detailed design of the ICM electronics and software							x	x	x							
Manufacturing and tests of electronics and control software									x	x	x					
Full test of OPM and of the control software											x	x	x			

9.2.5 Spectrograph (SPE)

Spectrograph	*1998*				*1999*				*2000*				*2001*			
Detailed specifications					x											
Preliminary study				x	x	x										
Detailed optical design					x	x	x									
Detailed mechanical design						x	x	x								
Manufacturing of the optics and the cryostat							x	x	x	x						
Manufacturing the mechanics								x	x	x	x					
Integration and tests of the spectrograph alone										x	x	x				

The cryostat of the cooled spectrograph is manufactured to the specifications by a small company. It must be ordered immediately after the PDR, to permit an integration of the spectrograph at Arcetri before the integration of the detector in the spectrograph. That implies that at the PDR, the detailed design of the spectrograph has been started. This is possible because of the availability of the Arcetri people in the first semester of 1999 and because the specifications of the spectrograph, which are already quite well defined can be completely frozen by February 99 (if we receive some immediate help from an optical engineer).

9.2.6 Detector (DET)

Detector	***1998***				***1999***				***2000***				***2001***			
Select electronics and chip	x	x	x													
Preliminary design and adaptation to ESO standards				x	x	x										
Chip order							x									
Detailed design							x	x								
Delivery engineering grade									x							
Delivery science grade										x						
Manufacturing and integration at MPIfR										x	x					
Tests at MPIfR											x	x				
Integration in the spectrograph and tests													x			

The detector chip must be ordered immediately after the PDR (spring 99) to be delivered in time for the integration at the MPIfR (2nd and 3rd terms 2000) and then in the cooled spectrograph (4th term 2000) before the MIR.

9.2.7 Observing Support Module (OSM)

Observing support software	***1998***				***1999***				***2000***				***2001***			
Instrument simulation software	x	x	x	x	x											
Software environment				x	x											
Functional analysis and preliminary design (partially with ICM)				x	x	x	x									
Detailed design							x	x	x							
Finalizing and testing the OSM software									x	x	x	x	x	x		
Full test of OSM with simulated data															x	x
Update of OSM from actual Paranal experience																x

After the last term of 2001, OSM will continue to include the actual observing experience in the software until the full handover to ESO in 2004.

9.2.8 Integration (INT)

Integration	*1998*				*1999*				*2000*				*2001*			
Defining the global integration « machine »					x	x	x									
Detailled design of the global integration « machine »							x	x	x							
Building, integrating and testing the global integration « machine »									x	x	x	x	x			
OPM alone											x	x				
ICM alone											x	x				
OPM+ICM													x			
SPE alone											x	x				
DET alone											x	x				
DET inside SPE													x			
General integration														x	x	
Performance evaluation															x	
OSM with simulated data															x	
Paranal tests																x

9.2.9 Science group (SGR)

Integration	*1998*				*1999*				*2000*				*2001*			
Defining the global integration « machine »					x	x	x									
Detailled design of the global integration « machine »							x	x	x							
Building, integrating and testing the global integration « machine »									x	x	x	x	x			
OPM alone											x	x				
ICM alone											x	x				
OPM+ICM													x			
SPE alone											x	x				
DET alone											x	x				
DET inside SPE													x			
General integration														x	x	
Performance evaluation															x	
OSM with simulated data															x	
Paranal tests																x

The tasks of the Science Group (SGR) are partially independent from the general milestones for the instrument development except in the beginning (SGR needs the instrument simulator OSM will finish for the end of 98) and at the end when the actual instrumental performances have to be used to refine the observing programs.

9.3 Budget

Note: n = number of telecopes, m =number of spectral bands.

9.3.1 Global Budget

GLOBAL BUDGET[5]								
Sub system	2 Telescopes				3 Telescopes			
	Partially to standard[6]		Fully to standard		Partially to standard		Fully to standard	
	MF	K€	MF	K€	MF	K€	MF	K€
DETector	1.31	199.6	1.31 + tbd	199.6 + tbd	1.31	199.6	1.31 + tbd	199.6 + tbd
Spectrograph[7]	0.73	111.1	1.03	187.3	0.73	111.1	1.03	187.3
OPtics and Mechanics	1.18	179.9	1.18	179.5	1.71	261.2	1.71	261.2
Instrument Control	0.81	123.5	1.16	176.5	0.90	136.7	1.46	222.1
Global Integration[8]	0.5	76.2	0.5	76.2	0.5	76.2	0.5	76.2
Travels and transport[9]	1.2	182.9	1.2	182.9	1.2	182.9	1.2	182.9
TOTAL[10]	**5.73**	**873.5**	**6.38**	**972.2**	**6.35**	**968.0**	**7.21**	**1099.1**

[5] Hypothesis: ESO provides software licences and development HP work stations.

[6] The single difference between *partially to standard* and *fully to standard* is the use of MACCON boards for the control of motors.

[7] *Fully to standard* extra-cost corresponds to one year of computer engineer work.

[8] Non deliverable to ESO. Very preliminary estimation from PFSU *piston generator assembly* which had a cost of about 60 K€ (380 KF).

[9] 300 KF per year. Includes all travels. For 2002, includes transport to Paranal, Paranal tests and first science observations.

[10] Induced cost to be added, starting mid-2002: about 600KF per year if operated by the consortium.

9.3.2 Optomechanics: warm optics and mechanics

OPTICAL COMPONENTS						
Component	Nbr	Unit Price KF	Total=f(m,n)	Total 2T (3b)	Total 3T (3b)	Comment
Black body	1	40	40	40	40	ESO ?
Laser diode J	1	8	8	8	8	
Laser diode H	1	11	11	11	11	
Laser diode K	1	11	11	11	11	
Fibers J, H, K	m.n	22	22 m .n	132	200	Includes higher price for K
Plane mirror Φ=60	1+4n	5	5 + 20 .n	45	65	
Polariser	n	10	10 n	20	30	
Dichroics	2.(m-1).n	4	8.(m-1).n	32	48	16 for 4 dichr.
Doublets Φ=50	2.m.n	10	20.m.n	120	180	30 for 3 doublets
Parabola Φ=200	1+n	15	15+15.n	45	60	Or two off axis Φ=60
Spherical Φ=10	n	3	3.n	6	9	
Slits	2.n	5	10.n	20	30	
Beam splitter Φ=60	N	10	10.n	20	30	
Cylindrical mirrors	“n”	30	30.n	60	90	
Refraction correctors	2.n	15	30.n	60	90	n may be enough. ESO ?
Control sensors	n	10	10.n	20	30	
TOTAL OPTICS KF				**650**	**932**	
TOTAL OPTICS K€				**99.1**	**142.1**	

MECHANICAL COMPONENTS						
Component	Nbr	Unit Price KF	Total=f(m,n)	Total 2T (3b)	Total 3T (3b)	Comment
Repositioning	1+(2+m).n	10	10+(20+10m)n	110	160	motors
Piezos x-y pos.	1+2.m.n	5	5+10.m.n	65	95	2 piezos
Precise trans.	m.n	10	10.m.(n-1)	30	60	0 OPD
Inserter	1+2.n	3	3+6.n	15	21	motors
Table	1	40	40	40	40	
Beam clean sup.	n	10	10.n	20	30	
Support for pl. mir	(2+m).n	5	(10+5.m).n	50	75	Non motorized
Rotations	4.n	5	50.n	100	150	
Material, small components			50.n	100	150	
TOTAL MECHANICS KF				**530**	**781**	
TOTAL MECHANICS K€				**80.8**	**119.1**	
TOTAL OPM KF				**1180**	**1713**	
TOTAL OPM K€				**179.9**	**261.2**	

9.3.3 Spectrograph: cooled optics and mechanics

SPECTROGRAPH COMPONENTS		
Component	Price (K€)	Comment
Optics	**29.6**	
Window	1	2 Ml
2 Gratings	3.8	7.3 Ml
2 Flat mirrors + 2 prisms	2.6	5 Ml
Filters J,H,K	3.1	6 Ml
Order sorting filter	2.1	4 Ml
3 mirrors with aluminum	17	33 Ml
Cryogenics and mechanics	**67.5**	
Consulting for Dewar and mechanical study	12.9	25 Ml
Dewar manufacturing	36.2	70 Ml
3 Motorizations	15.3	6K$ each, including mechanics, power and driver
Control PC, boards, connectors	3.1	6 Ml, useful in spectrograph integration phase
Additional costs	**14**	
Integration tools	5.2	10 Ml
Manpower	8.8	17 Ml for 1 “post-laurea” scholarship
TOTAL SPECTROGRAPH KF	**729**	
TOTAL SPECTROGRAPH K€	**111.1**	215.1 Ml

9.3.4 Detector and data acquistion

DETECTOR and DATA ACQUISITION COMPONENTS		
Component	Price (K€)	Comment
Detector	**147.4**	
Chip Hawaii (scien.+eng.+mux)	127.1	150 K$ (40 K$ at order, 50 K$ o+5 m, 60 K$ o+14 m)
Fanout board with detector mount + connectors	3.4	4 K$
Test dewar HDL-8	16.9	20 K$
Electronics	**12.3**	
Metal box for electronics boards	4.1	8 KDM
Printed circuit boards, components, connectors	5.1	10 KDM
Power supply, cables	2.0	4 KDM
Optical fiber cables	1.0	2 KDM
Data acquisition and storage	**31.7**	
Computer data interface	1.0	2 KDM
Online computer with real time display	15.3	30 KDM
Control computer, data storage and distribution	15.3	30 KDM
Environment	**5.1**	
Cooling system	5.1	10 KDM
Additional tools	**3.1**	
Flat field lamp + shutter	2.6	5 KDM
Shutter controller	0.5	1 KDM
TOTAL DETECTOR and DATA ACQUISITION KF	**1309**	
TOTAL DETECTOR and DATA ACQUISITION K€	**199.6**	390.4 KDM

9.3.5 Instrument control and observing support

INSTRUMENT CONTROL COMPONENTS									
Component			Price KF						Comment
Work stations			100						ICM WS
Cabinets			100						
Connectors and wires			100						
Training to ESO std			100						Travels
Logical I/O board, time boards and back plane			50						
Miscellaneous			100						
Total common features			**550**						
Piezo control	2T: 24 piezos				3T: 36 piezos				
	2 boards 16 A Outputs		40		3 boards 16 A Outputs		60		
	Controllers		48		Controllers		72		
Sensors	2T: 4 sensors				3T: 6 sensors				
	ADC boards		20		ADC boards		30		
Total piezos + sensors			**108**				**162**		
Motor control	2T: 24 motors				3T: 35 motors				
	Partial ESO std		Full ESO std		Partial ESO std		Full ESO std		
	1 VME LCU	30	2 VME LCU	60	1 VME LCU	30	3 VME LCU	90	
	1 VME bus draw	30	2 VME bus draw	60	1 VME bus draw	30	3 VME bus draw	90	
	1 serial board	20	6 Macon boards	200	1 serial boards	20	9 Macon boards	300	
	24 motor+pw bds	72	24 power boards	120	35 motor+pw bds	105	35 power boards	175	
			2 drawers	60			3 drawers	90	
Total motors		**152**		**500**		**185**		**745**	
TOTAL ICM KF	**2T, partial std**	**810**	**2T, full std**	**1158**	**3T, partial std**	**897**	**3T, full std**	**1457**	
TOTAL ICM K€	**2T, partial std**	**123.5**	**2T, full std**	**176.5**	**3T, partial std**	**136.7**	**3T, full std**	**222.1**	

9.3.6 Financing plan and spending timetable

TOTAL: 873 K€
France: 457 K€ (3 MF, INSU: 2 MF, Regions: 1MF)
MPIfR[11]: 208.1 K€ (407 kDM)
OAA[12]: 208.1 K€ (402.9 ML)

TENTATIVE SPENDING SCHEDULE					
Sub System	S. S. total	1999	2000	2001	2002
Detector	199.6	85	114.6		
Spectrograph	111.2	50	61.2		
Optics and Mechanics	180.0	30	120	30	
Instrument Control	123.5	30	60	33.5	
Global Integration	76.2		38.2	38	
Travels and transport	183.0	45.8	45.7	45.8	45.7
Total K€	**873.5**	**240.8**	**439.7**	**147.3**	**47.5**
Total France[13] K€	**457.3**	**130**	**200**	**100**	**27.3**
3 telescopes option	94.5			47.3	47.2
Total 3T K€	968	240.8	439.7	194.6	94.7
Total France 3T K€	551.8	130	200	147.3	74.5

[11] At the present moment, the guaranteed MPIfR contribution is 152 K€ (1 MF). Extension is the matter of pending negociations.
[12] At the present moment, the guaranteed OAA contribution is 152 K€ (1 MF). Extension is the matter of pending negociations.
[13] The present spending timetable for the French contribution corresponds to the previsions of INSU. The global spending timetable still has to be discussed with MPIfR and OAA.

9.4 Operation plan

The operation plan would include the following steps:

July 2001: Beginning of the global integration in Grenoble and beginning of ESO AMBER operators.

Fall 2001: Paranal laboratory and siderostats test. AMBER team will contain typically 6 to 8 people. Provision for this travels is made in AMBER budget.

December 2001: First observations with the UTs.

Mid 2002: First observations with the ATs (differential mode). AMBER team reduced to 3 people.

2nd semester 2002: first UT differential observations for the direct detection of hot giant extra solar planets[14]

End of 2002: Full ESO operation of the basic mode (two-telescope visibility in each spectral channel).

2003: First observations with 3 telescopes (1UT+2AT or 3AT if available).

Mid 2003: Full ESO operation of differential modes (visibility and phase as a function of wavelength).

End of 2003: Full ESO operation of phase closure observations.

1st semester 2004: Full ESO operation of the infrared instrument (including observations with non filtered mode)[15].

The teams making observations in modes not yet fully managed by ESO would be paid by AMBER when the consortium is the main beneficiary of the observations. This will represent typically one or two runs per semester by a three people team (including ATs and UTs). Observations in full ESO operated modes will be managed in a classical ESO way. Observations in non ESO managed modes for scientists outside the AMBER consortium can be handled by AMBER teams for a TBD counterpart in terms of guaranteed time.

The repartition of the AMBER guaranteed time has still to be analyzed.

[14] Good success in the analysis of this mode for this program might push toward its early implementation.

[15] The development and commissioning of visible instrument (2002-2005) is not included in the present operation plan. This phase will need additional agreements, timetables and budget. An important contribution of CRAL is expected for this future phase.

This issue is still discussed inside the consortium and with our sponsoring Institutes and is still subject to major changes. The dates are likely to be modified after a more precise analysis. Also the order of implementation of the different modes can be modified as a result of the Scientific demand as it will be refined by the AMBER Science Group. A more precise formulation of the Operation plan proposed by AMBER will be presented at the CDR.

Appendix A

Glossary

ADC: Analog / Digital Converter or Atmospheric Dispersion Compensator depending on context

AGB: Asymptotic Giant Branch

AGN: Active Galactic Nucleus

AIT: Assembly, Integration and Tests module

AMBER: Astronomical Multi-BEam Recombiner

AO: Adaptive Optics

ARC: Atmospheric Refraction Compensator

AT: 1.8-m Auxiliary Telescope

AU: Astronomical Unit

CDR: Conceptual Design Review

CRAL: Centre de Recherche Astrophysique de Lyon

DL: Delay Line

DDL: Differential Delay Line

DET: DETector module

DSP: Digital Signal Processor

EGP: Extrasolar Giant Planet

ESO: European Southern Observatory

FCR: Final Concept Review

FLUOR: Fiber-Linked Unit for Optical Recombination

FSU: Fringe Sensor Unit

FOV: Field Of View

GI2T: Grand Interféromètre à 2 Télescopes (*Grand Interferometer with 2 Telescopes*)

GUI: General User Interface

HPVM: High Precision Visibility Mode

HSRM: High Spectral Resolution Mode

IAP: Institut d'Astrophysique de Paris

ICM: Instrument Control Module

IGR: Interferometric GRoup

IM: Imaging Mode

INT: Integration group

IOTA: Infrared and Optical Telescope Array

ISAC: Interferometry Science Advisory Committee

IR: InfraRed

IRCOM: Institut de Recherche en Communications Optiques et Microondes in Limoges

LAOG: Laboratoire d'Astrophysique de l'Observatoire de Grenoble

LBV: Luminous Blue Variable

MIDI: MID-Infrared instrument

MOU: Memorandum of Understanding

MPIfR: Max Planck Institute für Radioastronomie in Bonn

MSPS: ????

OAA: Osservatorio Astrofisico di Arcetri in Firenze

OCA: Observatoire de la Côte d'Azur in Nice

OdP: Observatoire de Paris

ONERA: Office National d'Études et de Recherches Aérospatiales in Paris

OPD: Optical Path Difference

OPM: OPto-Mechanical module

OSM: Observing Support Module

PFSU: Prototype Fringe Sensor Unit

PRIMA: Phase Reference Imaging and Micro-Arcsecond Astrometry

PTV: Peak-To-Valley

QLA: Quick Look Analysis

QSO: Quasi-Stellar Object

RMS: Root Mean Square

RON: Read-Out Noise

SFDR: ???????

SGR: Scientific GRoup

SPE: SPEctrograph module

SNR: Signal-to-Noise Ratio

TBD: To Be Done

TBC: To Be Confirmed

UT: 8-m Unit Telescope

VCM: Variable Curvature Mirror

VINCI: VLT INterferometer Commissioning Instrument

VLTI: Very Large Telescope Interferometer

VLTICS: Very Large Telescope Interferometer Control Software

WFE: WaveFront Error

WFS: WaveFront Sensor

YSO: Young Stellar Object

Appendix B

References

B.1 AMBER documentation

The AMBER documentation is available on the AMBER Web site:

`http://www-laog.obs.ujf-grenoble.fr/amber`

B.2 Bibliography

Beletic J., et al. 1998, Experim. Astron. 8, 13

ISAC report, 1996, *A new start for the VLTI*, The ESO Messenger, 83

Ciddor, P.E. 1996, Appl. OPt. 35, 1566

Coudé du Foresto V., Mariotti J.-M., Perrin G. 1996, *Direct observation of extrasolar planets with an infrared interferometer*, in Proc. of ESO conference "Science with the VLT Interferometer", Garching, Germany, F. Paresce ed., pp. 86–87.

Coudé du Foresto V., Perrin G., Mariotti J.-M., Lacasse M. and Traub W. 1996. *The FLUOR/IOTA fiber stellar interferometer.* In proc. of the AstroFib'96 conference on "Integrated Optics For Astronomical Interferometry", Grenoble, Observatoire de Grenoble, P. Kern and F. Malbet eds., pp. 115–125.

Coudé du Foresto V. 1996. *Fringe benefits: the spatial filtering advantage of single-mode fibers.* In proc. of the AstroFib'96 conference on "Integrated Optics For Astronomical Interferometry", Grenoble, Observatoire de Grenoble, P. Kern and F. Malbet eds., pp. 27–30.

Mourard D., Tallon-Bosc I., Blazit A., Bonneau D., Merlin G., Morand F., Vakili F., Labeyrie A. 1994, A&A 283, 705

Malbet F., Coudé du Foresto V., Mékarnia D., Petrov R., Reynaud F., Tallon M. 1997a, *AMBER Report 1 – Preliminary study of the near-infrared/red instrumentation of VLTI and GI2T*

Malbet F., Perrin G., Petrov R., Richichi A., Schöller M. 1997b, *AMBER Report 2 – The imaging and spectroscopic VLTI focal instrument*, available on the AMBER Web (AMB-REP-002).

Petrov R.G., Malbet F., Richichi A., and Hofmann K.-H. 1998, The ESO Messenger, 92, 11, *AMBER, the near-infrared / red VLTI focal instrument*

Malbet F., Berger J.-P., Colavita M. M., Koresko C. D., Beichman C., Boden A. F., Kulkarni S. R., Lane B. F., Mobley D. W., Pan X. P., Shao M., van Belle G. T., and Wallace J. K., 1998, ApJL, in press, *FU Orionis resolved by infrared long-baseline interferometry at a 2-AU scale*

Millan-Gabet R., et al. 1998, in preparation

Richichi A., Stecklum, Herbst T. & Lagage P.-O. 1998, A&A 334, 585

Malbet F., Petitjean P., and Henri G., 1997, *AGN Models and Fringe Visibilities*, in Paresce F. (ed.), Science with the VLT Interferometer. ESO Astrophysics Symposia, Springer, Heidelberg (Germany), p. 102

Index